

Two-photon ionization of atomic inner-shells

Inaugural-Dissertation
zur Erlangung der
Doktorwürde der Naturwissenschaften
(Dr. rer. nat.)

vorgelegt beim Fachbereich Naturwissenschaften
der Universität Kassel

von
Peter Koval
aus Majkop, Russland

January 2004

1. Gutachter: Dr. Stephan Fritzsche

2. Gutachter: Prof. Dr. Burkhard Fricke

weitere Mitglieder der Prüfungskommission:

1. Prüfer: Prof. Dr. Thomas Baumert

2. Prüfer: Prof. Dr. Réne Matzdorf

Tag der Disputation: 19. März 2004

Contents

1	Introduction	1
2	Perturbative methods in description of multiphoton ionization	5
2.1	Time-dependent perturbation theory	6
2.2	Direct summation method	11
2.3	Differential equation method	13
2.4	Green's function method	14
3	Relativistic and multipole effects in two-photon ionization	15
3.1	Differential and total cross sections for hydrogen-like ions	17
3.2	Total ionization cross section for heavy hydrogen-like ions	19
3.2.1	Basic features of the total cross section	19
3.2.2	Relativistic effects	21
3.2.3	Multipole effects	22
3.2.4	Dependence of the total cross section on the nuclear charge	23
3.3	Electron angular distribution in the two-photon ionization	25
3.4	Conclusion	28
4	Two-photon ionization of many-electron atoms	29
4.1	Single-active-electron approximation	30
4.2	Total cross section in the SAE approximation	30
4.3	Dirac-central-field Green's function	31
4.3.1	Defining equation for the Dirac-central-field Green's function	31
4.3.2	Separation of the Dirac-central-field Green's function	32
4.3.3	Calculation of the radial part of Dirac-central-field Green's function	33
4.4	Two-photon ionization of the lithium outer-shell	36
4.5	Two-photon ionization of He and He-like ion of neon	38
4.6	Two-photon ionization of the argon K- and L-shells	39
4.6.1	Stretching of theoretical cross sections	39
4.6.2	Two-photon ionization of the argon K-shell	40
4.6.3	Two-photon ionization of the argon L-shell	41
4.6.4	Polarization dependence of subshell cross sections	43
4.7	Conclusion	45

5	Summary and Outlook	47
	German summary (Zusammenfassung)	49
A	One-electron radiative matrix elements	51
A.1	First-order radiative matrix element	51
A.2	Second-order radiative matrix element	53
B	Calculation of Kummer and Tricomi functions	55
B.1	Mathematical formulae for Kummer and Tricomi functions	55
B.2	Round-off error in the realization of numerical algorithms	57
B.3	Self-validation algorithm for the computation of the Kummer function	57
B.4	Self-validation algorithm for the computation of the Tricomi function	59
C	Calculation of Hartree potentials	63
C.1	Hartree potential	63
C.2	Hartree-plus-statistical-exchange potential	64
D	Numerical tests for the Dirac-central-field Green's function	65
E	Publications	67
E.1	Relativistic wave and Green's functions for hydrogen-like ions	69
E.2	Relativistic and retardation effects in the two-photon ionization of H-like ions .	89
E.3	Electron angular distributions in the two-photon ionization of H-like ions . . .	97
	Acknowledgment	119
	Curriculum Vitae	121

Chapter 1

Introduction

Multiphoton absorption belongs to those phenomena which have first been predicted *theoretically*. At the middle of 1920-s, Schrödinger (1926) and Dirac (1926) developed the *first-order* perturbation theory and applied it to one-photon absorption processes. Moreover, Dirac also discussed the applications for the *second-order* perturbation theory. He applied the second-order perturbation theory to the electron scattering which is a *two-photon* process. Only by 1931, however, Göppert-Mayer noticed that the second-order perturbation theory is able to describe another—different from the scattering—process of *two-photon absorption*. In the two-photon absorption, the two photons simultaneously transfer their energy to the atom. Furthermore, it became clear after Göppert-Mayer's work that *higher-order* perturbation theory reveals *multiphoton absorption* processes.

Since the discovery of lasers in 1960-s, the multiphoton excitation and ionization processes have received an increasing interest, both from the experimental as well as from the theoretical side. For example, the measurements of the two-photon ionization in alkali and alkaline atoms have confirmed the theoretical predictions on *total cross sections* and electronic angular distributions (Delone and Krainov 1999). The multiphoton spectroscopy of alkaline outer-shells contributed to the identification of their—otherwise difficult to interpret—excited states (Wynne *et al* 1977) and made evident the importance of an AC Stark shift and the possibility of a higher-order harmonic generation (Delone and Krainov 1999). The latter possibility wake up recently a theoretical interest to these—rather hard to treat—atoms (McKenna and Hugo 2003, Luc-Koenig *et al* 1997).

From a *theoretical* point of view, the most often studied atom is certainly the *hydrogenic atom*. Although there are not many experiments dealing with the multiphoton ionization of hydrogen, the simplicity of the hydrogenic atom made it possible to calculate the total cross section and the electron angular distribution already in a first attempt by Zernik (1964) who had considered the two-photon ionization of the $2s$ metastable state of the hydrogen atom. The following investigations by Bebb and Gold (1966), Gontier and Trachin (1968), Rapoport *et al* (1969) were devoted to the few-photon ionization of the hydrogen atom in the ground state as well as in the metastable states. These studies elucidated the resonance structure of the multiphoton cross section and reached a numerical reliability in computation of the absolute cross section values. Further on, the dependence of the multiphoton ionization yield on the

photon polarization was studied by Zon *et al* (1971) and by Arnous *et al* (1973). In contrary to the one-photon ionization, the two-photon ionization shows a strong dependence not only on the photon energy but also on the polarization of the light.

First theoretical studies on the multiphoton ionization/excitation were all done within the perturbation theory which requires a calculation of *perturbative sums* over the whole spectrum of *intermediate states* of the atom. Already in first theoretical works, these sums had been calculated by means of *implicit summation methods* which convert the summation into the solving of a relevant differential equation. Although one of the implicit methods—the *differential equation method*—had been implemented firstly, yet another *Green's function method* became wide-spread. The Green's function method replaces the summation over the complete atomic spectrum by the calculation of a relevant *Green's function*.

The relevant Green's function for hydrogen—Coulomb Green's function—can be obtained analytically in many forms. Despite a formal equivalence of these forms, there are large differences by the accuracy and in the efficiency by actual computations of the multiphoton cross sections. For instance, an *integral representation* (Klarsfeld 1969) of the Coulomb Green's function is the slowest, while a *product representation* (Laplanche *et al* 1976) allows already a faster computation. Furthermore, an expansion of the Coulomb Green's function on a *Sturmian basis* seems to be most efficient in the *matrix element calculation* (Karule and Pratt 1991).

Although the theoretical predictions in the multiphoton ionization are far more accurate than the present experimental measurements, the experimental research determines *general directions* for new theoretical developments. The present technique of the light production develops in two main directions: (1) sources of electromagnetic radiation become more powerful and (2) their wavelength become shorter.

(1) The strength of the field in modern lasers exceed the intrinsic field in the atomic outer-shells. This circumstance leads to new, non-perturbative phenomena like the above-threshold-ionization, AC Stark shift and high-order-harmonic generation. These phenomena require a non-perturbative treatment based on a direct solution of time-dependent Schrödinger equation (Gebarowski *et al* 1997).

(2) On the other-hand, it is always desirable that the wavelength of the produced radiation would be shorter. Aside from many other applications (TESLA 2003), the short-wavelength radiation—either from capillary discharge (Rus *et al* 2002, Rocca *et al* 2003) or from free-electron sources (Andruszkow J *et al* 2000)—will facilitate applications in the atomic physics of heavy systems like *highly-charged ions* or *inner-shells*. For instance, a coherent, high-photon-energy output from a free-electron laser will be used in the experiments on the two-photon ionization of the inner-shells of neon atom (TESLA 2003).

At the same time, the theoretical predictions in the multiphoton ionization of heavy atoms are still scarce and need to be extended (Kornberg *et al* 2002).

In this work, I am going to study the two-photon ionization of atomic inner-shells and to accomplish two main tasks. Firstly, I will investigate the *relativistic and multipole*¹ *effects* and, secondly, I will investigate the *many-particle effects* in the two-photon ionization of atomic inner-shells. The relativistic effects are those differences between the non-relativistic (based

¹ *Multipole* (or *retardation*) effects arise from an inclusion of higher, non-dipole terms into an expansion of electro-magnetic plane wave $e^{i\mathbf{k}\mathbf{r}}$ over the spherical partial waves (see page 22).

on the Schrödinger equation) and the relativistic (based on the Dirac equation) descriptions of the atom which arise when the electronic energy get higher, i. e. when the heavier atoms are considered. The relativistic effects are *fundamental* in that sense that they do not depend on the complexity of the atom, but on the energy of electrons. Similarly to the relativistic effects, the multipole effects relate to the energy of the absorbed/emitted photons, i. e. they may show up already in the simplest one-electron atoms. Hence, it is worth to study the relativistic and multipole effects in the simplest heavy atomic systems: hydrogen-like ions. The simplicity of hydrogen-like ions allows to study in Chapter 3 both the *total cross section* as well as the *electron angular distribution* in the two-photon ionization.

Since the field strength of any today X-ray machine is far below of the intrinsic atomic field, I will treat the two-photon ionization by means of the perturbation theory. The perturbative treatment requires a calculation of perturbative sums over the whole atomic spectrum. This is a difficult task even in case of the simplest, one-electronic atom. The difficulty arises mainly because of the continuum part of the atomic spectrum and can be overcome by means of *implicit summation methods*. I will present one of the implicit summation methods—Green’s function method—in Chapter 2 and use it all over this work.

In Chapter 4, I will utilize the Green’s function method and investigate the *many-electron effects* within the so-called *single-active-electron* (SAE) approximation. Although the SAE approximation is the simplest extension of the hydrogen-like model of the inner-shell, it will allow to estimate the effects arising due to the *electron-electron interaction* in a number of atomic systems.

Finally, in Chapter 5, I will give some conclusion and short outlook on further applications of the Green’s function method.

Chapter 2

Perturbative methods in description of multiphoton ionization

Atoms certainly belong to the most frequently studied quantum systems. They consist of a heavy nucleus and one- or many light electrons. Since the nucleus carries a positive electric charge, it attracts electrons which reside nearby to the nucleus. The positive and negative charges of the nucleus and electrons compensate and the atom normally looks like a neutral particle. However, an atom changes its properties when immersed in an external electromagnetic field.

For example, a *time-independent* electromagnetic field changes the position of atomic energy levels, splits spectroscopic lines and even ionizes the atom. The manifold of mentioned phenomena enormously increases if one studies how a *time-dependent* electromagnetic field influences the atom. There are two reasons for this increase. Firstly, a conventional source of time-dependent field (i. e. a source of electromagnetic waves) creates a much stronger field than sources of constant fields are able to produce. Secondly, time-dependent fields bring into play *different mechanisms* of studied phenomena. For instance, in this thesis I will study the ionization of an atom by the time-dependent electromagnetic field. Although both time-dependent as well as time-independent fields can ionize the atom, ionization mechanisms differ significantly. In case of time-independent electromagnetic field the ionization takes place due to a tunnel effect while an electromagnetic wave acts on the atom by transmitting a certain amount of its energy. This energy can excite or even release the atomic electron(s).

The field of a monochromatic plane wave can be imagined as an ensemble of photons each of which possesses an energy E_γ and move in the same direction. If such an ensemble of photons meets an atom, the atomic electron(s) can take up the energy of one or many photons. When the electron absorbs an energy which is larger than a *threshold* energy, it leaves the atom and becomes a "free" electron. Such release of electrons from the atom is known as *photoionization* since an initially neutral atom becomes a positive *ion* due to the absorption of *photon(s)*. If the electron is released by absorption of only one single photon then the ionization probability will be proportional to the number of photons which interact with the atom. Hence, in one-photon ionization the probability *linearly* depends on the number of interacting photons, i. e. depends *linearly* on the photon flux.

Apart from the one-photon ionization, there are other photoionization processes possible. For instance, atom may absorb the energy of two photons simultaneously. In this case, the ionization probability is proportional to the number of couples of photons. Hence, the ionization probability will depend on the square of the photon flux as it is explained in the Figure 2.1.

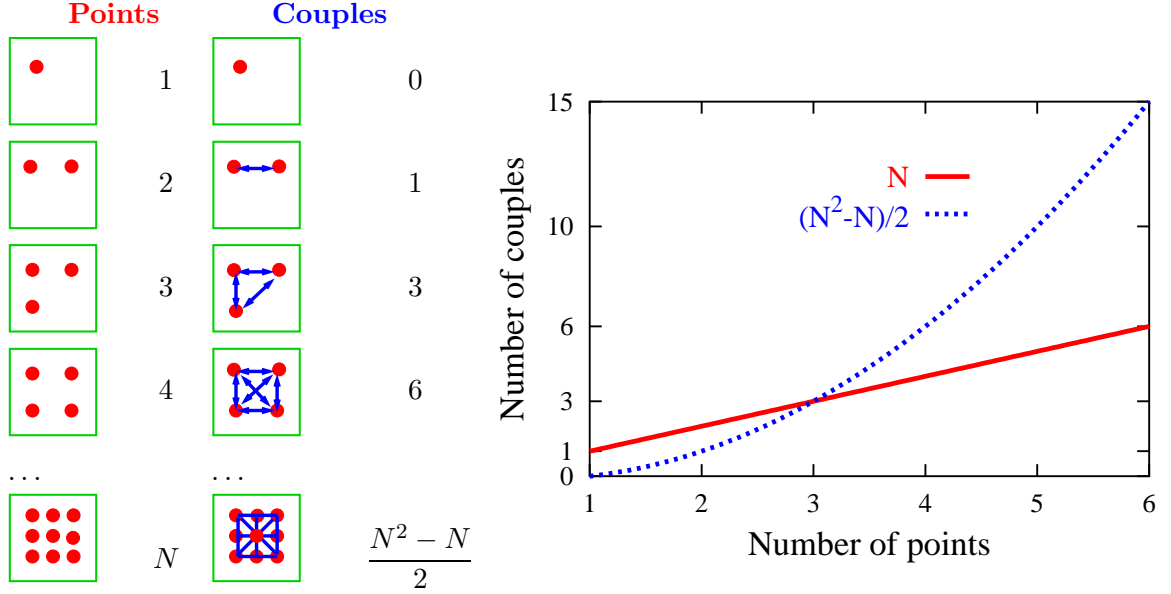


Figure 2.1: One can assume that the atom interacts only with photons inside of a volume and model this volume by a box. The probability of the one-photon ionization is proportional to the number of photons inside of the box, since the absorption of just one single photon ionizes the atom. In contrary, the probability of the two-photon ionization is proportional to the number of couples of photons inside of the box, since only a simultaneous absorption of two photons ionizes the atom. Thus, the probability of the one-photon ionization is proportional to the photon flux and the probability of the two-photon ionization is proportional to the square of the photon flux.

In this chapter, I will consider a multiphoton ionization process from the viewpoint of conventional quantum mechanics. In the following section, I will treat the one- and two-photon ionization within the time-dependent second-order perturbation theory. The probability of two-photon ionization will be derived for the case when a single plane wave ionizes the atom. *Second-order matrix elements*, which arise in this perturbative treatment, are rather difficult to treat. Hence, in Sections 2.2, 2.3 and 2.4, I will discuss these difficulties and present two accurate methods to calculate these second-order matrix elements.

2.1 Time-dependent perturbation theory

From a point of view of modern quantum mechanics, the properties of free atom and the atom in the external field can be explained solving a Schrödinger type equation

$$\hat{H} \Psi = i \frac{\partial}{\partial t} \Psi \quad (2.1)$$

with a suitable Hamilton operator \hat{H} . For instance, the energy levels of a *free* N -electron atom can be described by means of a Dirac-Coulomb Hamilton operator (Grant 1988)

$$\hat{H}_{DC} = \sum_{i=1}^N \left\{ c \boldsymbol{\alpha}(i) \mathbf{p}_i + [\beta(i) - 1]c^2 - \frac{Z}{|\mathbf{r}_i|} \right\} + \sum_{i,j}^N \frac{1}{|\mathbf{r}_i - \mathbf{r}_j|}. \quad (2.2)$$

This relativistic operator contains the kinetic energy of electrons, the rest mass energy of electrons and the potential energy of the electrostatic interactions between nucleus and electrons¹.

If one considers the action of the light on the atom, the Equation (2.1) remains still valid. However, the Hamilton operator \hat{H} will contain new terms which describe the action of the light on the unperturbed, free atom. In order to write the Hamilton operator for atom in the field of electromagnetic wave (in radiation gauge), one must replace the momentum of free electron \mathbf{p} to the momentum of electron in the electromagnetic field (Messiah 1990b)

$$\mathbf{p} \rightarrow \mathbf{p} - \frac{e\mathbf{A}}{c}. \quad (2.3)$$

Performing the latter substitution in the operator H_{DC} (2.2), one receives the Hamilton operator \hat{H} for the atom in the external field of electromagnetic waves

$$\hat{H} = \sum_{i=1}^N \left\{ c \boldsymbol{\alpha}(i) \left(\mathbf{p}_i - \frac{\mathbf{A}(\mathbf{r}_i, t)}{c} \right) + [\beta(i) - 1]c^2 - \frac{Z}{r_i} \right\} + \sum_{i,j}^N \frac{1}{r_{ij}}. \quad (2.4)$$

Certainly, a solution of Equation (2.1) with the Dirac Hamilton operator (2.4) can be obtained only by means of *approximation* methods.

One can distinguish between *perturbative* and *non-perturbative* approximation methods. Non-perturbative methods do not accept any assumption about strength of external and internal fields acting upon and in the atom. Absence of such assumption makes non-perturbative methods more general than perturbative methods. However, the non-perturbative methods require much larger computational effort and, as consequence, they have been developed only for non-relativistic atomic systems with one or two active electrons (Lambropoulos *et al* 1998).

The aim of this work is to study two-photon ionization in heavy atomic systems like inner-shells of atoms and ions. Study of inner-shell processes requires, in general, a relativistic theory. Additionally, the strength of modern light sources in UV and X-ray ranges is much lower than the strength of internal field in the inner-shell. Therefore, later on I will consider only the perturbative approach to deal with Equation (2.1).

The perturbation theory assumes that the Hamilton operator \hat{H} can be separated in two parts: unperturbed operator \hat{H}_0 and a small perturbation \hat{H}'

$$\hat{H} = \hat{H}_0 + \hat{H}'. \quad (2.5)$$

¹The fundamental problem of the relativistic Hamilton operator (2.2) is what is known as "Brown-Ravenhall disease". The many-body Hamilton operator (2.2) has no bound (normalizable) eigen-states (Brown and Ravenhall 1951). This disease is cured by Dirac's suggestion that all negative single-particle continuum states are occupied by electrons. Hence, if one excludes (project out) all negative states, then the Hamilton operator (2.2) describes the bound states of the atom (Grant 1988).

For instance, one can separate the Hamilton operator (2.4) of the atom in the external field of an electromagnetic wave in two parts: Hamilton operator of the free atom $\hat{H}_0 = \hat{H}_{DC}$ (2.2) and a perturbation $\hat{H}'(t)$ due to the external field (Karazija 1996, page 58)

$$\hat{H}'(t) = - \sum_{i=1}^N \alpha(i) \mathbf{A}(\mathbf{r}_i, t). \quad (2.6)$$

Due to perturbation theory, one uses the solutions $\Psi_n(t)$ of Equation (2.1) with the unperturbed Hamilton operator $\hat{H} = \hat{H}_0 = \hat{H}_{DC}$ (2.2)

$$\hat{H}_0 \Psi_n(t) = i \frac{\partial}{\partial t} \Psi_n(t) \quad (2.7)$$

as a basis set to build the solution Ψ of Equation (2.1) with the perturbed Hamilton operator $\hat{H} = \hat{H}_0 + \hat{H}'(t)$

$$\Psi = \sum_n c_n(t) \Psi_n(t). \quad (2.8)$$

The Hamilton operator of unperturbed atom $\hat{H}_0 = \hat{H}_{DC}$ (2.2) does not depend on time. Therefore, the solution $\Psi_n(t)$ of unperturbed atom is separable into a time-dependent and a time-independent parts

$$\Psi_n(t) \equiv \Psi_n = e^{iE_n t} \psi_n(\mathbf{r}), \quad (2.9)$$

where E_n is the eigen-energy and vector \mathbf{r} represents all $3N$ spatial coordinates of N electrons and the eigen-solution $\psi_n(\mathbf{r})$ does not depend on time

$$\hat{H}_0 \psi_n(\mathbf{r}) = E_n \psi_n(\mathbf{r}). \quad (2.10)$$

If one inserts the ansatz (2.8) into Equation (2.1) then one obtains a system of differential equations for coefficients $c_n(t)$

$$\sum_n c_n(t) \int d\mathbf{r} \Psi_m^\dagger \hat{H}'(t) \Psi_n = i \frac{\partial}{\partial t} c_m(t). \quad (2.11)$$

which is still equivalent to the initial Equation (2.1). It means that the solution of the latter equation is also a tedious task. In order to obtain an approximate and hence a simpler solution, the perturbation theory accepts an *iterative procedure* to evaluate the coefficients $c_m(t)$. Namely, it assumes, the system initially being in the state Ψ_i and chooses the coefficient $c_m(t)$ in form

$$c_m(t) = \delta_{mi} + c_{mi}^{(1)}(t). \quad (2.12)$$

Inserting this form back into Equation (2.11), one receives

$$\sum_n (\delta_{ni} + c_{ni}^{(1)}(t)) \int d\mathbf{r} \Psi_m^\dagger \hat{H}'(t) \Psi_n = i \frac{\partial}{\partial t} c_{mi}^{(1)}(t). \quad (2.13)$$

One can neglect the $c_{mi}^{(1)}(t)$ on the left hand side, if perturbation $\int d\mathbf{r} \Psi_m \hat{H}'(t) \Psi_n$ is weak. Such neglect allows to express a *first-order correction* $c_{mi}^{(1)}(t)$

$$c_{mi}^{(1)}(t) = \frac{1}{i} \int_0^t dt' \int d\mathbf{r} \Psi_m^\dagger \hat{H}'(t') \Psi_i. \quad (2.14)$$

The first-order correction $c_{mi}^{(1)}$ is sufficient in many applications. For instance, one can calculate the probability to find the system in a final state Ψ_f

$$w(t) = |\langle \Psi_f | \Psi \rangle|^2 = |c_{fi}^{(1)}(t)|^2. \quad (2.15)$$

and hereunder study the *one-photon* excitation or ionization.

As I mentioned in Introduction, the two-photon processes naturally appear in the perturbation theory of *second-order*. Therefore, I will perform a second iteration in solving of the system (2.11). Namely, one adds a *second-order correction* $c_{mi}^{(2)}(t)$ in the Equation (2.12)

$$c_m(t) = \delta_{mi} + c_{mi}^{(1)}(t) + c_{mi}^{(2)}(t). \quad (2.16)$$

One can insert this formula back into Equation (2.11) and, taking into account the approximation (2.14) for first-order correction, obtain the second-order correction $c_{mi}^{(2)}(t)$

$$c_{mi}^{(2)}(t) = \frac{1}{i^2} \sum_{\nu}^{\int} \int_0^t dt'' \int d\mathbf{r}'' \Psi_m^\dagger \hat{H}'(t'') \Psi_\nu \cdot \int_0^{t''} dt' \int d\mathbf{r}' \Psi_\nu^\dagger \hat{H}'(t') \Psi_i, \quad (2.17)$$

where notation \sum_{ν}^{\int} represents a *sum over whole spectrum* of the unperturbed Hamilton operator H_0 , i. e. a sum over discrete spectrum plus an integral over continuum spectrum.

Now, having the approximate solution Ψ (2.8) with coefficients given by Equations (2.14) and (2.17), one can derive the ionization rate in the second-order perturbation theory

$$\left. \frac{dw}{t} \right|_{t \rightarrow \infty} = \lim_{t \rightarrow \infty} \frac{d|\langle \Psi_f | \Psi \rangle|^2}{t} = \lim_{t \rightarrow \infty} \frac{d|c_{fi}^{(1)}(t) + c_{fi}^{(2)}(t)|^2}{t}. \quad (2.18)$$

I will calculate coefficients $c_{fi}^{(1)}(t)$ and $c_{fi}^{(2)}(t)$ for a perturbation when a monochromatic plane wave acts on the atom.

The vector potential of the plane wave reads

$$\mathbf{A} = A_0 \mathbf{u}_\lambda (e^{i(E_\gamma t - \mathbf{k}\mathbf{r})} + e^{-i(E_\gamma t - \mathbf{k}\mathbf{r})}), \quad (2.19)$$

where A_0 , \mathbf{u}_λ , E_γ and \mathbf{k} are amplitude, polarization vector, frequency and wave vector.

If one inserts Equations (2.19) and (2.9) into Equation (2.14) and takes into account only the ionization process (when $E_f > E_i$), then one can obtain for $c_{fi}^{(1)}(t)$ (Messiah 1990a)

$$c_{fi}^{(1)}(t) = A_0 \frac{1 - e^{it(E_f - E_\gamma - E_i)}}{E_f - E_\gamma - E_i} \langle \psi_f | \hat{O} | \psi_i \rangle, \quad (2.20)$$

where the *first-order matrix element* $M_1^{fi} \equiv \langle \psi_f | \hat{O} | \psi_i \rangle$ is time-independent

$$M_1^{fi} = \langle \psi_f | \hat{O} | \psi_i \rangle = \int d\mathbf{r} \psi_f^\dagger(\mathbf{r}) \sum_{i=1}^N \boldsymbol{\alpha} \mathbf{u}_\lambda e^{i\mathbf{k}\mathbf{r}_i} \psi_i(\mathbf{r}). \quad (2.21)$$

Analogously, inserting vector potential \mathbf{A} (2.19) and solution Ψ_n (2.9) into Equation (2.17), I obtain for second-order correction $c_{fi}^{(2)}(t)$

$$c_{fi}^{(2)}(t) = A_0^2 \frac{1 - e^{it(E_f - 2E_\gamma - E_i)}}{E_f - 2E_\gamma - E_i} M_2^{fi} \quad (2.22)$$

with a time-independent *second-order matrix element* M_2^{fi}

$$M_2^{fi} = \sum_{\nu}^f \frac{\langle \psi_f | \hat{O} | \psi_\nu \rangle \langle \psi_\nu | \hat{O} | \psi_i \rangle}{E_\nu - E_i - E_\gamma}. \quad (2.23)$$

The limit $\lim_{t \rightarrow \infty}$ in transition rate (2.18) can be calculated taking into account a relation for the Dirac δ -function

$$\lim_{t \rightarrow \infty} \frac{1}{t} \left| \frac{1 - e^{it\omega}}{\omega} \right|^2 = 2\pi \delta(\omega). \quad (2.24)$$

This relation allows to represent the transition rate (2.18) as a sum of the one-photon and two-photon rates. I insert the Equations (2.20) and (2.22) into Equation (2.18) and, taking into account property (2.24), obtain

$$\frac{dw}{t} \Big|_{t \rightarrow \infty} = 2\pi \delta(E_f - E_i - E_\gamma) A_0^2 |M_1^{fi}|^2 + 2\pi \delta(E_f - E_i - 2E_\gamma) A_0^4 |M_2^{fi}|^2. \quad (2.25)$$

If one fixes the initial energy E_i and photon energy E_γ , then δ -functions in the latter equation represent the density of final states. It tells namely that there are two allowed energies of final states: $E_f = E_i + E_\gamma$ and $E_f = E_i + 2E_\gamma$, i. e. such δ -like density interpretes the first and the second-order matrix elements M_1^{fi} and M_2^{fi} as amplitudes of one- and two-photon ionization correspondingly.

The generalization of rate Equation (2.25) on the n -photon case can now be guessed easily. Moreover, one can integrate over the energy spectrum of final states and write the transition rate $\frac{w}{t}$ in form of power series over the photon flux $F = A_0^2 E_\gamma / (2\pi c)$ (McGuire 1981)

$$\frac{w}{t} = \sum_{n=1}^{\infty} \sigma_n F^n. \quad (2.26)$$

The n -photon cross section σ_n relates to the n -th order amplitude M_n^{fi}

$$\sigma_n = \frac{8\pi^3}{E_\gamma^n} |M_n^{fi}|^2, \quad (2.27)$$

where n -th order amplitude M_n^{fi} can be obtained in the perturbation theory of n -th order and expressed with $(n-1)$ -fold summation over the whole spectrum (Lambropoulos *et al* 1998)

$$M_n^{fi} = \sum_{j_0}^f \dots \sum_{j_\xi}^f \sum_{j_\nu}^f \frac{\langle \psi_f | \hat{O} | \psi_o \rangle}{E_o - E_i - (n-1)E_\gamma} \dots \frac{\langle \psi_\xi | \hat{O} | \psi_\nu \rangle}{E_\xi - E_i - 2E_\gamma} \frac{\langle \psi_\nu | \hat{O} | \psi_i \rangle}{E_\nu - E_i - E_\gamma}. \quad (2.28)$$

In this work I am mainly interested in the two-photon ionization, i. e. the second-order amplitude M_2^{fi} (2.23) will be calculated. The second-order amplitude M_2^{fi} (2.23) is more difficult to calculate than the first-order amplitude M_1^{fi} (2.21). The difficulty arises mainly because of the continuum part of spectrum. The conventional integration over atomic continuum is difficult to prepare, even in the simplest case of hydrogen atom. At the same time, the neglect of continuum brings about gross mistakes and is generally impossible in any accurate calculation. However, there are few methods exist which allow an accurate calculation of the second-order amplitude. In the following, I will discuss two of them: *differential equation method* and *Green's function method*. Moreover, in order to demonstrate the need of integration over continuum part, I firstly discuss a *direct summation method* which takes into account only discrete part of atomic spectrum.

2.2 Direct summation method

The direct summation method leaves out the integration over continuum in the n -th-order matrix element M_n^{fi} (2.28), although the integral over continuum part has basically as large magnitude as the magnitude of the discrete sum. Moreover, the magnitude and sign of continuum part depends on the energy $E_i + n E_\gamma$ and differs, in general, to the magnitude and sign of the discrete part. Therefore, the direct summation only over discrete spectrum leads, as a rule, to serious errors which depend on the photon energy.

In order to clarify these points, I compare two calculations of second-order matrix element: one takes the continuum part into account, another lets it out.

I calculate two-photon total cross section σ_2 for hydrogen atom in ground state²

$$\sigma_2 = \frac{8\pi^3}{E_\gamma^2} |M_2^{fi}|^2, \quad (2.29)$$

where the second-order amplitude M_2^{fi} (2.23) reads explicitly

$$M_2^{fi} = \sum_\nu \frac{\langle \psi_f | \hat{O} | \psi_\nu \rangle \langle \psi_\nu | \hat{O} | \psi_i \rangle}{E_\nu - E_i - E_\gamma} + \int_E \frac{\langle \psi_f | \hat{O} | \psi_E \rangle \langle \psi_E | \hat{O} | \psi_i \rangle}{E - E_i - E_\gamma} dE. \quad (2.30)$$

Two methods will be compared: the direct summation only over the discrete spectrum and the Green's function method. In the Green's function method, the integral over continuum part is taken *implicitly* into account. The comparison will show the need of continuum part as well as conditions when continuum part can be nevertheless neglected.

Two-photon ionization *dominates* over all other ionization processes when the photon energy lies below threshold energy E_T and above half threshold energy

$$E_T/2 < E_\gamma < E_T. \quad (2.31)$$

²In this formula, the initial and final states are defined by its energy. Since the initial and final states can be degenerated, one must perform the summation over final and an average over the initial states. An example for such summation and average can be seen in Equation (3.10).

In this *dominant range*, the one-photon ionization is forbidden by energy conservation law. Higher-order ionization processes are allowed, but have much smaller influence on the electronic yield and can be neglected. Thus, the cross section (2.29) will be plotted in the dominant range.

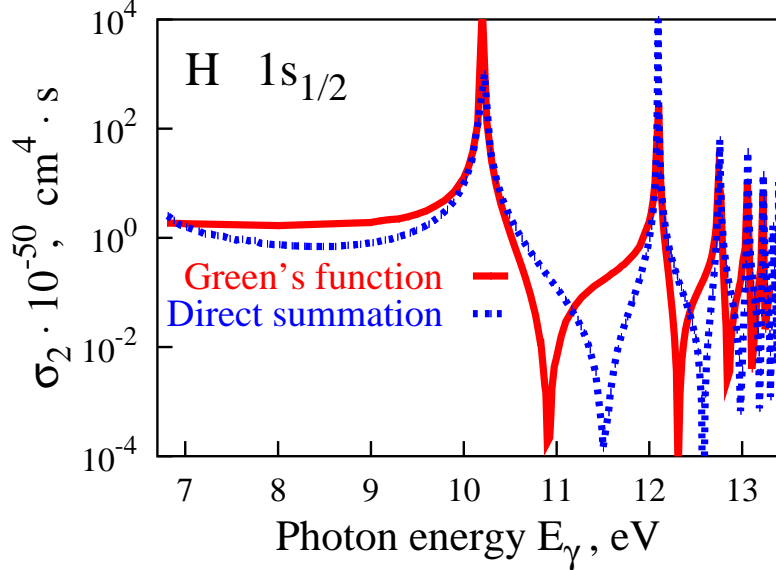


Figure 2.2: Two-photon total cross section σ_2^{circ} for hydrogen vs photon energy. Direct summation and Green's function methods are compared. One can see that the methods agree only nearby the resonances.

Figure 2.2 shows the total cross section σ_2 which is calculated in the *long-wavelength approximation* (see Equation 3.13), for circular polarized light. Cross section is plotted against photon energy E_γ in the dominant range (2.31). One can see that the cross section has a *non-resonance* range in the first half of the dominant range, and *resonances* and *anti-resonances* in the second half. The resonance structure is determined by denominator in second-order amplitude (2.23). Denominator $E_\nu - E_i - E_\gamma$ turns to zero when the energy $E_i + E_\gamma$ is equal to a bound state energy E_ν . Hence, in the vicinity of resonance with the bound state ν , the ν -th summand becomes much larger than other summands in discrete spectrum as well as the integral over continuum spectrum. Thus, *in the vicinity of resonance, the Green's function method gives at limit the same cross section as direct summation method.*

However, when the photon energy lies far off a resonance, the interference in the discrete sum and in the continuum integral leads to large discrepancies in two-photon cross section. The Green's function method produces a flat behaviour in the non-resonance range, while the direct summation forms a valley. The difference between two methods reaches a factor of 3 and even more in the non-resonance region. In the resonance domain, the discrepancy is much larger. In the resonance range, the magnitude and sign of summands depends on the photon energy. Namely, the sign of ν -th term changes to the opposite when the photon energy E_γ transits from range before ν -th resonance $E_\gamma < E_\nu - E_i$ to a nearby range $E_\gamma > E_\nu - E_i$. These changes of magnitude and sign produce *anti-resonances*. Second-order amplitude M_2^{fi} has a zero value on the anti-resonance. Both direct summation and Green's function methods show the anti-resonances. However, the positions of anti-resonances are different because of the continuum part. This position difference leads to the *large* (in electric dipole approximation

infinite) disagreement between direct summation and Green's function methods.

One can see now the importance of integration over continuum spectrum in calculation of second-order amplitude. The same point applies certainly also to the n -th-order amplitude (2.28). In fact, this importance had been recognized long time ago when very first calculations of n -th-order amplitude by Zernik (1964) and Bebb and Gold (1966) appeared.

Since the pioneer works by Schwartz (1959) and Schwartz and Tieman (1959), there were few methods invented to evaluate the n -th-order amplitude accurately, taking into account the integration over continuum spectrum. In the following, I will discuss two of them: *differential equation method* and *Green's function method*. Both methods allow to evaluate the perturbative sum in n -th order matrix element implicitly, solving an inhomogeneous equation.

2.3 Differential equation method

The differential equation method has been invented by Schwartz and Tieman (1959) and applied by Zernik (1964) to the two-photon ionization of the metastable $2s$ -state of hydrogen atom. This technique has been used later in many calculations for multi-photon ionization for hydrogen atom (Gontier and Trachin 1968, and Karule 1977) and two-photon ionization of helium atom (Victor 1967, Ritchie 1977, and Aymar and Crance 1980). The insight of differential equation method was well explained by Xingdong and Crasemann (1988).

In order to evaluate the second-order amplitude (2.23), one defines a function

$$F_E = \sum_{\nu}^f \frac{|\psi_{\nu}\rangle\langle\psi_{\nu}|\hat{O}|\psi_i\rangle}{E_{\nu} - E} \quad (2.32)$$

which represents an atomic transition through an *intermediate state* with energy E .

One uses the function $F_E(\mathbf{r})$ and rewrite the second-order amplitude M_2^{fi} in a form which is similar to the conventional first-order matrix element M_1^{fi}

$$M_2^{fi} = \langle\psi_f|\hat{O}|F_{E_i+E_{\gamma}}\rangle. \quad (2.33)$$

The trick is now to calculate the function $F_E(\mathbf{r})$ not directly by Formula (2.32) but to find a *differential equation* to which the function $F_E(\mathbf{r})$ satisfies and use a solution of this equation in calculation of the second-order amplitude M_2^{fi} (2.33).

In order to find the differential equation for the function $F_E(\mathbf{r})$, one can build an operator $(\hat{H}_0 - E)$ with Hamilton operator \hat{H}_0 for unperturbed atom

$$\hat{H}_0 \psi_{\nu} = E_{\nu} \psi_{\nu}. \quad (2.34)$$

One acts with this operator on the function $F_E(\mathbf{r})$ and herewith obtains

$$(\hat{H}_0 - E) F_E = \sum_{\nu}^f \frac{|\hat{H}_0 - E|\psi_{\nu}\rangle\langle\psi_{\nu}|\hat{O}|\psi_i\rangle}{E_{\nu} - E} = \sum_{\nu}^f |\psi_{\nu}\rangle\langle\psi_{\nu}|\hat{O}|\psi_i\rangle. \quad (2.35)$$

Hence, using a closure relation for the eigen-solutions $\psi_{\nu}(\mathbf{r})$

$$\sum_{\nu}^f |\psi_{\nu}\rangle\langle\psi_{\nu}| = \delta(\mathbf{r} - \mathbf{r}'), \quad (2.36)$$

one finds the sought differential equation

$$(\hat{H}_0 - E) F_E(\mathbf{r}) = \hat{O} |\psi_i\rangle. \quad (2.37)$$

Solution of this equation can be found in analytic form (Zernik 1964) for hydrogen atom with Schrödinger Hamilton operator \hat{H}_0 and a electric dipole transition operator $\hat{O} = \varepsilon \mathbf{r}$. For more complex model of atom, a numerical method can be applied (Victor 1967, Ritchie 1977, and Aymar and Crance 1980).

2.4 Green's function method

The basic idea of the Green's function method is similar to the idea of the differential equation method. However, instead to introduce the function $F_E(\mathbf{r})$ by Equation (2.32), one brings in a—more general—Green's function $G_E(\mathbf{r}, \mathbf{r}')$

$$G_E = \sum_{\nu}^f \frac{|\psi_{\nu}\rangle\langle\psi_{\nu}|}{E_{\nu} - E} \quad (2.38)$$

and rewrites the second-order amplitude M_2^{fi} in form of a two-dimensioned integral, when compare with first-order matrix element M_1^{fi} .

$$M_2^{fi} = \int d\mathbf{r} d\mathbf{r}' \psi_f^{\dagger}(\mathbf{r}) \hat{O} G_{E_i+E_{\gamma}}(\mathbf{r}, \mathbf{r}') \hat{O} \psi_i(\mathbf{r}') \equiv \langle\psi_f | \hat{O} | G_{E_i+E_{\gamma}} | \hat{O} | \psi_i\rangle. \quad (2.39)$$

The calculation of the Green's function $G_E(\mathbf{r}, \mathbf{r}')$ proceeds by solving a *defining differential equation* for Green's function. One can obtain this equation analogously to the differential equation method. Acting with operator $(H_0 - E)$ on the Green's function, one obtains

$$(\hat{H}_0 - E) G_E = \sum_{\nu}^f \frac{|\hat{H}_0 - E | \psi_{\nu}\rangle\langle\psi_{\nu}|}{E_{\nu} - E} = \sum_{\nu}^f |\psi_{\nu}\rangle\langle\psi_{\nu}|. \quad (2.40)$$

Further on, taking into account the closure relation for eigen-states (2.36), one obtains an inhomogeneous differential equation for the Green's function

$$(\hat{H}_0 - E) G_E(\mathbf{r}, \mathbf{r}') = \delta(\mathbf{r} - \mathbf{r}'). \quad (2.41)$$

The Green's function $G_E(\mathbf{r}, \mathbf{r}')$ for pure Coulomb field is well known analytically, both for the Schrödinger and Dirac Hamilton operator \hat{H}_0 . If one considers a more complex atomic system, the Equation (2.41) can be solved numerically. Although it is more cumbersome to deal with the two times more dimensioned Green's function $G_E(\mathbf{r}, \mathbf{r}')$ than with function $F(\mathbf{r})$, the Green's function method has been often utilized in study of few-photon ionization/excitation and two-photon decay processes (Maquet *et al* 1998).

In Chapter 3, the relativistic and multipole effects in two-photon ionization will be studied on example of heavy hydrogen-like ions. I will use the Green's function method with an analytical solution for Dirac-Coulomb Green's function. Further on in Chapter 4, I describe a relativistic *central-field* Green's function and present a numerical method to evaluate its radial part. This Dirac-central-field Green's function will be utilized in a study of the many-electron effects in the two-photon ionization of inner-shells of argon, helium and helium-like neon.

Chapter 3

Relativistic and multipole effects in two-photon ionization

Inner-shell electrons have the largest binding energy amongst other electrons in atom. One may expect, therefore, that the *relativistic effects* become important in the processes involving the inner-shell electrons and investigate these *fundamental effects* before any discussion of the many-electron effects. In this chapter, I will study the *relativistic and multipole* effects in the two-photon ionization. In order to keep these effects separately from the many-particle effects, I investigate the simplest atomic systems: a hydrogenic atom and heavy hydrogen-like ions.

The hydrogenic atom consists of a charged nucleus (proton, deuteron or triton) around which a *single electron* moves. The simplest protonic nucleus is about 1836 times as heavy as the electron, so one can treat the motion of the electron as a motion of a light charged particle in the pure *Coulomb field* created by a static point nucleus.

Although hydrogen is the simplest atom, it can demonstrate such *general features* of two-photon processes as *two-photon selection rules*, a *resonance structure* and a dependence of electron yield on the polarization of incident radiation.

Any selection rule is a consequence of a conservation law. For instance, the conservation of angular momentum results in a restriction on the possible pairs of initial and final states (Messia 1990a, and Landau and Lifshitz 1986). Namely, in a one-photon process the electric dipole transitions take place only between states whose angular momentum differs by unity

$$\Delta l = \pm 1. \tag{3.1}$$

The two-photon transitions obey another selection rules, since there are two photons whose angular momenta appear in the conservation law. Namely, in a two-photon process, the electric dipole transitions take place only between states whose angular momentum does either not differ or it differs by two (Göppert-Mayer 1931, and Zernik 1964)

$$\Delta l = 0, \pm 2. \tag{3.2}$$

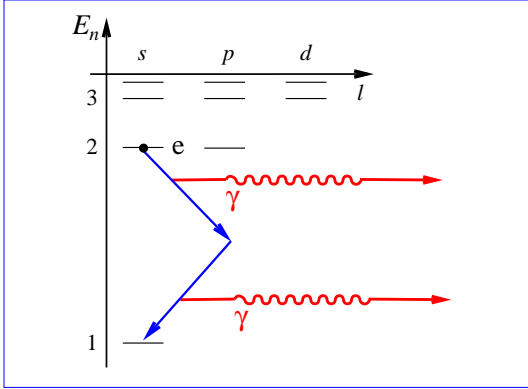


Figure 3.1: Electric dipole transitions in two-photon decay.

Inverted with respect to the two-photon decay, two-photon *excitation* occurs at the photon energy twice as low as the one-photon process would require. The electric dipole transitions allow already two channels and two final states which are unreachable in one-photon excitation. Moreover, the two-photon excitation depends strongly on the polarization of light since both electric dipole channels $s \rightarrow p \rightarrow d$ and $s \rightarrow p \rightarrow s$ are open in case of linearly polarized light, but only $s \rightarrow p \rightarrow d$ channel is open for circularly polarized light.

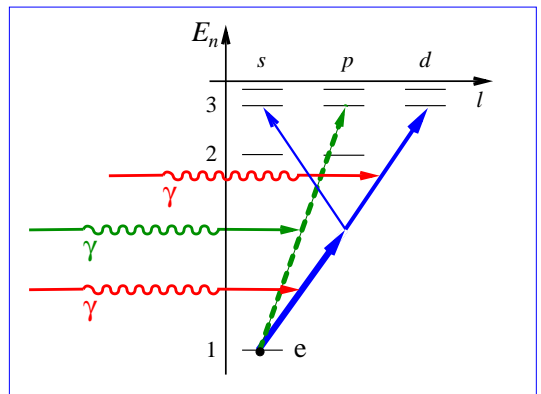


Figure 3.2: Electric dipole transitions in two-photon excitation.

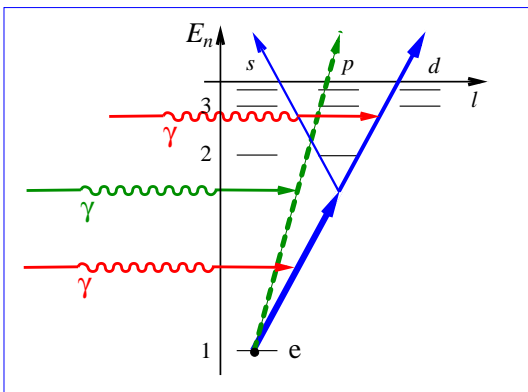


Figure 3.3: Electric dipole transitions in two-photon ionization.

hydrogen atom. Since our goal is to consider the relativistic and multipole effects in the inner-shells, it is better to look at *hydrogen-like ions*. The electron in hydrogen-like ions has a larger energy and must show the larger relativistic effects the heavier the nucleus is. Moreover, a hydrogen-like ion with an appropriate nuclear charge Z_{eff} can model quite well a K -shell of heavy atoms but still remains as simple as hydrogen in theoretical consideration.

Hydrogen-like ion resembles very much the hydrogen atom: it contains one electron and

One can demonstrate the electric dipole selection rules in the two-photon processes of decay, excitation and ionization.

In two-photon decay, one has to consider a single *electric dipole channel* $s \rightarrow p \rightarrow s$ only. Although the $2s$ metastable state of hydrogen can decay due to the one-photon *magnetic dipole* transition, the two-photon transition issues in a much more strong rate and dominates the decay process.

The two-photon ionization resembles the two-photon excitation. The only difference to the excitation is that, in the ionization process, one has no restriction on the angular momentum of the final state. It results in the infinite number of the allowed final states in case when *higher multipoles* are taken into account. Similar to the two-photon excitation, the two-photon ionization cross section depends on the photon energy (see Figure 2.2) and on the photon polarization (see Figure 3.6).

Thus, as one can see from the above discussion, many properties of two-photon processes (like two-photon selection rules, dependence on the photon energy and polarization) shown up already in the

a nucleus which is heavier than the hydrogenic nuclei. Amongst other properties of nucleus, its electrical charge Z has a major importance for the electron's motion. Although the heavy nucleus contains a large number of protons and neutrons, it is still very compact in comparison with the electron orbits. Therefore, the problem of the electron motion in hydrogen-like ions can be treated as the motion of electron in the Coulomb field of a static point electric charge.

The problem of the electron motion in the pure Coulomb field is one of the few problems in quantum mechanics which can be solved exact, with an *analytical* answer. The electron wave functions and Green's function for the Coulomb problem are well known analytically. Hence, the Dirac-Coulomb wave functions and Dirac-Coulomb Green's function (Swainson and Drake 1991a, 1991b, and Koval and Fritzsche 2003) will be used in calculation of the two-photon ionization cross sections.

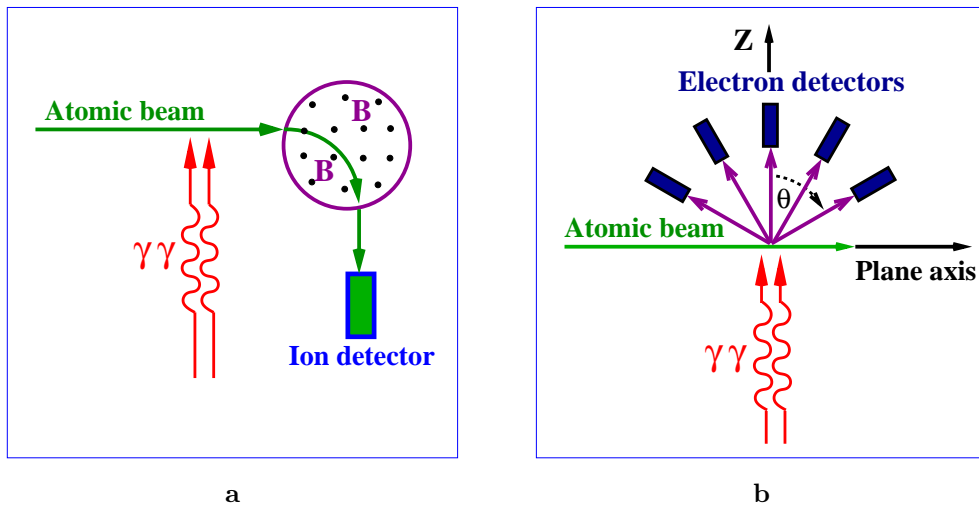


Figure 3.4: Detection of the ionization (a) by measurement of the ion yield and (b) by measurement of the electron yield. If one counts the number of produced ions, then one can measure only the *total cross section*. If one counts the number of electrons which move in certain direction, then one can measure both *differential* and total cross sections. The differential cross section provides surely the finer information on the ionization process.

In the following section, I will present the Dirac Hamilton operator for Coulomb field and shortly discuss the properties of its eigen-solutions. After this discussion, it will be easier to introduce the two-photon *total* and *differential* cross sections. These cross sections are appropriate in calculation of the total electron yield (Figure 3.4a) and the electron angular distribution (Figure 3.4b). The relativistic and multipole effects will be studied in Sections 3.2 and 3.3 for the total and differential cross sections, accordingly.

3.1 Differential and total cross sections for hydrogen-like ions

The total cross section of two-photon ionization is given by Equation (2.29). In order to apply this formula to the hydrogen-like ions, one can insert the well known Coulomb wave functions and Coulomb Green's function (Swainson and Drake 1991a, 1991b, and Koval and Fritzsche 2003) into this equation and perform summations over the (degenerated) initial and final states. In this section I go another way. I write the differential cross section $\frac{d\sigma_2}{d\Omega}$ and

then, by integrating it over the solid angle, I will arrive to the total cross section σ_2 .

The motion of the relativistic electrons in the heavy hydrogen-like ion can be described by Dirac Equation (2.1) with the Dirac's Hamilton operator

$$\hat{H}_D = \left\{ c \boldsymbol{\alpha} \mathbf{p} + [\beta - 1] c^2 - \frac{Z}{r} \right\}, \quad (3.3)$$

where $\boldsymbol{\alpha} = \{\alpha_x, \alpha_y, \alpha_z\}$ and β are Dirac matrices, $\mathbf{p} = -i\nabla$ is operator of electron momenta, Z is the nuclear charge and r is the distance from the nuclear charge. The solution of the Dirac Equation (2.1) with Hamilton operator \hat{H}_D (3.3) is well known (Swainson and Drake 1991a). The spectrum of eigen-solutions has a discrete "bound" and a continuum "free" parts.

The eigen-function $\psi_{n\kappa m}$ of a bound state depends on three (integer) quantum numbers (n, κ, m) while the eigen-energy of bound state $E_{n\kappa}$ depends only on the principal quantum number n and on the angular momentum number κ . The eigen-function $\psi_{E\kappa m}$ of a free state has a continuum energy spectrum. It means that the energy E of a free state takes any real positive value.

A bound state represents the electron moving nearby the nucleus, attracted by the nucleus field, while a free state represents the outgoing electron. I will use the bound eigen-functions $\psi_{n_i \kappa_i m_i}$ in order to describe the initial state ψ_i of the ion and the free eigen-functions $\psi_{E_f \kappa_f m_f}$ to describe the ionized electron of energy E_f .

The angular distribution of ionized electrons can be calculated if one knows the spatial momentum \mathbf{p}_f of ionized electron instead of the angular momentum κ_f and its projection m_f . The free state with a well defined asymptotic momentum \mathbf{p}_f and an electron spin projection m_s on the direction of Z -axis can be expanded into the wave functions in partial wave representation $\psi_{E_f \kappa_f m_f}$ (Eichler and Meyerhof 1995)

$$\psi_{\mathbf{p}_f m_s} = 4\pi \sum_{\kappa_f m_f} i^{l_f} e^{-i\Delta_{\kappa}} \langle l_f m_f - m_s, 1/2 m_s | j_f m_f \rangle Y_{l_f m_f - m_s}^*(\mathbf{p}_f) \psi_{E_f \kappa_f m_f}(\mathbf{r}), \quad (3.4)$$

where Δ_{κ_f} is the *Coulomb phase*, $\langle | \rangle$ denotes the Clebsch-Gordan coefficient, $l_f = l_f(\kappa)$ and $j_f = j_f(\kappa)$ denote the orbital and total angular momentum of the electron.

Inserting the final state with the well defined momentum (3.4) to the two-photon cross section (2.29) one can obtain the angular differential cross section $\frac{d\sigma_2}{d\Omega}$

$$\frac{d\sigma_2}{d\Omega} = \frac{\pi}{2\alpha^2 E_\gamma^2} \frac{1}{2j_i + 1} \sum_{m_s m_i} \left| M_2^{fi}(\mathbf{p}_f, \lambda) \right|^2. \quad (3.5)$$

The second-order amplitude $M_2^{fi}(\mathbf{p}_f, \lambda_2, \lambda_1)$ has the Coulomb wave functions $\psi_{n_i \kappa_i m_i}$ and $\psi_{\mathbf{p}_f m_s}$ as the initial and final states, accordingly

$$M_2^{fi}(\mathbf{p}_f, \lambda) = \langle \psi_{\mathbf{p}_f m_s} | \boldsymbol{\alpha} \mathbf{u}_\lambda e^{-i\mathbf{k}\mathbf{r}} | G_{E_{n_i \kappa_i} + E_\gamma} | \boldsymbol{\alpha} \mathbf{u}_\lambda e^{-i\mathbf{k}\mathbf{r}'} | \psi_{n_i \kappa_i m_i} \rangle, \quad (3.6)$$

where G_E is a Dirac-Coulomb Green's function (Swainson and Drake 1991b, and Drake 1996).

Since the initial states are distinguished only by their energy $E_i = E_{n_i \kappa_i}$ and the final states only by their spatial momenta \mathbf{p}_f , one averages the cross sections over the magnetic quantum number m_i and sums over all possible spin states of the final state $m_s = \pm 1/2$ in Equation

(3.5). The unit polarization vector \mathbf{u}_λ can describe either a circularly [$\mathbf{u}_{\pm 1} = (\mathbf{x} \pm i\mathbf{y})/\sqrt{2}$] or a linearly [$\mathbf{u}_3 \equiv \mathbf{x} = (\mathbf{u}_{+1} + \mathbf{u}_{-1})/\sqrt{2}$] polarized beams; \mathbf{k} is the photon wave vector.

The total cross section σ_2 can be obtained from the Equation (3.5) by integrating it over the solid angle $d\Omega = \sin\theta d\theta d\varphi$. Hence, the total cross section σ_2 reads

$$\begin{aligned} \sigma_2 &= \int d\Omega \frac{d\sigma_2}{d\Omega} = \sum_{m_s m_i} \frac{\pi}{2\alpha^2 E_\gamma^2} \frac{1}{2j_i + 1} \times \\ &\times \int d\Omega \sum_{\kappa_f m_f} \sum_{\kappa'_f m'_f} 4\pi i^{-l_f} e^{i\Delta_{\kappa_f}} \langle l_f m_f - m_s, 1/2 m_s | j_f m_f \rangle Y_{l_f m_f - m_s}(\mathbf{p}_f) \times \\ &\times 4\pi i^{l'_f} e^{-i\Delta_{\kappa'_f}} \langle l'_f m'_f - m_s, 1/2 m_s | j'_f m'_f \rangle Y_{l'_f m'_f - m_s}^*(\mathbf{p}_f) M_2^{fi*}(\lambda) M_2^{f'i}(\lambda), \end{aligned} \quad (3.7)$$

where the second-order amplitude $M_2^{fi}(\lambda)$ with the final state $\psi_{E_f \kappa_f m_f}$ is defined to

$$M_2^{fi}(\lambda) = \langle \psi_{E_f \kappa_f m_f} | \boldsymbol{\alpha} \mathbf{u}_\lambda e^{-i\mathbf{k}\mathbf{r}} | G_{E_{n_i \kappa_i} + E_\gamma} | \boldsymbol{\alpha} \mathbf{u}_\lambda e^{-i\mathbf{k}\mathbf{r}'} | \psi_{n_i \kappa_i m_i} \rangle. \quad (3.8)$$

If one takes into account the orthogonality of the spherical harmonics $Y_{lm}(\mathbf{p}_f)$ and a summation property of the Clebsch-Gordan coefficients (Varshalovich *et al* 1989)

$$\sum_{m_l m_s} \langle l m_l, 1/2 m_s | j m \rangle \langle l m_l, 1/2 m_s | j' m' \rangle = \delta_{j j'} \delta_{m m'}, \quad (3.9)$$

one obtains the two-photon total cross section

$$\sigma_2 = \frac{8\pi^3}{\alpha^2 E_\gamma^2} \sum_{\kappa_f m_f} \frac{1}{2j_i + 1} \sum_{m_i} |M_2^{fi}(\lambda)|^2. \quad (3.10)$$

3.2 Total ionization cross section for heavy hydrogen-like ions

The total cross section σ_2 for hydrogen-like ions depends on the nuclear charge Z , on the photon energy E_γ and on the polarization of the light λ . In the following subsection, I will discuss the dependence on the photon energy $\sigma_2(E_\gamma)$ and on the photon polarization while, the dependence on the nuclear charge Z will be discussed later, in Subsection 3.2.4.

The basic features of the total cross section σ_2 include *resonances*, *anti-resonances*, and a behavior of the *polarization ratio* $R = \sigma_2^{\text{circ}}/\sigma_2^{\text{lin}}$. These features will be discussed for hydrogen atom while relativistic effects are shown for heavy hydrogen-like ions.

3.2.1 Basic features of the total cross section

The two-photon total cross section σ_2 of the hydrogenic atom depends on the photon energy E_γ on a more complex way than the one-photon cross section does. The one-photon cross section decreases regularly when the photon energy increases (Amusia 1990) and does not depend on the polarization of light. In contrary, the two-photon cross section (3.10) strongly depends on the polarization of the light and possesses maxima (resonances) and minima (see Figure 2.2).

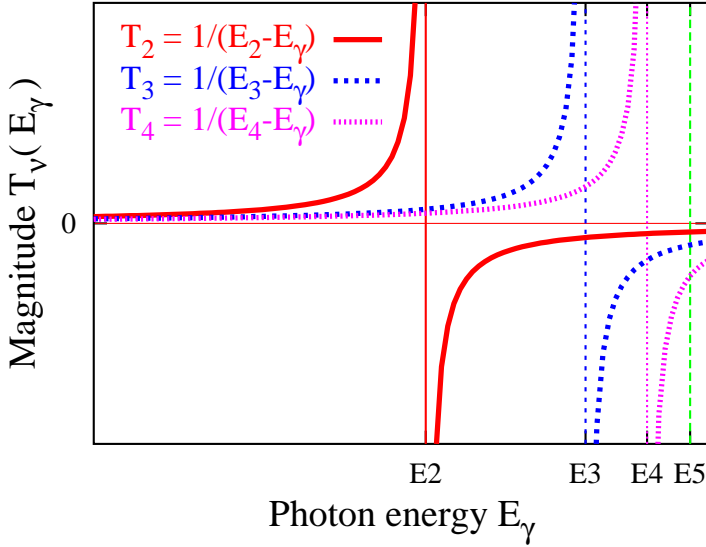


Figure 3.5: Dependence of the terms in two-photon amplitude $M_2^{fi} = \sum_{\nu} T_{\nu}$ on the photon energy E_{γ} . The magnitude of a ν -th term changes in the infinite limits when the photon energy passes a resonance energy $E_{\nu} - E_i$.

its magnitude in infinite limits when the photon energy E_{γ} passes a resonance energy $E_{\nu} - E_i$ while the other terms behave regularly (see Figure 3.5). Hence, at a certain photon energy the second-order amplitude M_2^{fi} becomes zero¹.

If the ionizing radiation is linearly polarized, then two-photon cross section σ_2^{lin} (see Figure 3.6) does not have the anti-resonances. This circumstance can be explained if one considers the selection rules in the two-photon ionization.

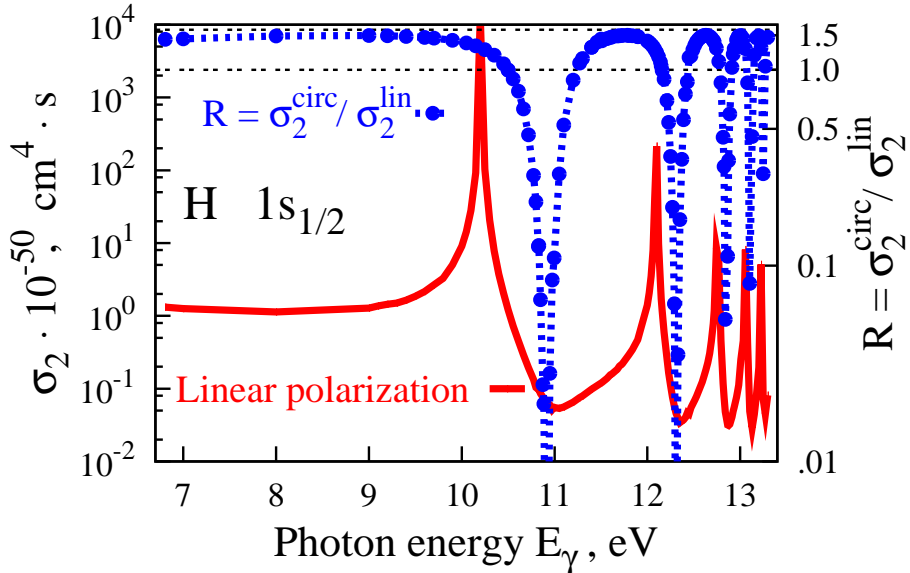


Figure 3.6: Two-photon total cross section σ_2 for linearly polarized incident radiation and polarization ratio $R = \sigma_2^{\text{circ}}/\sigma_2^{\text{lin}}$ versus photon energy E_{γ} for hydrogen atom in ground state.

¹The name "anti-resonance" can be easily understood if one looks at the dependence $\sigma = \sigma(E_{\gamma})$ on the logarithmic scale (see Figure 2.2): zeros lay infinitely deep and look like inverted resonances.

The electric dipole selection rules result in two possible *electric dipole channels*: $s \rightarrow p \rightarrow d$ and $s \rightarrow p \rightarrow s$ for two-photon ionization of $1s$ initial state (see Figure 3.3). In case of circularly polarized light, however, the $s \rightarrow p \rightarrow s$ channel is closed due to the conservation of the projection of angular momentum: two equally polarized photons must change the angular momentum projection m by ± 2 , while the difference between momentum projections for $s \rightarrow p \rightarrow s$ channel does not exceed unity. Hence, the second-order amplitude $s \rightarrow p \rightarrow d$ determines the behavior of the two-photon cross section when the radiation is circularly polarized. Namely, if the second-order amplitude of the $s \rightarrow p \rightarrow d$ channel vanishes, then the cross section σ_2^{circ} becomes necessarily zero. In contrary, in case of linearly polarized radiation, the $s \rightarrow p \rightarrow s$ channel remains open, and the two-photon cross section, according to Equation (3.10), can be written as a sum of two terms

$$\sigma_2^{\text{lin}} = \left| M_2^{fi}(s \rightarrow p \rightarrow s) \right|^2 + \left| M_2^{fi}(s \rightarrow p \rightarrow d) \right|^2. \quad (3.11)$$

Although, both terms vanish when the photon energy takes a designated value, this photon energy differs for different channels and the cross section σ_2^{lin} remains non-zero at any photon energy. The polarization dependence of the two-photon cross section can be represented in a form of the *polarization ratio* $R = \sigma_2^{\text{circ}} / \sigma_2^{\text{lin}}$. In the non-relativistic case of hydrogen atom, the polarization ratio does not exceed a factor of 1.5 and has infinite dips which are placed between resonances. These dips correspond, obviously, to the anti-resonances.

3.2.2 Relativistic effects

The features of the two-photon ionization of hydrogen atom, which were discussed in the previous subsection, are characteristic also for all hydrogen-like ions. The relativistic effects, in contrary, come into play when the nuclear charge becomes larger. For instance, a well known relativistic effect of the level splitting due to the spin-orbit interaction reveal itself in a splitting of two-photon resonances. The p levels of hydrogen-like ion consist of two sublevels. For instance, the $2p$ level is split on $2p_{1/2}$ and $2p_{3/2}$ sublevels which possess different energies. This energy difference leads to the doubling of each two-photon resonance.

The energy splitting between the $2p_{1/2}$ and $2p_{3/2}$ sublevels depends on the square of the nuclear charge Z^2 . It is very small for the hydrogen atom

$$(E_{2p_{1/2}} - E_{2p_{3/2}}) / E_{1s_{1/2}} < \mathbf{3.4 \cdot 10^{-6}}, \text{ for } Z = 1,$$

but becomes comparable with threshold energy $|E_{1s_{1/2}}|$ for the hydrogen-like uranium

$$(E_{2p_{1/2}} - E_{2p_{3/2}}) / E_{1s_{1/2}} \approx \mathbf{3.5 \cdot 10^{-2}}, \text{ for } Z = 92.$$

The splitting of the p -levels dominates the relativistic resonance behavior of the two-photon cross section which can be seen most clearly for the hydrogen-like uranium (Figure 3.7).

Since the spin-orbit interaction leads to a splitting of possible angular momentum channels the second-order amplitude M_2^{fi} can be separated in the two terms

$$M_2^{fi} = M_2^{fi}(i \rightarrow p_{1/2} \rightarrow f) + M_2^{fi}(i \rightarrow p_{3/2} \rightarrow f), \quad (3.12)$$

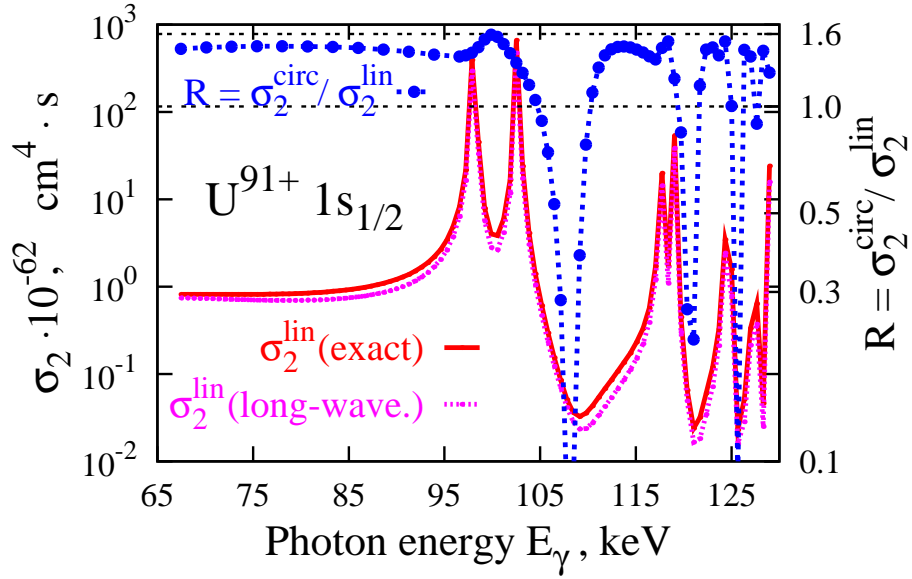


Figure 3.7: Two-photon total cross section σ_2^{lin} versus photon energy E_γ for hydrogen-like uranium U^{91+} ion in ground state. An *exact relativistic* and *long-wavelength* multipole approximations are presented (see Subsection 3.2.3). Polarization ratio $R = \sigma_2^{\text{circ}}/\sigma_2^{\text{lin}}$ is presented for the exact relativistic formulation.

each of which has $p_{1/2}$ or $p_{3/2}$ symmetry in the intermediate states. The resonance energies $E_\gamma(np_{1/2})$ and $E_\gamma(np_{3/2})$ corresponding to the $p_{1/2}$ and $p_{3/2}$ intermediate states

$$E_\gamma(np_{1/2}) = E_{np_{1/2}} - E_{1s_{1/2}} \quad \text{and} \quad E_\gamma(np_{3/2}) = E_{np_{3/2}} - E_{1s_{1/2}}$$

are significantly different for hydrogen-like uranium and resonances split visibly.

3.2.3 Multipole effects

Until now I have discussed the properties of two-photon cross section assuming the so-called *long-wavelength approximation* when the spatial part $e^{\pm i\mathbf{k}\mathbf{r}}$ of the electromagnetic plane wave is replaced to unity

$$e^{\pm i\mathbf{k}\mathbf{r}} \approx 1. \quad (3.13)$$

Although the long-wavelength approximation seems to be fully justified for the hydrogen atom, it must be proved for the heavier hydrogen-like ions. In order to calculate the second-order matrix element M_2^{fi} beyond long-wavelength approximation, one expands the plane wave into the electromagnetic multipoles (Rose 1957)

$$\mathbf{u}_\lambda e^{i\mathbf{k}\mathbf{r}} = \sqrt{2\pi} \sum_{L=1}^{\infty} \sum_{M=-L}^L i^L \sqrt{2L+1} \left(\mathcal{A}_{LM}^{(m)}(\mathbf{r}) + i\lambda \mathcal{A}_{LM}^{(e)}(\mathbf{r}) \right) D_{M\lambda}^L(\varphi_k, \theta_k, 0). \quad (3.14)$$

The latter expansion allows to reduce the second-order amplitude M_2^{fi} to radial matrix elements (see Appendix A).

If one includes the non-dipole terms ($L > 1$) in the multipole expansion (3.14), then one can achieve a certain convergency when the inclusion of higher multipoles brings only a negligible

contribution to the cross section σ_2 . If such convergency is achieved, one speaks about *exact* approximation.

As one can see in the Figure 3.7, the exact and the long-wavelength approximations do not differ significantly even in the case of the extremely relativistic hydrogen-like uranium. The values of two-photon cross section σ_2 in the exact and in the long-wavelength approximations are different by less than 10% everywhere in the dominant range². It means that the *long-wavelength approximation proves to be sufficient in calculation of two-photon total cross section*.

3.2.4 Dependence of the total cross section on the nuclear charge

The dependence of the two-photon cross section of hydrogen-like ions on the nuclear charge Z can be summarized in an analytical Z -scaling rule (Zernik 1964, and Kornberg *et al* 2002)

$$\sigma_2(Z, E_\gamma) = \frac{1}{Z^6} \sigma_2(1, E_\gamma/Z^2). \quad (3.15)$$

The latter equation allows to determine the cross section $\sigma_2(Z, E_\gamma)$ once one knows the cross section $\sigma_2(1, E_\gamma/Z^2)$ of the hydrogen atom for a corresponding photon energy. This scaling rule works only in the non-relativistic case in the long-wavelength approximation. In the relativistic case, i. e. when one evaluates the cross section with Dirac functions, such a simple rule does not exist. However, one can try to extend the non-relativistic scaling rule (3.15) to the relativistic case. The relativistic contraction of the hydrogenic orbitals can be represented by means of a *scaling factor* and the photon energy must be scaled according to the relativistic dependence of a bound energy on the nuclear charge Z . The relativistic scaling rule can be written, for instance, in the following form (Koval *et al* 2003)

$$\sigma_2(Z, \varepsilon) = \frac{\xi(Z)}{Z^6} \sigma_2(Z = 1, \varepsilon), \quad (3.16)$$

where the photon energy E_γ is scaled by means of a *relative energy* $\varepsilon \equiv 2 E_\gamma/E_T$ and a scaling factor $\xi(Z)$ is introduced. Certainly, the relativistic scaling rule (3.16) transforms to the non-relativistic scaling rule (3.15) if one applies the non-relativistic formula for the threshold energy $E_T = Z^2/(2n^2)$ and sets the scaling factor to unity $\xi(Z) = 1$.

The scaling factor $\xi(Z)$ must give an idea about deviations which are caused by relativistic and multipole effects. I will plot this factor against the nuclear charge Z for a designated relative energy $\varepsilon = 1.15$ in the electric dipole and in the exact (see Subsection 3.2.3) approximations.

One can see from the Figure 3.8 that the scaling factor $\xi(Z)$ decreases with the increase of the nuclear charge Z . For $\varepsilon = 1.15$, the scaling factor for hydrogen-like uranium ($Z = 92$) is about 2.5 times smaller than for hydrogen atom. Hence, one can conclude that the relativistic effects are strong and lead to a decrease of the two-photon cross section. In contrary, the inclusion of higher multipoles does not change the scaling factor for more than few percents for any ion.

Obviously, the relativistic scaling rule (3.16) is approximate, i. e. the scaling factor $\xi(Z)$ depends not only on the nuclear charge Z but also on the relative energy $\xi(Z, \varepsilon)$. In the

²Dominant range (of the photon energy for two-photon ionization) starts at half of the threshold energy and ends at the threshold energy $E_T/2 < E_\gamma < E_T$. See Section 2.2 for a more general explanation.

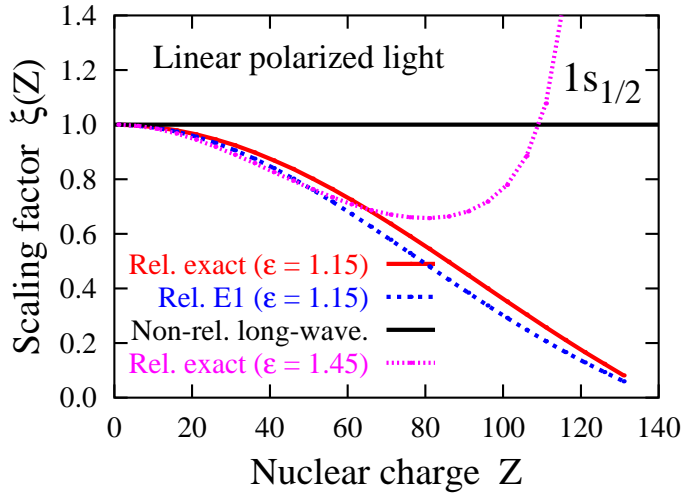


Figure 3.8: Scaling factor $\xi(Z)$ versus nuclear charge for different relative energies ε . In the non-resonance range of the photon energies $1.0 < \varepsilon < 1.4$ the scaling factor represents the relativistic contraction.

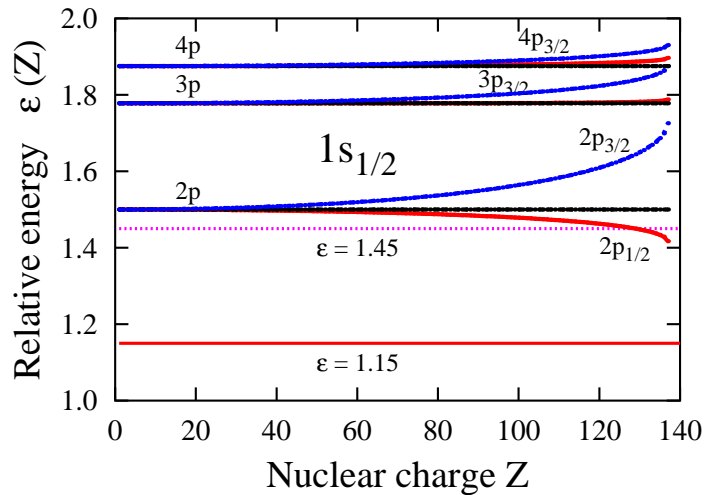


Figure 3.9: Relative photon energy ε of the first two-photon resonances versus nuclear charge.

non-resonance range, when the photon energy lies far from the resonances $1.0 < \varepsilon < 1.4$, the relativistic scaling factor behaves properly, i. e. shows the relativistic contraction of the $1s$ orbital. If the photon energy comes closer to the resonance, then the behavior of the scaling factor becomes arbitrary. For instance, it can exceed the unity, as it is shown for the relative energy $\varepsilon = 1.45$ in the Figure 3.8. The reason, why the relativistic scaling rule fails, lies in an improper scaling of the photon energy by means of the relative energy ε . For instance, the relative energy $\varepsilon = 1.45$ results in a photon energy E_γ below $2p_{1/2}$ resonance for ions $Z < 125$ and above $2p_{1/2}$ resonance for ions $Z > 125$ (see Figure 3.9).

3.3 Electron angular distribution in the two-photon ionization

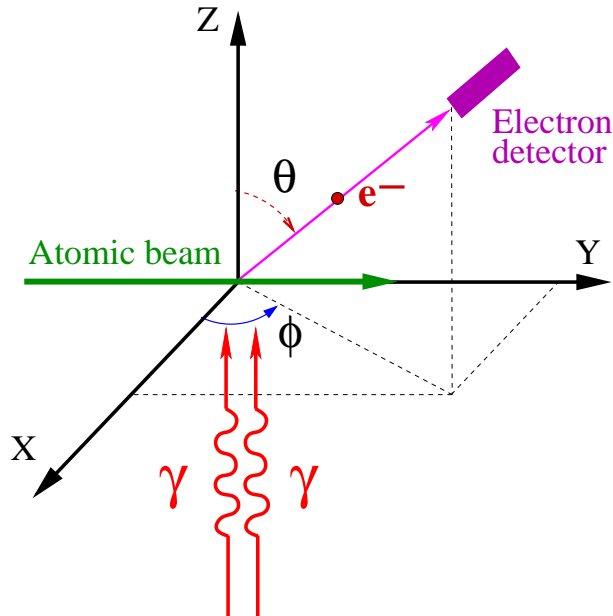


Figure 3.10: Geometry accepted in theoretical consideration of the electron angular distribution.

Although the inclusion of higher multipoles does not change the total cross section σ_2 significantly (see Section 3.2), the differential cross section $d\sigma_2/d\Omega$ (3.5) is more sensitive to the non-dipole contributions (Koval *et al* 2004). When the nuclear charge Z of the hydrogen-like ion increases, the inclusion of higher multipoles (see Subsection 3.2.3) become more and more important.

The electron angular distribution will be investigated in the simplest case when the photons possess an equal energy and polarization and propagate along Z -axis (see Figure 3.10). The direction of the outgoing electrons is determined by the spherical angles θ and ϕ . The flux of the outgoing electrons is proportional to the two-photon differential cross section $d\sigma_2/d\Omega$ which depends on the direction (θ, ϕ) . In this section, I am mainly interested in the dependence of the two-photon differential cross section $d\sigma_2/d\Omega$ on the polar angle θ and on the photon energy.

In the Figure 3.11, the differential cross section for the ground state of hydrogen and hydrogen-like uranium ion are presented. The electric dipole and the exact approximations are plotted in polar coordinates for the relative energy $\varepsilon = 1.4$ and the azimuthal angle $\phi = 0$. Indeed, one can see that the non-dipole contributions strongly influence the electron distribution in two-photon ionization of hydrogen-like ion of uranium and do not affect the electron distribution of hydrogen atom. The electron angular distribution for hydrogen-like uranium resembles that of hydrogen atom, but shows an asymmetry: the wings of angular distribution are bent to the direction of the photon's propagation. Apart from this, one can see that the *circularly polarized light* does not cause any electron emission in the direction of the light propagation. This can be explained by conservation of total angular momentum projection on Z -axis. Two left or right polarized photons carry ± 2 units of the angular momentum projection which must be transferred to the ion which is *initially* in $s_{1/2}$ state ($m_i = \pm 1/2$). The projection of spin of the *ionized electron* on the direction of propagation is always $m_s = \pm 1/2$.

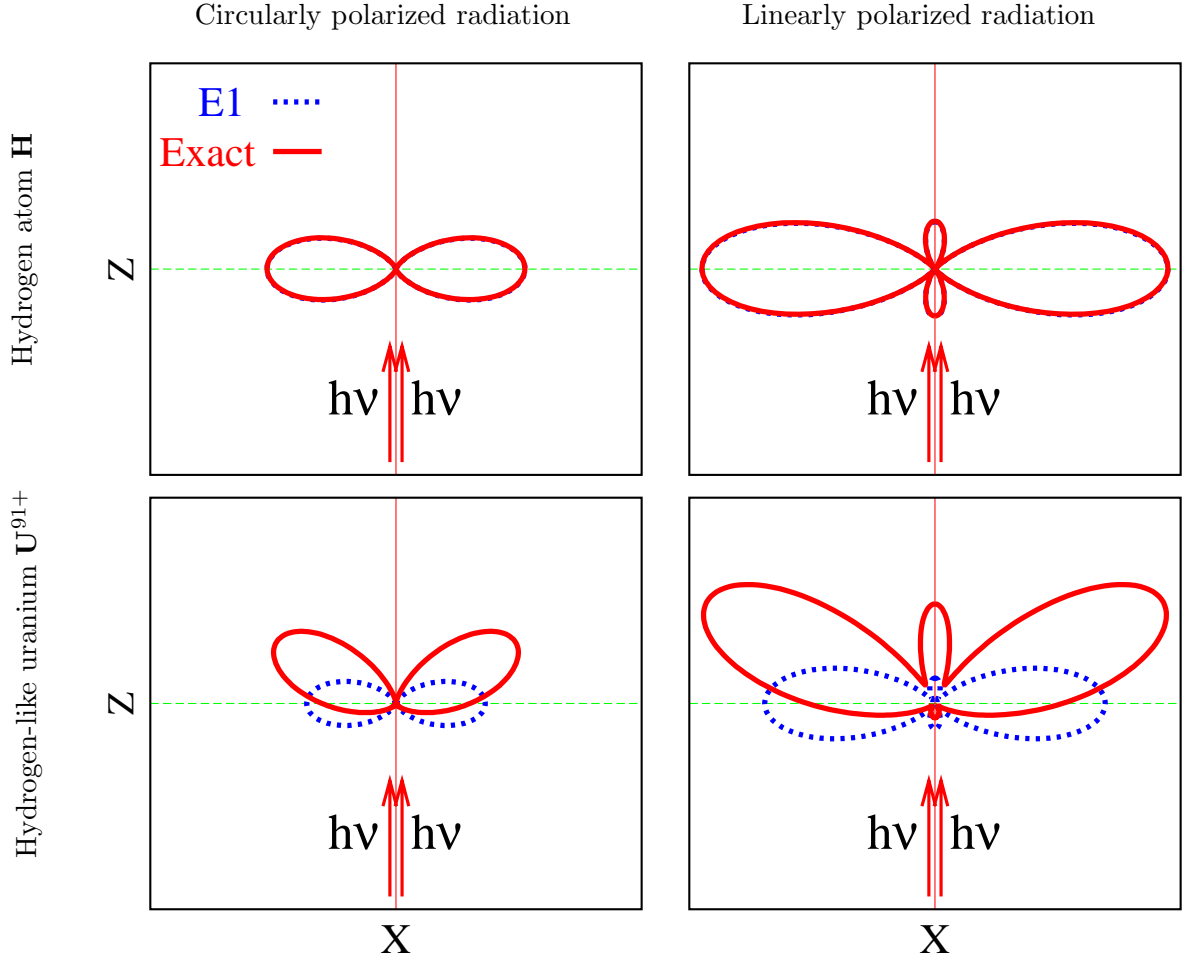


Figure 3.11: Electron angular distribution by two-photon ionization of hydrogen atom and hydrogen-like uranium ion in ground state. Relative energy $\varepsilon = 1.4$ and azimuthal angle $\phi = 0$. Electric dipole (E1) and the exact approximation are presented.

Therefore, if the ionized electron propagates along Z -axis, the projection of angular momentum can not be conserved

$$(\lambda_1 + \lambda_2 = \pm 2) + (m_i = \pm 1/2) \neq (m_s = \pm 1/2). \quad (3.17)$$

In contrast, if the light is *linearly polarized*, then the angular momentum projection of photons $J_{z1} + J_{z2}$ can take a *zero value*, i. e. there will be the possibilities to conserve the projection of angular momentum. This means that the electron can propagate along Z -axis after the two-photon ionization by the linearly polarized light.

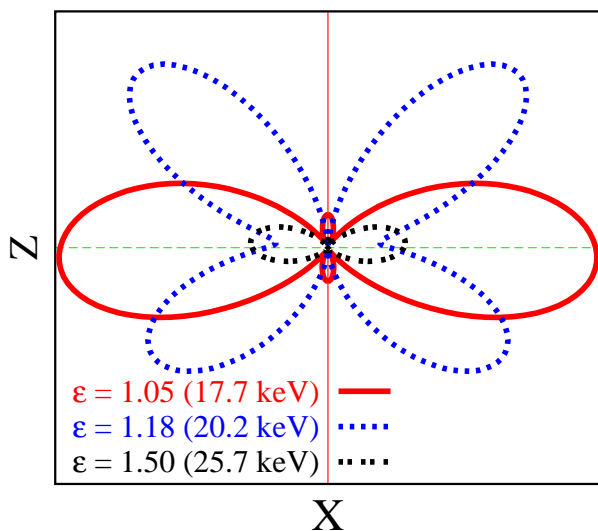


Figure 3.12: Electron angular distribution in the two-photon ionization of $2s_{1/2}$ metastable state U^{91+} ion with the linearly polarized light.

$1s_{1/2}$ state, the maxima of angular distribution for relative energy $\varepsilon = 1.05$ and $\varepsilon = 1.50$ are shifted slightly in the *backward direction*. Second, one has *two maxima* in the angular distribution when $\varepsilon = 1.18$, instead of *one maximum* in the other cases.

Such—rather difficult to explain—behavior is determined certainly by the energy denominator in the second-order amplitude M_2^{fi} (3.6). The entire second-order amplitude can be separated in two electric dipole channels like in Equation (3.12). The sign of each term depends on the photon energy: it changes to the opposite if the energy exceeds the corresponding resonance. Moreover, since the angular distribution is determined by a sum of spherical harmonics up to the d -symmetry, the angular distribution can show a manifold shape.

The shape of the angular distribution depends certainly on the photon energy E_γ . In order to show this dependence, I will consider the electron angular distribution after two-photon ionization of the hydrogen-like uranium ion in $2s_{1/2}$ metastable state.

In the Figure 3.12, the angular distributions are shown for three photon energies: below the $3p_{1/2}$ resonance when $\varepsilon = 1.05$ (17.7 keV), above the $3p_{3/2}$ resonance when $\varepsilon = 1.50$ (20.2 keV) and between $3p_{1/2}$ and $3p_{3/2}$ resonances when $\varepsilon = 1.18$ (25.7 keV). Two features should be mentioned with respect to the shape. First, in contrast to the ground

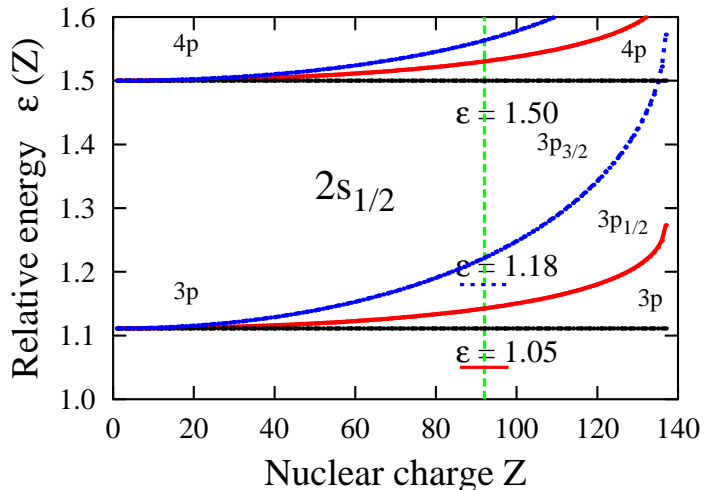


Figure 3.13: Relative energies ε of resonances in the two-photon ionization of $2s_{1/2}$ metastable state.

3.4 Conclusion

In this chapter, I discussed the influence of relativistic and multipole effects onto the total and differential cross sections. The total cross section is affected by relativistic effects which become increasingly important for higher nuclear charges. The relativistic effects are strong and must be taken into account for the hydrogen-like ions starting from the nuclear charge $Z \approx 30$. In contrary, the multipole corrections to the total cross section σ_2 are much weaker and do not exceed 10 % even for the very heavy ions. The relativistic and multipole effects can be treated like corrections in the so-called non-resonance range. In non-resonance range, the two-photon cross section calculated with Dirac theory is smaller than that calculated with Schrödinger theory. However, if one studies the two-photon ionization at an arbitrary photon energy, then one should take into account also the relativistic level shift and splitting.

Even more strongly than the total cross section, the relativistic effects influence the electron angular distributions. The differential cross sections show a strong dependence on the light polarization and on the photon energy. Apart from this, the angular distributions are sensitive to the inclusion of higher multipoles. Although, the shape of the angular distribution does not change qualitatively due to the inclusion of higher multipoles, it can be changed quantitatively rather strong.

The relativistic and multipole effects have been studied in our papers (Koval *et al* 2003 and Koval *et al* 2004) which can be found in Appendix E.

Chapter 4

Two-photon ionization of many-electron atoms

In the previous chapter I studied the relativistic and multipole effects in two-photon ionization of heavy hydrogen-like ions. I drew two main conclusions. First, the relativistic effects play an important role for both the total cross section as well as for the differential cross section. Second, the multipole effects strongly influence only the angular distributions of photoelectrons.

In this chapter, I will investigate the effects which arise in many-electron atomic inner-shells. Since the relativistic effects are fundamental effects and they are important for heavy hydrogen-like ions, the many-electron inner-shells will be investigated on the basis of the Dirac equation. Since the Dirac equation for a many-electron atom is much too hard to deal with, I will simplify the ionization model to a *single-active-electron* (SAE) approximation. The SAE approximation represents an atomic model of next sophistication level if compare SAE with hydrogenic model. It accounts for such atomic properties like energy levels or radiative rates better than the simplest hydrogenic approximation, and remains much simpler than a many-electron theory.

Although the SAE formalism is essentially an one-electron theory, it is able to take into account the effects which originate from the electron-electron interaction. Hence, if one compares the hydrogenic results with a proper SAE approximation, one will be able to assess the influence of exchange correlation effects in two-photon ionization.

In order to realize an accurate SAE calculation of two-photon ionization, one must be able to calculate a *central-field wave function* and a *central-field Green's function*. While the calculation of the central-field wave function is a relatively routine task, the calculation of Dirac-central-field Green's function has been less frequently discussed in the literature and is less known. I will present an algorithm to calculate the central-field Green's function in Section 4.3. Later, using this algorithm, I will calculate the two-photon cross sections for different atomic systems.

4.1 Single-active-electron approximation

Atoms with more than one electron show qualitatively new effects in the ionization and excitation processes. Namely, in a many-electron atom, two or more electrons can participate to the process, absorbing the energy of photon(s). For instance, in a *double ionization* two electrons absorb the energy of one or more photons. However, the probability of such *non-sequential* ionization is usually lower than the probability of one-electronic processes, i. e. the ionization can be considered within a single-active-electron approximation.

The SAE approximation assumes that only one electron changes its energy during ionization. All the other electrons are frozen, do not change their states and only create a mean-field for the *active electron*. This picture significantly simplifies the calculations because the whole theory remains an one-electronic theory. In order to perform a SAE computation, one must only specify the mean-field and the *initial state* of the active electron. These problems can be solved if one considers the structure of the many-electron atom.

It is well known that the dominant central symmetry of an atom and the Pauli's exclusion principle results in a shell-structure of the atom. It means that, in first approximation, the atomic electrons move independently in a central symmetric electrostatic field. Moreover, the Pauli's exclusion principle limits the number of electrons which belong to a shell and, what is more important, to a subshell. In the central-field approximation, the energy of an electron depends only on the quantum numbers n and κ which specify a subshell. Hence, the electrons in a many-electron atom are distributed over the subshells, in which the electrons have a certain energy and angular momentum.

The electrons within a subshell are called *equivalent electrons*. The mean field acting on these electrons is the same. Thus, once the initial subshell is specified, one can calculate the mean field and perform a SAE calculation.

In Section 4.2, I will present the formulae for calculation of two-photon cross section in the SAE approximation. These formulae will be used later to calculate the two-photon ionization of different atomic systems. It is clear that a proper choice of the mean field is crucial for the quality of the SAE predictions. Since, I will get the mean field out of a Hartree-Fock many-electron wave function (see Appendix C), one must choose a proper method to calculate this mean field. For this purpose, three test calculations using different potentials will be performed in Section 4.4 and 4.5. These calculations reveal a best potential which will be applied for two-photon ionization of the K- and L-shells of argon atom in Section 4.6.

4.2 Total cross section in the SAE approximation

The cross section in the SAE approximation will be calculated using an *one-electron cross section* $\sigma_2(n_i \kappa_i)$. The one-electron cross section, in turn, is completely similar to the hydrogenic cross section Equation (3.10). However, as it is clear from the previous, one must replace the radial parts of the Coulomb wave- and Coulomb Green's functions with corresponding central-

field functions. Thus, the one-electron cross section reads (in long-wavelength approximation)

$$\sigma_2(n_i \kappa_i) = \frac{8\pi^3 \alpha^2}{E_\gamma^2} \left| \langle \psi_f | \mathbf{p} \cdot \mathbf{u}_\lambda G_{E_i+E_\gamma} \mathbf{p} \cdot \mathbf{u}_\lambda | \psi_i \rangle \right|^2, \quad (4.1)$$

where \mathbf{p} is operator of electronic momentum, \mathbf{u}_λ is a polarization vector of ionizing radiation. The wave functions $|\psi_i\rangle$, $|\psi_f\rangle$ and Green's function G_E are Dirac-central-field functions. Calculation of these functions will be discussed below in Section 4.3.

Since there can be few equivalent electrons in a subshell, the one-electron cross sections must be multiplied with corresponding occupations. For instance, the s^2 subshells $1s^2, 2s^2, \dots, ns^2 \dots$ contain two equivalent electrons and the subshell cross section will be a corresponding one-electron cross section multiplied by an *occupation* of two.

Apart from this, a further detail should be mentioned here. Although, relativistic subshells are specified by quantum numbers n and κ , the energy difference between subshells with equal orbital momentum l is almost the same. Hence, it is useful sometimes to calculate a non-relativistic subshell cross section as a linear combination of the relativistic one-electron cross sections. For instance, the cross section for $2p^6$ initial subshell is a sum of the one-electron cross sections from $2p_{1/2}$ and $2p_{3/2}$ subshells multiplied with occupations $d_{2p_{1/2}} = 2$ and $d_{2p_{3/2}} = 4$

$$\sigma_2(2p^6) = d_{2p_{1/2}} \sigma_2(2p_{1/2}) + d_{2p_{3/2}} \sigma_2(2p_{3/2}). \quad (4.2)$$

4.3 Dirac-central-field Green's function

As it is shown in the previous section, the formulae for the two-photon cross section in the SAE approximation contain the central-field wave and central-field Green's functions. Although the calculation of central-field wave functions is a relatively well established task, the calculation of central-field Green's function is a less known problem. Hence, I will take one of the best algorithms for central-field wave function by Salvat *et al* (1995) and develop the own algorithm for Dirac-central-field Green's function.

Thus, in the following I am going to define the Dirac-central-field Green's function by means of a differential equation, separate this equation onto radial and angular parts, and detail the algorithm for calculation of the radial part.

4.3.1 Defining equation for the Dirac-central-field Green's function

The Dirac-central-field Green's function is determined by differential Equation (2.41)

$$(\hat{H}_0 - E) G_E(\mathbf{r}, \mathbf{r}') = \delta(\mathbf{r} - \mathbf{r}'), \quad (4.3)$$

where the Hamilton operator \hat{H}_0 describes the total energy of a single electron in the (arbitrary) mean field $U(r)$

$$\hat{H}_0 = \{ c \boldsymbol{\alpha} \mathbf{p} + [\beta - 1] c^2 + U(r) \}, \quad (4.4)$$

where conventional notation is already mentioned above in Section 3.1.

In the following, I will search for a solution of Equation (4.3) with boundary conditions as the ordinary wave function possesses. Namely, for each \mathbf{r}' , the Green's function obeys

$$\lim_{\mathbf{r} \rightarrow 0} G_E(\mathbf{r}, \mathbf{r}') = 0, \quad \lim_{\mathbf{r} \rightarrow \infty} G_E(\mathbf{r}, \mathbf{r}') = 0, \quad \text{for } E < 0. \quad (4.5)$$

Moreover, the Green's function obeys a symmetry relation

$$G_E(\mathbf{r}, \mathbf{r}') = G_E(\mathbf{r}', \mathbf{r}) \quad (4.6)$$

which defines the limiting properties completely.

If the $U(r)$ denotes a Coulomb field, i. e.

$$U(r) = -\frac{Z}{r}, \quad (4.7)$$

then the corresponding Green's function $G_E(\mathbf{r}, \mathbf{r}')$ can be obtained analytically (Swainson and Drake 1991, and Koval and Fritzsche 2003). In general, for an arbitrary mean field $U(r)$, it is still more convenient to write the mean field $U(r)$ with the aid of an *effective nuclear charge function* $Z(r)$

$$U(r) \equiv -\frac{Z(r)}{r}. \quad (4.8)$$

4.3.2 Separation of the Dirac-central-field Green's function on the radial and angular parts

The central-field Green's function for an arbitrary potential must be obtained by means of a numerical method. However, since the mean field possesses a central symmetry, one still can separate the central-field Green's function into angular and radial parts. This allow us to use the angular momentum algebra in the computation of second-order matrix element (2.39) and reduce the numerical computation only to the radial part of second-order matrix element. Details on the calculation of first- and second-order radiative matrix elements are collected in Appendix A. Here I will present the formulae which support the defining equation for a *radial part* of Dirac-central-field Green's function.

In order to derive the radial and angular parts of Dirac-central-field Green's function, I will use the expansion over eigen-states (2.38). The eigen-states of Hamilton operator H_0 (4.4) are the Dirac four-spinors (Grant 1988)

$$\psi_{n\kappa m}(\mathbf{r}) = \frac{1}{r} \begin{pmatrix} P_{n\kappa}(r) \Omega_{\kappa m}(\mathbf{r}) \\ -iQ_{n\kappa}(r) \Omega_{-\kappa m}(\mathbf{r}) \end{pmatrix} \equiv \frac{1}{r} \begin{pmatrix} g_{n\kappa}^L(r) \Omega_{\kappa m}(\mathbf{r}) \\ -ig_{n\kappa}^S(r) \Omega_{-\kappa m}(\mathbf{r}) \end{pmatrix}, \quad (4.9)$$

where $\Omega_{\kappa m}(\mathbf{r})$ are usual two-component spherical spinors (Beresteckij *et al* 1989, and Grant 1988). Large $P_{n\kappa}(r) \equiv g_{n\kappa}^L(r)$ and small $Q_{n\kappa}(r) \equiv g_{n\kappa}^S(r)$ radial components are real functions. Thus, performing the direct multiplication of 4-spinors (4.9), one can obtain the Dirac-central-field Green's function in form of a 4 by 4 matrix

$$\begin{aligned} G_E(\mathbf{r}, \mathbf{r}') &= \frac{1}{r r'} \sum_n \sum_{\kappa m} \frac{1}{E_{n\kappa} - E} \times \\ &\times \begin{pmatrix} g_{n\kappa}^L(r) g_{n\kappa}^L(r') \Omega_{\kappa m}(\mathbf{r}) \Omega_{\kappa m}^\dagger(\mathbf{r}') & -i g_{n\kappa}^L(r) g_{n\kappa}^S(r') \Omega_{\kappa m}(\mathbf{r}) \Omega_{-\kappa m}^\dagger(\mathbf{r}') \\ i g_{n\kappa}^S(r) g_{n\kappa}^L(r') \Omega_{-\kappa m}(\mathbf{r}) \Omega_{\kappa m}^\dagger(\mathbf{r}') & g_{n\kappa}^S(r) g_{n\kappa}^S(r') \Omega_{-\kappa m}(\mathbf{r}) \Omega_{-\kappa m}^\dagger(\mathbf{r}') \end{pmatrix}. \end{aligned} \quad (4.10)$$

If one defines radial parts of the central-field Green's function by $g_{E\kappa}^{TT'}(r, r') \equiv \sum_n \frac{g_{n\kappa}^T(r) g_{n\kappa}^{T'}(r')}{E_{n\kappa} - E}$, then the Green's function (4.10) will take the form

$$G_E(\mathbf{r}, \mathbf{r}') = \frac{1}{r r'} \sum_{\kappa m} \begin{pmatrix} g_{E\kappa}^{LL}(r, r') \Omega_{\kappa m}(\mathbf{r}) \Omega_{\kappa m}^\dagger(\mathbf{r}') & -i g_{E\kappa}^{LS}(r, r') \Omega_{\kappa m}(\mathbf{r}) \Omega_{-\kappa m}^\dagger(\mathbf{r}') \\ i g_{E\kappa}^{SL}(r, r') \Omega_{-\kappa m}(\mathbf{r}) \Omega_{\kappa m}^\dagger(\mathbf{r}') & g_{E\kappa}^{SS}(r, r') \Omega_{-\kappa m}(\mathbf{r}) \Omega_{-\kappa m}^\dagger(\mathbf{r}') \end{pmatrix}. \quad (4.11)$$

The radial parts of the central-field Green's function have to be obtained by a numerical method as a solution of corresponding differential equation. In order to derive this equation, one inserts the ansatz (4.11) into the defining Equation (4.3). Performing this substitution with the Hamilton operator (4.4) in spherical coordinates, one obtains the radial equation

$$\begin{pmatrix} \left[-\frac{\alpha Z(r)}{r} - \alpha E \right] & \left[\frac{\kappa}{r} - \frac{\partial}{\partial r} \right] \\ \left[\frac{\partial}{\partial r} + \frac{\kappa}{r} \right] & \left[-\frac{2}{\alpha} - \frac{\alpha Z(r)}{r} - \alpha E \right] \end{pmatrix} \begin{pmatrix} g_{E\kappa}^{LL} & g_{E\kappa}^{LS} \\ g_{E\kappa}^{SL} & g_{E\kappa}^{SS} \end{pmatrix} = \alpha \delta(r - r') \mathbf{I}_2, \quad (4.12)$$

where α is fine structure constant, and \mathbf{I}_2 is the 2 by 2 unit matrix.

In the following subsection, I will consider a method which allows to solve the defining Equation (4.12) once the potential $Z(r)$ is specified. The method was originally developed by McGuire (1981) for Schrödinger central-field Green's function. I am going to extend this method on the relativistic framework based on Dirac equation.

4.3.3 Calculation of the radial part of Dirac-central-field Green's function

In order to explain the algorithm, I will give a general idea of the method and explain all necessary details after. Thus, in order to get a more clear overview of the method, I will formalize the defining Equation (4.12)

$$(\hat{h} - E) g_E(r, r') = \delta(r - r'). \quad (4.13)$$

Solution of this *inhomogeneous equation* can be *separately determined* for each value of *second argument* r' by means of a *general solution* of a *corresponding homogeneous equation*

$$(\hat{h} - E) g_E(r) = 0. \quad (4.14)$$

There are two linearly independent solutions of the homogeneous Equation (4.14): regular at the origin and regular at the infinity solutions a linear combination of which form the general solution. The solution regular at the *origin will be determined* only in the closed interval

$0 < r < r'$. The solution regular at the infinity will be determined only in the interval $r > r'$. Afterwards, one matches the obtained solutions at $r = r'$ by a simple multiplication of one of the solutions. An obtained in this way *matched function* is mainly the Green's function for a given second argument r' . Now one should only normalize the matched function. In order to derive the normalization condition, one must integrate in the defining Equation (4.13) over a small range $r = r' - \varepsilon \dots r' + \varepsilon$

$$\int_{r'-\varepsilon}^{r'+\varepsilon} (\hat{h} - E) g_E(r, r') dr = \int_{r'-\varepsilon}^{r'+\varepsilon} \delta(r - r') dr = 1. \quad (4.15)$$

The latter equation results in an algebraic equation for the left-hand-side and the right-hand-side Green's function derivatives $\frac{\partial g_E}{\partial r}$ at the matching point $r = r'$, i. e. Equation (4.15) imposes an incontinuity of the first derivative. Moreover, Equation (4.15) determines a *normalization factor* for the matched function.

Below, I will detail the procedure sketched above. As follows from Equation (4.12), the system of four equations separates in two couples of equations for $g_{E\kappa}^{LL}$, $g_{E\kappa}^{SL}$ and $g_{E\kappa}^{SS}$, $g_{E\kappa}^{LS}$ components. I will consider only the procedure for $g_{E\kappa}^{LL}$ and $g_{E\kappa}^{SL}$ components because the procedure for $g_{E\kappa}^{SS}$ and $g_{E\kappa}^{LS}$ components is similar.

Thus, the couple of differential equations, one is interested in, reads

$$\left[-\frac{\alpha Z(r)}{r} - \alpha E \right] g_{E\kappa}^{LL}(r, r') + \left[\frac{\kappa}{r} - \frac{\partial}{\partial r} \right] g_{E\kappa}^{SL}(r, r') = \alpha \delta(r - r'), \quad (4.16)$$

$$\left[\frac{\partial}{\partial r} + \frac{\kappa}{r} \right] g_{E\kappa}^{LL}(r, r') + \left[-\frac{2}{\alpha} - \frac{\alpha Z(r)}{r} - \alpha E \right] g_{E\kappa}^{SL}(r, r') = 0. \quad (4.17)$$

Expressing the component $g_{E\kappa}^{SL}$ from Equation (4.17) and inserting it into Equation (4.16), one obtains a second-order inhomogeneous differential equation for the component $g_{E\kappa}^{LL}$

$$\left(\frac{\kappa}{r} - \frac{\partial}{\partial r} \right) \left(\frac{\left(\frac{\partial}{\partial r} + \frac{\kappa}{r} \right) g_{E\kappa}^{LL}(r, r')}{-\frac{2}{\alpha} - \frac{\alpha Z(r)}{r} - \alpha E} \right) - \left(-\frac{\alpha Z(r)}{r} - \alpha E \right) g_{E\kappa}^{LL}(r, r') = \alpha \delta(r - r'). \quad (4.18)$$

In order to determine the general solution of the latter equation, the effective nuclear charge function $Z(r)$ will be approximated piecewise by lines

$$Z(r) = Z_{0i} + Z_{1i} r, \text{ for } r_i \leq r \leq r_{i+1}, \quad (4.19)$$

where the index i ranges between 1 and a maximal value i_{\max} .

This linear approximation allows an *analytical general solution* of the *corresponding homogeneous equation*

$$\left(\frac{\kappa}{r} - \frac{\partial}{\partial r} \right) \left(\frac{\left(\frac{\partial}{\partial r} + \frac{\kappa}{r} \right) g_{E\kappa}^{LL}(r)}{-\frac{2}{\alpha} - \frac{\alpha Z(r)}{r} - \alpha E} \right) - \left(-\frac{\alpha Z(r)}{r} - \alpha E \right) g_{E\kappa}^{LL}(r) = 0 \quad (4.20)$$

on each piece $r_i \leq r \leq r_{i+1}$.

The regular at the origin $M_{E\kappa}^i(r)$ and regular at the infinity $W_{E\kappa}^i(r)$ *piece-solutions* will be used to built up the general solution of the Equation (4.20) in the whole range $r = 0 \dots r_{i_{\max}}$ of r coordinate. The piece-solutions $M_{E\kappa}^i(r)$ and $W_{E\kappa}^i(r)$ can be written in the following form

$$M_{E\kappa}^i(r) = r^{s_i} e^{-q_i r} [t_i M(-t_i + 1, 2s_i + 1, 2q_i r) + (\kappa - Z_{0i}/q_i) M(-t_i, 2s_i + 1, 2q_i r)], \quad (4.21)$$

$$W_{E\kappa}^i(r) = r^{s_i} e^{-q_i r} [(\kappa + Z_{0i}/q_i) U(-t_i + 1, 2s_i + 1, 2q_i r) + U(-t_i, 2s_i + 1, 2q_i r)], \quad (4.22)$$

where $M(a, b, z)$ and $U(a, b, z)$ are the confluent hypergeometric functions regular at the origin and at the infinity (Abramowitz and Stegun 1965, and Spanier and Keith 1987, Appendix B) and where the quantities s_i , t_i and q_i read

$$s_i = \sqrt{\kappa^2 - \alpha^2 Z_{0i}^2}, \quad t_i = \frac{\alpha Z_{0i}((E + Z_{1i})\alpha^2 + 1)}{\sqrt{1 - ((E + Z_{1i})\alpha^2 + 1)^2}} - s_i,$$

$$q_i = \sqrt{-(E + Z_{1i})((E + Z_{1i})\alpha^2 + 2)}.$$

The solution of the inhomogeneous Equation (4.18) will be constructed separately for each r' , piecewise on the grid on which the potential was represented (see Equation (4.19)). The piece-solution of the inhomogeneous Equation (4.18) will be written as a linear combination of piece-solutions $M_{E\kappa}^i(r)$ and $W_{E\kappa}^i(r)$ of the homogeneous Equations (4.21, 4.22)

$$g_{E\kappa}^{LL}(r, r') = f_{i,1}(r') \cdot M_{E\kappa}^i(r) + f_{i,2}(r') \cdot W_{E\kappa}^i(r), \quad \text{for } r_i \leq r \leq r_{i+1}, \quad i = 1 \dots i_{\max}. \quad (4.23)$$

Hence, if the coefficients $f_{i,1}(r')$, $f_{i,2}(r')$ are determined for each piece i , the Green's function will be found.

The coefficients $f_{i,1}(r')$ and $f_{i,2}(r')$ will be obtained first in the region $r < r'$, i. e. on the pieces $i = 1 \dots i_{\text{mid}}$. For the first piece $i = 1$, the coefficients $f_{1,1}(r')$ and $f_{1,2}(r')$ are assumed to be one and zero. The latter assumption keeps the solution regular at the origin.

The continuity of the solution and its derivative results in the following recurrence equations

$$\begin{aligned} f_{i,1}(r') M_{E\kappa}^i(r_i) + f_{i,2}(r') W_{E\kappa}^i(r_i) &= f_{i+1,1}(r') M_{E\kappa}^{i+1}(r_i) + f_{i+1,2}(r') W_{E\kappa}^{i+1}(r_i), \\ f_{i,1}(r') M'_{E\kappa}^i(r_i) + f_{i,2}(r') W'_{E\kappa}^i(r_i) &= f_{i+1,1}(r') M'_{E\kappa}^{i+1}(r_i) + f_{i+1,2}(r') W'_{E\kappa}^{i+1}(r_i) \end{aligned} \quad (4.24)$$

which determine f_{i+1} coefficient if f_i coefficient is known. The calculation of the f coefficients is stopped on the i_{mid} -th piece in which an inequality $r_{i_{\text{mid}}} \leq r' < r_{i_{\text{mid}}+1}$ is satisfied.

Hereon, the f coefficients are determined on the pieces $i = i_{\max} \dots i_{\text{mid}}+1$ i. e. in the region $r' < r$. Since the regular at the infinity solution have to be constructed, one assumes $f_{i_{\max},1} = 0$ and $f_{i_{\max},2} = 1$. One uses a backward recurrence and evaluate the coefficients $f_{i_{\max},1} \dots f_{i_{\text{mid}}+1,1}$ and $f_{i_{\max},2} \dots f_{i_{\text{mid}}+1,2}$. Backward recurrence is based, of course, also on the continuity Equations (4.24).

Next, the value of the Green's function $g_{E\kappa}^{LL}(r, r')$ at the matching point $r = r'$ must be continuous. One can achieve this continuousness, for instance, by multiplication of coefficients $f_{i_{\text{mid}}+1,1} \dots f_{i_{\text{max}},1}$ and $f_{i_{\text{mid}}+1,2} \dots f_{i_{\text{max}},2}$ to a *continuousness factor* f_c

$$f_c = \frac{f_{i_{\text{mid}},1}(r') M_{E\kappa}^{i_{\text{mid}}}(r') + f_{i_{\text{mid}},2}(r') W_{E\kappa}^{i_{\text{mid}}}(r')}{f_{i_{\text{mid}}+1,1}(r') M_{E\kappa}^{i_{\text{mid}}+1}(r') + f_{i_{\text{mid}}+1,2}(r') W_{E\kappa}^{i_{\text{mid}}+1}(r')}. \quad (4.25)$$

Finally, all the coefficients $f_{i,1}$ and $f_{i,2}$ have to be normalized according to a δ -like inhomogeneity on the right hand-side in Equation (4.18). If one integrates the differential Equation (4.18) over a small interval $r = r' - \varepsilon \dots r' + \varepsilon$, the following algebraic equation can be obtained

$$\left. \frac{\partial}{\partial r} g_{E\kappa}^{LL}(r, r') \right|_{r=r'-\varepsilon}^{r=r'+\varepsilon} = -\alpha \left(-\frac{2}{\alpha} - \frac{\alpha Z(r')}{r'} - \alpha E \right). \quad (4.26)$$

This equation determines a normalization factor f_n by which all the determined f coefficients must be multiplied.

Having the component $g_{E\kappa}^{LL}(r, r')$ in form of a piecewise-analytical function, the component $g_{E\kappa}^{SL}(r, r')$ can be easily obtained out of the Equation (4.17)

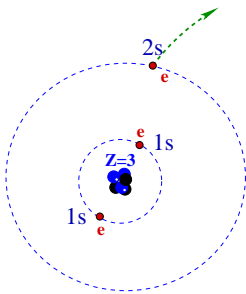
$$g_{E\kappa}^{SL}(r, r') = -\frac{\left(\frac{\partial}{\partial r} + \frac{\kappa}{r} \right) g_{E\kappa}^{LL}(r, r')}{-\frac{2}{\alpha} - \frac{\alpha Z(r)}{r} - \alpha E}. \quad (4.27)$$

The values of $g_{E\kappa}^{LL}(r, r')$ component and its derivative $\frac{\partial g_{E\kappa}^{LL}}{\partial r}$ can be calculated on each piece using already determined f coefficients and piece-solutions (4.21, 4.22).

In this way, one is able to obtain numerically the Dirac-central-field Green's function. Since the described algorithm is quite complex, one may wish to check the generated functions before using it in calculation of second-order matrix elements. Two simple, but rather strong methods to check the central-field Green's functions are detailed in Appendix D.

Further on, I will use the Dirac-central-field Green's function in the SAE calculations of the total cross section σ_2 .

4.4 Two-photon ionization of the lithium outer-shell



The alkali metal atoms contain a relatively compact close-shell core and a single electron in the outer-shell. The outer electron moves relatively far away from the core. It may be considered in a very good approximation as an electron moving in a central symmetric electrostatic field. Thus, the SAE approximation must work well in alkali atoms, therefore I will justify the method comparing our calculations for lithium outer-shell with an available (non-relativistic) calculation by McGuire (1981).

By studying two-photon ionization of lithium and helium (see the following Section 4.5), I pursue two goals: to check our calculations as whole and to choose a most suitable method for calculation of the mean field. The latter purpose is very important, since the rightness of the SAE approximation totally depends on the quality of the mean field model. In order to choose a most realistic model, I will compare the total cross sections of two our calculations: SAE with a Hartree potential and the SAE with a Hartree-plus-statistical-exchange potential. The latter potential had been developed by Cowan (1965, 1981) who denoted it as the HX-potential. While Hartree potential takes into account only the potential energy of an electron in the averaged field of nucleus and all other electrons, HX-potential takes additionally into account the effects of electron spin-spin interaction. With other words, the HX-potential is more realistic because a two-body part of the full energy of the atom, which is neglected in Hartree potential, is taken partially into account in the HX-potential.

Both potentials can be calculated once one has a Hartree-Fock wave function and specify the subshell where the electron moves. The formulae to calculate the Hartree and HX-potentials are collected in Appendix C.

In the Figure 4.1a, the Hartree and HX-potentials are shown for 2s electron of lithium atom. One can see that the asymptotic behavior of both potentials is the same: the effective nuclear charge strives to the nuclear charge at the origin $Z_{\text{eff}}(0) = Z_{\text{nuc}}$ and becomes unity at the infinity $Z_{\text{eff}}(\infty) = 1$. However, the exchange-correlation leads to a more strong binding of the outer electron to the atomic core. The stronger binding, in turn, results in a smaller two-photon cross section.

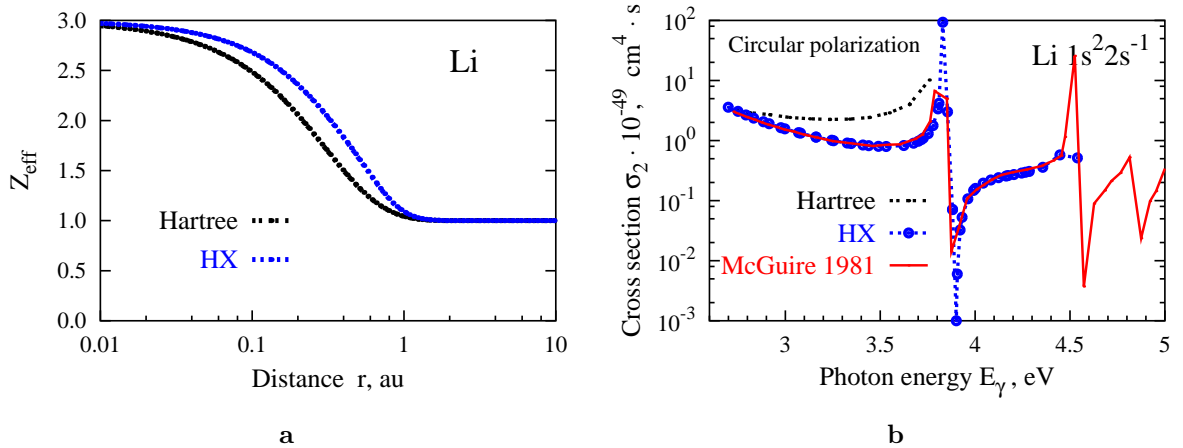
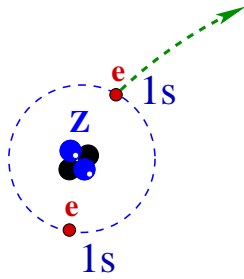


Figure 4.1: Two-photon ionization cross section σ_2 for 2s outer electron of lithium atom.

Two-photon total cross sections are compared in the Figure 4.1b. One can see that the cross section for the HX-potential coincides indeed with calculation by McGuire (1981), while the cross section for the Hartree potential deviates strongly. It means that the HX-potential can be considered as a more realistic approximation for the atomic mean field.

4.5 Two-photon ionization of He and He-like ion of neon



Further test of the SAE model is devoted to the two-electronic inner-shells. Since I am going to perform a new calculation for the K- and L-shells of argon, I have to test the method on the inner-shells which contain two equivalent electrons. In these premises, I will calculate the total cross section σ_2 for helium atom in ground state and for a helium-like ion of neon.

I will compare the SAE calculation with a corresponding *two-active-electron calculation*. The two-active-electron calculation utilizes a *discretized continuum method* to perform the summation over whole two-electronic spectrum (Lambropoulos *et al* 1998). This relatively new method had been tested in the two-photon ionization of helium atom by Saenz and Lambropoulos (1999) and on alkaline outer-shells by Nikolopoulos (2003). The latter article describes a computer program which I used to calculate the reference cross sections for helium-like neon.

The SAE calculations include three test cases of the mean field: pure Coulomb, Hartree and the HX-potentials. As one can see in the Figure 4.2a, the HX-model coincides with the two-active-electron calculation better than Coulomb-model or Hartree-model. Moreover, Coulomb-model provides a better account than Hartree-model in the non-resonance range. For this reason, I will calculate the SAE cross sections of argon inner-shells only with pure Coulomb potential and the HX-potential, leaving out the Hartree potential.

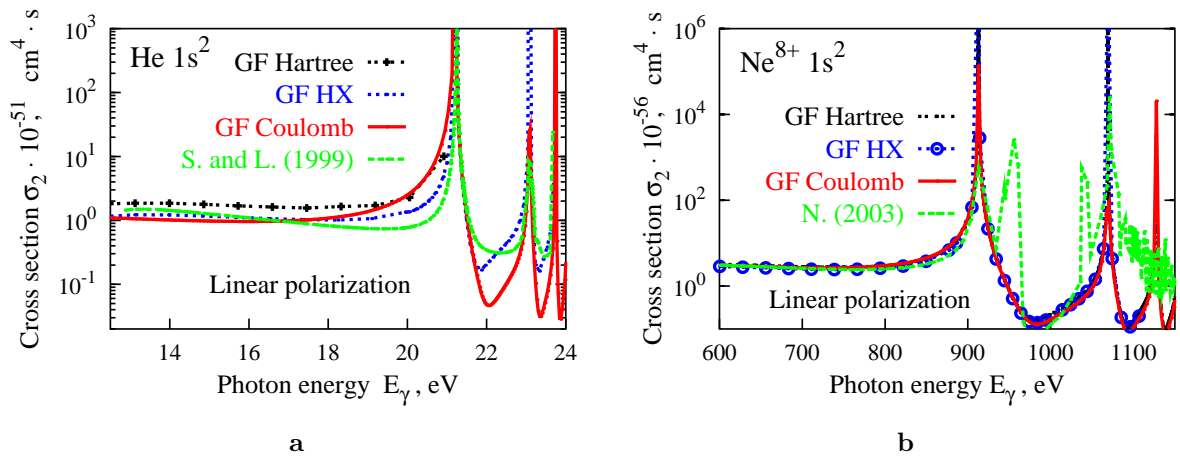


Figure 4.2: Two-photon ionization cross section σ_2 for helium and helium-like ion of neon. The curves denoted as S. and L. (1999) on panel **a** and N. (2003) on panel **b** refer to the paper by Saenz and Lambropoulos (1999) and our computation with a computer program by Nikolopoulos (2003) accordingly.

If one compares the Figures 4.2a and b, one will see that the effects of electron-electron interaction become weaker for helium-like ions. All four curves coincide well¹ and resonances become distributed like in hydrogenic case (compare with Figure 3.6). This gives a hint that

¹Fluctuations in the curve N. (2003) after first resonance should not be taken into account. Although, I was able to use the program by Nikolopoulos (2003) to calculate the two-photon cross section for helium-like neon ion, I didn't arrive, obviously, to properly optimize whole manifold of program parameters.

the effects of electron-electron interaction are also unimportant in the K-shell of neutral atom.

4.6 Two-photon ionization of the argon K- and L-shells

The comparisons, which are presented above, revealed the HX-potential as a best mean field and justified our computation as whole. Hence, one is able now to perform an analogous calculation for atom which was not under study before. For instance, heavy rare gas atoms represent interesting examples since the two-photon ionization of their inner-shells was studied only scarcely (Kornberg *et al* 2002). In this section, I am going to present the SAE calculations for the two-photon ionization of the argon K- and L-shells.

I will calculate the total cross section σ_2 for linearly polarized light with two potential models: a Coulomb potential and a HX-potential. Comparison of these calculations allows to assess the importance of *exchange correlation effects* in two-photon ionization. Additionally, I will present the polarization ratio $R = \sigma_2^{\text{circ}}/\sigma_2^{\text{lin}}$ and elucidate its quite unusual behavior in case when the $2p^6$ subshell is ionized.

4.6.1 Stretching of theoretical cross sections

Unfortunately, the calculated energies of bound states are rather unequal for different models of the mean field and to the experimental energies (see Tables 4.1, 4.2). Hence, the positions of two-photon resonances will not coincide and a graphical comparison of the two-photon cross sections would be difficult to perform. For this reason, I will stretch both theoretical cross sections between the corresponding experimental resonance energies.

Transition	Energy, eV			Width ^b $\Gamma(K)$, eV
	CF, $Z = 17.7$	HX _{1s-1}	Exp. ^a	
$1s \rightarrow 2p$	3213.710	2950.696	2955.566	0.68
$1s \rightarrow 3p$	3806.181	3220.825	3190.490	
$1s$ edge	4280.455	3240.948	3202.933	

^a NIST (2003).

^b Gräf and Hink (1985).

Table 4.1: The energies of two-photon resonances by ionization of the argon K-shell.

Directly on resonances, the denominator in second-order amplitude (2.23) turns to zero, i. e. the cross section would be infinitely large. Therefore, if one calculates the height of resonances, one must take into account a finite *level widths* of the intermediate states. In order to do this, one can replace in Equation (2.23)

$$E_\nu \rightarrow E_\nu + i\Gamma_\nu/2. \quad (4.28)$$

As the level widths Γ_ν , the *experimental level widths* by Gräf and Hink (1985) were accepted and the height of three best resolved resonances $1s \rightarrow 2p$, $2s \rightarrow 3p$ and $2p \rightarrow 3s$ are estimated. In order to calculate the transition amplitude M_2^{fi} (2.23) nearby resonances, I have used a

Transition	Energy, eV			Width ^b
	CF, $Z = 13.85$	HX _{1s²2s²2p⁻¹}	Exp. ^a	$\Gamma(L)$, eV
$2p \rightarrow 3s$	362.16	226.83	221.52 ^c	0.13
$2p \rightarrow 3d$	362.65	257.75	–	
$2p \rightarrow 4s$	489.43	255.43	–	
$2p \rightarrow 4d$	489.71	258.43	–	
$2p$ edge	652.89	259.33	250.57	
$2s \rightarrow 2p$	1.6769	64.451	–	
$2s \rightarrow 3p$	364.33	306.28	311.36 ^c	1.63
$2s \rightarrow 4p$	491.32	321.20	–	
$2s$ edge	654.56	323.79	326.30	

^a NIST (2003).

^b Gräf and Hink (1985).

^c Theoretical value.

Table 4.2: The energies of two-photon resonances by ionization of the argon L-shell.

direct summation only over bound states instead of the Green's function method. The direct summation only over bound states proves to be a correct means to calculate the resonance heights, since the Green's function method and the direct summation method result in equal cross sections nearby the resonances. Thus, if the photon energy meets a resonance, the infinite sum over complete spectrum can be reduced to the sum over the discrete spectrum. In fact, one can restrict in the discrete summation to just very few intermediate states.

4.6.2 Two-photon ionization of the argon K-shell

Figure 4.3 shows the total cross sections $\sigma_2(1s^2)$ for Ar atom for linearly polarized light: the SAE approximation with pure Coulomb field ($Z_{\text{eff}} = 17.7$) and the SAE approximation with the HX-potential are compared.

One can see that the cross sections $\sigma_2(1s^2)$ agree with each other surprisingly well, although the bound energies are reproduced in the SAE approximation with the Coulomb potential much worse than in the SAE approximation with the HX-potential (see Table 4.1) and the asymptotic behavior of Coulomb field differs significantly to the right asymptotic behavior

$$Z_{\text{eff}}(r \rightarrow 0) = Z_{\text{nuc}}, \quad Z_{\text{eff}}(r \rightarrow \infty) = 1.$$

In non-resonance range, when the photon energy lies between 1600...2800 eV, both cross sections possess a flat behavior, typical for hydrogenic atom. Unlike of hydrogenic case, the two-photon resonances are shifted to K-edge, i. e. two-photon ionization of the argon K-shell happens in a *non-resonant regime* over the largest part of dominant range. The only one resonance lies relatively far away from K-edge. On this $1s \rightarrow 2p$ resonance, the cross section increases and reaches a magnitude as greater as 10^5 if compare with an average non-resonance value.

The polarization ratio $R = \sigma_2^{\text{circ}}/\sigma_2^{\text{lin}}$ of cross sections for circularly and linearly polarized

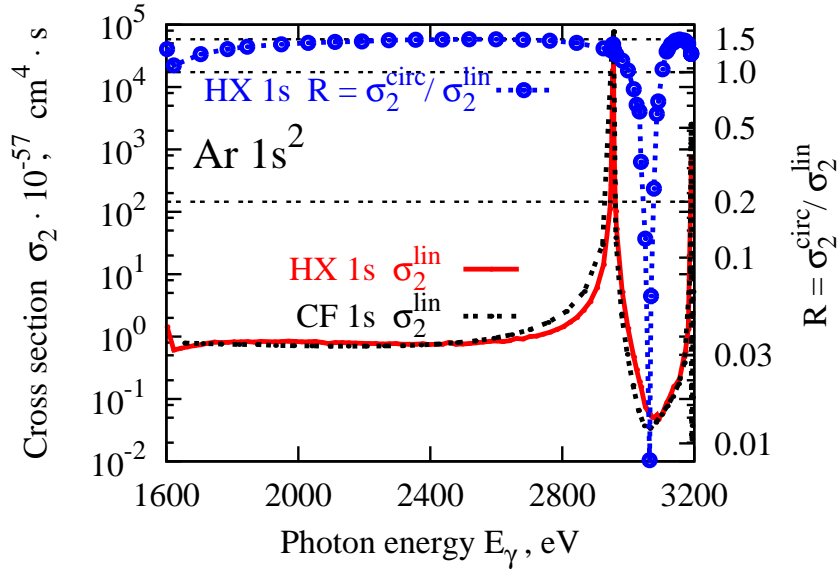


Figure 4.3: Two-photon ionization cross section σ_2^{lin} and polarization ratio $R = \sigma_2^{\text{circ}}/\sigma_2^{\text{lin}}$ versus photon energy for $1s^2$ subshell of argon.

light is only plotted for the HX-model. It shows a typical hydrogenic behavior which will be discussed later, in Subsection 4.6.4.

4.6.3 Two-photon ionization of the argon L-shell

Figure 4.4 shows the total cross sections $\sigma_2(2s^2)$ for Ar atom for linearly polarized light. Again, as I did for $1s^2$ subshell, the SAE approximation with the Coulomb field ($Z_{\text{eff}} = 13.85$) and the SAE approximation with the HX-potential are compared.

In contrast to $1s^2$ subshell, one can see a large discrepancy between two models. The cross sections disagree by a factor of 40...70 in almost whole dominant range. This disagreement is connected to the difference of hydrogen-like spectrum if compare with experimental spectrum or with the HX-spectrum. While the HX-model reproduces the experimental resonance positions and edge energies at a better than 2.3 % accuracy (see Table 4.2), the hydrogen-like resonance and edge energies can differ to the experimental values by factor of two. Moreover, the hydrogen-like resonances are distributed *else qualitatively* over the dominant range than the experimental or HX-resonances. For instance, the hydrogen-like model predicts a $2s \rightarrow 3p$ resonance at the beginning of the theoretical dominant range, while its right position locates at the end of dominant range.

Since the HX-spectrum coincides with experimental spectrum quite well, the HX-model must be appreciated as a more credible by contrast with the hydrogen-like model. Hence, further on I will discuss only the HX-model.

In contrast to the $1s^2$ subshell, the cross section $\sigma_2(2s^2)$ shows a rising behavior at the beginning of dominant range. This can be explained if one mentions a $2s \rightarrow 2p \rightarrow \epsilon d$ term in the second-order amplitude (2.23). Since the "resonance energy" of this term (see Table 4.2) lies below the dominant range, the whole dominant range becomes put *between resonances*. Thus, the dominant range becomes entirely a *resonance range* although all visible resonances

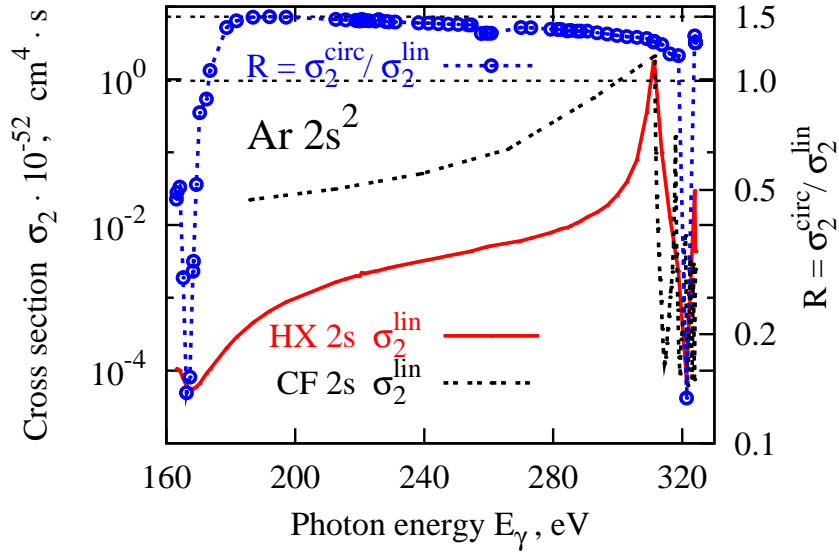


Figure 4.4: Two-photon ionization cross section σ_2^{lin} and polarization ratio $R = \sigma_2^{\text{circ}}/\sigma_2^{\text{lin}}$ versus photon energy for $2s^2$ subshell of argon.

are strongly shifted to the L_1 -edge. Herewith, the most pronounced $2s \rightarrow 3p$ resonance is only 10^3 times as larger as typical non-resonance cross section since a large level width $\Gamma(L_1) = 1.63$ eV dumps this resonance strongly.

Figure 4.5 shows the two-photon cross section of argon $2p^6$ subshell. A large discrepancy between hydrogen-like- and HX-models remains also in case of $2p^6$ subshell. Therefore, I do not present a less favorable calculation with the Coulomb potential and draw the cross section σ_2^{lin} and the polarization ratio $R = \sigma_2^{\text{circ}}/\sigma_2^{\text{lin}}$ only for the HX-model.

The dominant range of $2p^6$ subshell must be considered also as *resonance range* since there are available terms $2p \rightarrow 2s \rightarrow \varepsilon p$ and $2p \rightarrow 1s \rightarrow \varepsilon p$ in second-order amplitude. However, they are located far below the dominant range, they have a negative "resonance energy" and act only on a weak $2p \rightarrow ns \rightarrow \varepsilon p$ channel. For these reasons, the slope of cross section $\sigma_2(2p^6)$ at the beginning of dominant range is less steep than in case of $2s^2$ subshell.

The cross section $\sigma_2(2p^6)$ is roughly 10 times as large as $2s^2$ cross section. This discrepancy arises due to the two reasons. First, the *number of electrons* in $2p^6$ subshell and $2s^2$ subshell is different. Second, the $2p$ and $2s$ orbitals have *different size*: the electron in $2p^6$ subshell is less bounded and moves therefore farther away from the nucleus.

The structure of resonances of $2p^6$ subshell cross section differs to the resonance structure of $2s^2$ subshell cross section. *Electric dipole selection rules* allow two electric dipole *channels* in two-photon ionization of s^2 subshell: a major $s \rightarrow p \rightarrow d$ and a minor $s \rightarrow p \rightarrow s$ channels. Both channels have p -symmetry in the intermediate states, therefore there is only *one series* of resonances: $s \rightarrow np$. In contrast, there are three electric dipole channels open in two-photon ionization of a p subshell

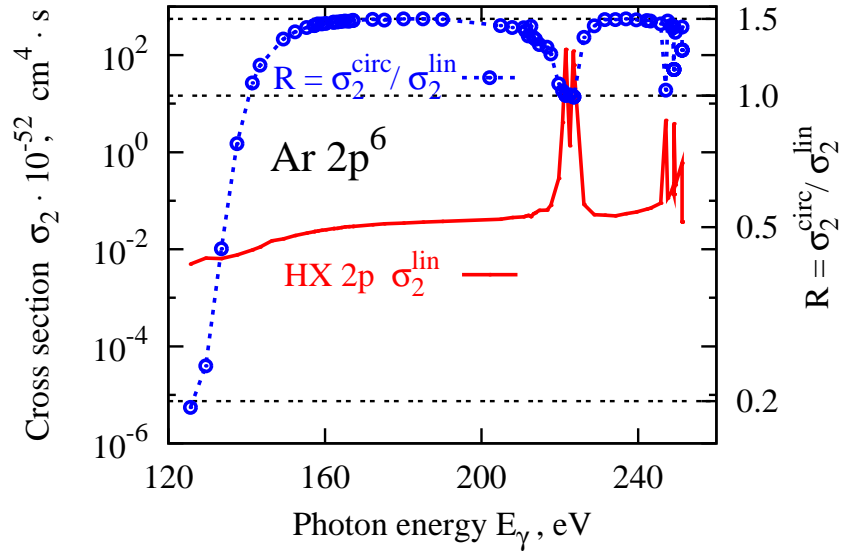


Figure 4.5: Two-photon ionization cross section σ_2^{lin} and polarization ratio $R = \sigma_2^{\text{circ}}/\sigma_2^{\text{lin}}$ versus photon energy for $2p^6$ subshell of argon.

$$\begin{aligned}
 p &\rightarrow d \rightarrow f, \\
 p &\rightarrow d \rightarrow p, \\
 p &\rightarrow s \rightarrow p.
 \end{aligned}
 \tag{4.29}$$

Since, there are two allowed symmetries in the intermediate states, two series of resonances are available: $p \rightarrow ns$ and $p \rightarrow nd$ series.

In case of argon $2p^6$ subshell, the $2p \rightarrow nd$ resonances are strongly shifted to the edge. Therefore, they are hardly resolvable. In contrast, the $2p \rightarrow ns$ resonances are less shifted and form the highest peaks in cross section $\sigma_2(2p^6)$ Figure 4.5. However, the only $2p \rightarrow 3s$ resonance is placed far off the L_2 -edge. The height of this resonance is governed by the width of $2p$ level $\Gamma(L_2, L_3) = 0.13$ eV. The cross section on $2p \rightarrow 3s$ resonance reaches about $2 \cdot 10^3$ times as larger value as typical non-resonance cross section.

4.6.4 Polarization dependence of subshell cross sections

As I have seen above, two-photon ionization cross sections strongly depend on the photon energy E_γ . Apart from this, cross sections depend also on the polarization of light. For instance, as I mentioned already in Subsection 4.6.2, the polarization ratio $R = \sigma_2^{\text{circ}}/\sigma_2^{\text{lin}}$ for $1s^2$ subshell shows a typical hydrogenic dependence on the photon energy (see Figure 4.3). It means that the polarization ratio has an almost constant value $R \approx 1.5$ in the non-resonance range and the deep holes between resonances.

Such behavior can be explained if one considers the properties of (two-photon) electric dipole channels with s -initial-symmetry

$$\begin{aligned}
s &\rightarrow p \rightarrow d, \\
s &\rightarrow p \rightarrow s.
\end{aligned}
\tag{4.30}$$

Both channels are open in case of linearly polarized radiation, while only $s \rightarrow p \rightarrow d$ channel is open in case of circularly polarized light. Moreover, second-order amplitudes of both channels vanish at a certain photon energies between resonances. These circumstances necessarily lead to a zero value of the cross section σ_2^{circ} between resonances, but the cross section σ_2^{lin} does not usually vanish. The latter circumstance takes place almost throughout because the second-order amplitudes of different channels turn to zero usually at *different photon energies*. The vanishing of the cross section σ_2^{circ} and non-vanishing of the cross section σ_2^{lin} determines minimum values of polarization ratio ($R_{\text{min}} = 0$ in electric dipole approximation) which locate between resonances.

In case of $2s^2$ initial subshell, the polarization ratio has a deep gap also at the beginning of the dominant range (see Figure 4.4). This can be explained if one again pays attention to the $2s \rightarrow 2p \rightarrow \varepsilon d$ term in second-order amplitude (2.23). The "resonant energy" of this term lies below the dominant range (see Table 4.2), but the second-order amplitude vanishes in the dominant range.

Polarization ratio for $2p^6$ initial subshell is shown in the Figure 4.5. Behavior of this ratio differs significantly to that of $1s^2$ and $2s^2$ subshells. The polarization ratio for $2p^6$ initial subshell has a flat plateau between resonances. There is nowhere holes between resonances, but small dips with value $R = 1.0$ *on the resonances*. The reason for such behavior consist therein that all electric dipole channels (4.29) *remain open* both for linearly as well as for circularly polarized light.

At the beginning of the dominant range, the polarization ratio for $2p^6$ subshell has a steep descent. The origin of this descent can be understood if one considers the contribution of electric dipole channels (4.29) to the two-photon cross section.

Although, every channel is open, the contribution of channels to the cross section is certainly different. Furthermore, this contribution depends on polarization of light. For instance, the $p \rightarrow d \rightarrow p$ channel contributes to the σ_2^{lin} approximately 70 times stronger than to the σ_2^{circ} , while the $p \rightarrow s \rightarrow p$ channel contributes equally in case of either circularly or linearly polarized light.

Figure 4.6 shows a *particular total cross section* $\sigma_2^{\text{lin}}(\text{channel})$ for linearly polarized radiation. The particular total cross section is calculated following the Formula (4.2) in which only matrix elements of corresponding channel are left. As one can see, the $p \rightarrow d \rightarrow p$ channel is the strongest at the beginning of the dominant range. Moreover, since the contribution of $p \rightarrow d \rightarrow p$ channel to the cross section σ_2^{lin} is approximately 70 times stronger than to the σ_2^{circ} , the polarization ratio R is strongly affected at the beginning of dominant range.

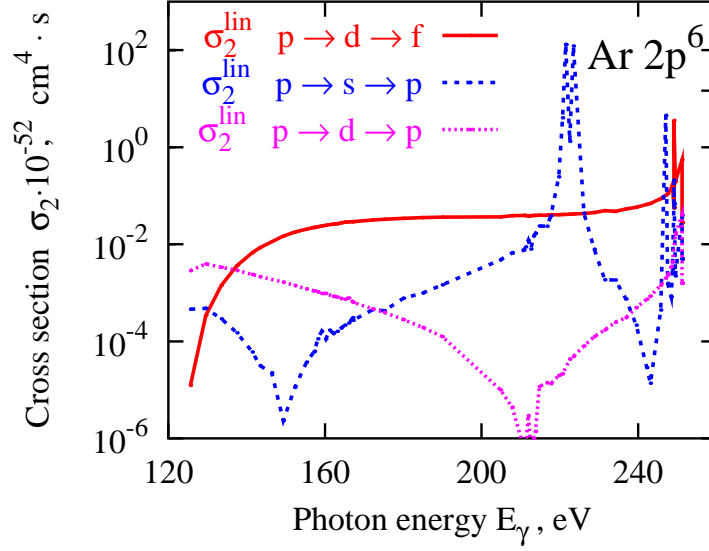


Figure 4.6: Particular two-photon cross sections σ_2 for linearly polarized light versus photon energy for $2p^6$ subshell of argon.

4.7 Conclusion

In this Chapter I studied the many-electron effects arising in the two-photon ionization. First, I presented single-active-electron approximation as a simple model which is able to assess the effects of electron-electron interaction. Second, I developed a Dirac-central-field Green's function as an accurate means to perform the summation over whole spectrum. Next, I compared the cross sections calculated within the SAE approximation with different mean fields and chose the Hartree-plus-statistical-exchange potential as a best model for the atomic field.

Finally, I performed the calculation on the two-photon ionization of inner-shells of argon atom. I compared the hydrogen-like and the HX-models of $1s^2$, $2s^2$ and $2p^6$ subshells of argon atom in order to estimate the influence of many-electron effects on the two-photon total ionization cross section. While both models issue similar cross sections for the K-shell, they are significantly different in case of the L-shell. This allows us to assess the exchange correlation effects as important for the L-shell and negligible for the K-shell. Furthermore, I discussed a quite anomalous behavior of polarization ratio in case of $2p^6$ initial subshell. This behavior and a rather large cross section $\sigma_2(2p^6)$ make the L-shell an interesting candidate for an experimental study.

Chapter 5

Summary and Outlook

In this thesis I have studied the two-photon ionization process in heavy atomic systems. I considered the ionization on the basis of Dirac equation, which was treated by means of the second-order perturbation theory. The infinite summation over the whole atomic spectrum, which arise in second-order perturbation theory, has been calculated by means of a *Green's function method*. The Green's function method requires the computation of different Green's functions: a Coulomb Green's function for the hydrogenic atom and a central-field Green's function for the many-electron atoms. With the aid of these Green's functions, I studied the two-photon ionization in a number of atomic systems:

- hydrogen-like ions in order to reveal the importance of *relativistic* and *multipole effects*,
- outer-shell of lithium atom, helium atom and helium-like neon in ground state in order to choose a suitable model for the atomic mean-field,
- K- and L-shells of argon atom in order to assess the *many-particle effects*.

Concluding, relativistic effects result in a *general decrease* of the two-photon cross section. Herewith, a factor of two difference was obtained in total cross section of hydrogen-like uranium ion. Apart from this relativistic *contraction*, a relativistic *splitting* of the intermediate p levels starts to be visible in the heavy ions from $Z_{\text{nuc}} \approx 50$. In contrary to the relativistic effects, the multipole effects almost do not affect the total cross section, i. e. even a long-wavelength approximation works well in calculations of the two-photon total cross sections.

In contrast to the two-photon total cross section, the *differential cross section* is influenced by relativistic effects on a more impressive manner: depending on the photon energy, the shape of the electron angular distribution can change *qualitatively*. Moreover, the multipole effects show up strongly since the higher multipoles can change the electronic yield by a factor of three.

The many-particle effects in the two-photon ionization were analyzed by means of the K- and L-shells of argon atom. The total cross sections have been calculated in a single-active-electron (SAE) approximation. It was found that the electron-electron interaction results in a significant change of L-shell cross section, but not K-shell cross section. It means that, the total cross section of the two-photon ionization of K-shell can be calculated within a SAE

approximation with a pure Coulomb field, while in case of L-shell a SAE approximation with a Hartree-plus-statistical-exchange potential or even a more sophisticated model is required. Apart from this, the ionization of the L-shell electrons brings into play an initial subshell with p symmetry. The cross section of argon $2p$ subshell shows a quite unusual dependence on the photon energy and on the polarization of light. These dependencies were elucidated analyzing the contribution of the *electric dipole channels* to the total ionization cross section.

The results for hydrogenic atom had been obtained by means of a Dirac-Coulomb Green's function which is well known from the literature. In contrary, the results for the many-electronic atoms have been obtained with a Dirac-central-field Green's function which has been calculated by means of a numerical algorithm. This numerical algorithm was originally invented by McGuire (1981) for a Schrödinger-central-field Green's function. In this work, the McGuire's algorithm was extended *on the relativistic framework*. Our algorithm uses the *Kummer and Tricomi functions* which are computed by means of a *reliable* but yet rather slow program.

The slowness of our program limits the range of the problems which can be efficiently solved by means of our implementation of the central-field Green's function. In principle, the central-field Green's function can be used in all the problems which require a summation over the whole atomic spectrum.

One can mention here few possible tasks for the central-field Green's function

- Calculation of two-photon decay rates,
- Calculation of two-photon excitation and ionization cross sections,
- Calculation of multi-photon excitation/ionization cross sections,
- Construction of an atomic many-electron Green's function.

Amongst these tasks, only the first two could be solved within a reasonable time. For the latter two tasks, our implementation is too slow and must be further improved.

In order to *improve the efficiency* of the central-field Green's function, I suggest to explore the advantages of a *Sturmian basis set*, i. e. to expand the central-field Green's function on an appropriate Sturmian basis set. The Sturmian basis set allows to expand the Green's function over *bound-like functions* (Avery and Avery 2003, and Szmytkowski 1997) and allows to use the one-dimensional integration for the radial matrix elements calculation. The usage of the one-dimensional functions in the radial integrals will certainly lower the *memory requirements* to store the central-field Green's function and may *increase the speed* of calculation of the radial matrix elements. Moreover, one can hope it will be possible to use a *purely numerical algorithm* for the calculation of the radial parts of Dirac-central-field Sturmians.

Zusammenfassung

In dieser Arbeit wurde die *Zweiphotonenionisierung* schwerer atomarer Systeme studiert. Die Ionisierung wurde im Rahmen der Störungstheorie zweiter Ordnung mit der Dirac-Gleichung behandelt. Die Summation über des vollständige Spektrum des Atoms, die in der Störungstheorie zweiter Ordnung vorkommt, wurde mit Hilfe der Greenschen Funktion Methode berechnet. Die Methode der Greenschen Funktion verlangt die Berechnung der unterschiedlichen Greenschen Funktionen: eine Coulomb-Greensche-Funktion im Fall von wasserstoffähnlichen Ionen und eine Zentral-feld-Greensche-Funktion im Fall des Vielelektronen-Atoms. Die entwickelte Greensche Funktion erlaubte uns die folgenden atomaren Systeme in die Zweiphotonenionisierung der folgenden atomaren Systeme zu untersuchen:

- wasserstoffähnliche Ionen, um relativistische und Multipol-Effekte aufzudecken,
- die äußere Schale des Lithium; Helium und Helium-ähnliches Neon im Grundzustand, um taugliche Modelle des atomaren Feldes zu erhalten,
- K- und L-Schalen des Argon, um die Vielelektronen-Effekte abzuschätzen.

Zusammenfassend, die relativistische Effekte ergeben sich in einer allgemeinen Reduzierung der Zweiphotonen Wirkungsquerschnitte. Zum Beispiel, beträgt das Verhältnis zwischen den nichtrelativistischen und relativistischen Wirkungsquerschnitten einen Faktor zwei für wasserstoffähnliches Uran. Außer dieser *relativistischen Kontraktion*, ist auch die relativistische *Aufspaltung* der Zwischenzustände für mittelschwere Ionen sichtbar. Im Gegensatz zu den relativistischen Effekten, beeinflussen die Multipol-Effekte die totalen Wirkungsquerschnitte sehr wenig, so daß die *Langwellennäherung* mit der exakten Näherung für schwere Ionen sogar innerhalb von 5% übereinstimmt.

Die winkelaufgelösten Wirkungsquerschnitte werden durch die relativistischen Effekte auf eine beeindruckende Weise beeinflusst: die Form der differentiellen Wirkungsquerschnitte ändert sich (qualitativ) abhängig von der Photonenenergie. Außerdem kann die Berücksichtigung der höheren Multipole die elektronische Ausbeute um einen Faktor drei ändern.

Die Vielelektronen-Effekte in der Zweiphotonenionisierung wurden am Beispiel der K- und L-Schalen des Argon analysiert. Hiermit wurden die totalen Wirkungsquerschnitte in einer *Ein-aktives-Elektron-Näherung* (*single-active-electron approximation*) berechnet. Es hat sich herausgestellt, daß die Elektron-Elektron-Wechselwirkung sehr wichtig für die L-Schale und vernachlässigbar für die K-Schale ist. Das bedeutet, daß man die totalen Wirkungsquerschnitte mit wasserstoffähnlichen Modellen im Fall der K-Schale beschreiben kann, aber für die L-Schale fortgeschrittene Modelle erforderlich sind.

Die Ergebnisse für Vielelektronen-Atome wurden mittels einer Dirac-Zentral-feld-Greenschen Funktion erlangt. Ein numerischer Algorithmus wurde ursprünglich von McGuire (1981) für der Schrödinger-Zentral-feld-Greensche Funktion eingeführt. Der Algorithmus wurde in dieser Arbeit zum ersten Mal für die Dirac-Gleichung angewandt. Unser Algorithmus benutzt die Kummer- und Tricomi-Funktionen, die mit Hilfe eines zuverlässigen, aber noch immer langsamen Programmes berechnet wurden.

Die Langsamkeit des Programms begrenzt den Bereich der Aufgaben, die effizient gelöst werden können. Die Zentral-feld-Greensche Funktion konnte bei den folgenden Problemen benutzt werden:

- Berechnung der Zweiphotonen-Zerfallsraten,
- Berechnung der Zweiphotonenanregung und -ionisierungs-Wirkungsquerschnitte,
- Berechnung die Multiphotonenanregung und -ionisierungs-Wirkungsquerschnitte,
- Berechnung einer atomaren Vielelektronen-Green-Funktion.

Von diesen Aufgaben können nur die ersten beiden in angemessener Zeit gelöst werden. Für die letzten beiden Aufgaben ist unsere Implementierung zu langsam und muss weiter verbessert werden.

Appendix A

One-electron radiative matrix elements of first- and second-order

A.1 First-order radiative matrix element

The transition probability for an one-electron atomic system to jump from an initial state ψ_α to a final state ψ_β and absorb one photon is proportional to the square of a *radiative first-order matrix element* $M_{\beta\alpha}^1$. Most general form of this matrix element can be found in Grant (1974). In this section, I am going to present the formulas for the first-order matrix element $M_{\beta\alpha}^1$ as it was given by Grant and rearrange them to a new form which is more appropriate to extend to the case of two-photon absorption. The first-order matrix element $M_{\beta\alpha}^1$ reads (Grant 1974, and Goldman and Drake 1981)

$$M_{\beta\alpha}^1 = \int (P_\beta(r) \Omega_{\kappa_\beta}^{m_\beta\uparrow}(\mathbf{n}), -iQ_\beta(r) \Omega_{-\kappa_\beta}^{m_\beta\uparrow}(\mathbf{n})) \tilde{A}_\lambda^* \begin{pmatrix} P_\alpha(r) \Omega_{\kappa_\alpha}^{m_\alpha}(\mathbf{n}) \\ iQ_\alpha(r) \Omega_{-\kappa_\alpha}^{m_\alpha}(\mathbf{n}) \end{pmatrix} dr d\mathbf{n}, \quad (\text{A.1})$$

where the transition operator \tilde{A}_λ^* reads

$$\tilde{A}_\lambda^* = \boldsymbol{\alpha}(\mathbf{u}_\lambda + G \mathbf{k}_\lambda) e^{-i\mathbf{k}_\lambda \mathbf{r}} - G e^{-i\mathbf{k}_\lambda \mathbf{r}}, \quad (\text{A.2})$$

where, in turn, \mathbf{u}_λ is a polarization vector, \mathbf{k}_λ is a photon momentum operator, and G is an arbitrary gauge parameter.

The operator \tilde{A}_λ^* (A.2) possesses a partial-wave expansion

$$\tilde{A}_\lambda^* = \sum_{LMq} [\mathbf{e}_\lambda \cdot \mathbf{Y}_{LM}^{(q)}(\mathbf{k}_\lambda)] \tilde{a}_{LM}^{(q)}(r)^*, \quad (\text{A.3})$$

where \mathbf{e}_λ is now an arbitrary polarization vector (not necessary transverse). $\mathbf{Y}_{LM}^{(q)}(\mathbf{k}_\lambda)$ are electric ($q = 1$), magnetic ($q = 0$) and longitudinal ($q = -1$) multipoles by Varshalovich *et al* 1989 and the matrix element $\langle \beta | \tilde{a}_{LM}^{(q)}(r)^* | \alpha \rangle$ is given by

$$\begin{aligned} \langle \beta | \tilde{a}_{LM}^{(q)}(r)^* | \alpha \rangle &= (-1)^{j_\alpha - m_\alpha} \begin{pmatrix} j_\alpha & L & j_\beta \\ -m_\alpha & M & m_\beta \end{pmatrix} (-i)^{L+q-1} (-1)^{j_\beta - 1/2} \left(\frac{4\pi}{2L+1} \right)^{1/2} \times \\ &\times [j_\alpha, j_\beta]^{1/2} \begin{pmatrix} j_\alpha & L & j_\beta \\ 1/2 & 0 & -1/2 \end{pmatrix} \Pi(\kappa_\beta, L, q, \kappa_\alpha) \overline{M}_{\beta\alpha}^{q,L}, \end{aligned} \quad (\text{A.4})$$

where the radial matrix elements $\overline{M}_{\beta\alpha}^{q,L}$ are defined to

$$\overline{M}_{\beta\alpha}^{1,L} = \left(\frac{L}{L+1} \right)^{1/2} [(\kappa_\alpha - \kappa_\beta) I_{L+1}^+ + (L+1) I_{L+1}^-] - \left(\frac{L+1}{L} \right)^{1/2} [(\kappa_\alpha - \kappa_\beta) I_{L-1}^+ - L I_{L-1}^-], \quad (\text{A.5})$$

$$\overline{M}_{\beta\alpha}^{0,L} = \frac{(2L+1)}{[L(L+1)]^{1/2}} (\kappa_\alpha + \kappa_\beta) I_L^+, \quad (\text{A.6})$$

$$\overline{M}_{\beta\alpha}^{-1,L} = -G[(2L+1) J_L + (\kappa_\alpha - \kappa_\beta)(I_{L+1}^+ + I_{L-1}^+) - L I_{L-1}^- + (L+1) I_{L+1}^-], \quad (\text{A.7})$$

$$I_L^\pm = \int_0^\infty (P_\alpha Q_\beta \pm Q_\alpha P_\beta) j_L(kr) dr, \quad (\text{A.8})$$

$$J_L = \int_0^\infty (P_\alpha P_\beta + Q_\alpha Q_\beta) j_L(kr) dr. \quad (\text{A.9})$$

The parity factor $\Pi(\kappa_\beta, L, q, \kappa_\alpha)$ is defined to

$$\Pi(\kappa_\beta, L, q, \kappa_\alpha) = \begin{cases} (-1)^{L+1}, & \text{if } q = 1 \text{ and } L + l_\beta + l_\alpha \text{ is odd;} \\ (-1)^L, & \text{if } q = 0 \text{ and } L + l_\beta + l_\alpha \text{ is even;} \\ 0, & \text{otherwise.} \end{cases} \quad (\text{A.10})$$

where l_α and l_β are orbital momenta defined to

$$l = \begin{cases} \kappa, & \text{if } \kappa > 0; \\ -\kappa - 1, & \text{if } \kappa < 0. \end{cases}$$

Explicitly written, the matrix element $M_{\beta\alpha}^1$ (A.1) takes the form

$$M_{\beta\alpha}^1 = \sum_{LMq} [e_\lambda \cdot \mathbf{Y}_{LM}^{(q)}(\mathbf{k}_\lambda)] \langle \beta | \tilde{a}_{LM}^{(q)}(r)^* | \alpha \rangle. \quad (\text{A.11})$$

I will rewrite the matrix element $\overline{M}_{\beta\alpha}^{q,L}$ Equations (A.5, A.6, A.7) using a more general radial matrix element

$$R_{\beta\Lambda\alpha}^{T_\beta T_\alpha} = \int_0^\infty g_\beta^{T_\beta}(r) j_\Lambda(kr) g_\alpha^{T_\alpha}(r) dr, \quad (\text{A.12})$$

instead of I_L^\pm and J_L radial integrals (A.8, A.9). The subscripts T_β and T_α in latter formula controls which components of radial spinor (large $T = 1$ or small $T = -1$) appear in the radial integral $R_{\beta\Lambda\alpha}^{T_\beta T_\alpha}$

q	r	T_β	T_α	$C_{T_\beta T_\alpha}^{qr}(\beta, L, \alpha, G)$
-1	-1	1	-1	$G(-\kappa_\alpha + \kappa_\beta - L)$
-1	-1	-1	1	$G(-\kappa_\alpha + \kappa_\beta + L)$
-1	0	-1	-1	$-G(2L + 1)$
-1	0	1	1	$-G(2L + 1)$
-1	1	1	-1	$G(-\kappa_\alpha + \kappa_\beta + L + 1)$
-1	1	-1	1	$G(-\kappa_\alpha + \kappa_\beta - L - 1)$
0	0	1	-1	$\frac{(2L+1)(\kappa_\alpha+\kappa_\beta)}{\sqrt{(L(L+1))}}$
0	0	-1	1	$\frac{(2L+1)(\kappa_\alpha+\kappa_\beta)}{\sqrt{(L(L+1))}}$
1	-1	1	-1	$\sqrt{\frac{L+1}{L}}(-\kappa_\alpha + \kappa_\beta - L)$
1	-1	-1	1	$\sqrt{\frac{L+1}{L}}(-\kappa_\alpha + \kappa_\beta + L)$
1	1	1	-1	$\sqrt{\frac{L}{L+1}}(\kappa_\alpha - \kappa_\beta - L - 1)$
1	1	-1	1	$\sqrt{\frac{L}{L+1}}(\kappa_\alpha - \kappa_\beta + L + 1)$

Table A.1: Nonzero values of $C_{T_\beta T_\alpha}^{qr}(\beta, L, \alpha, G)$

$$g_\alpha^1(r) = P_\alpha(r), \quad g_\alpha^{-1}(r) = Q_\alpha(r).$$

By means of new radial matrix element $R_{\beta\Lambda\alpha}^{T_\beta T_\alpha}$, the matrix element $\overline{M}_{\beta\alpha}^{q,L}$ can be rewritten as an uniform sum

$$\overline{M}_{\beta\alpha}^{q,L} = \sum_{r=-1}^{+1} \sum_{T_\beta T_\alpha} C_{T_\beta T_\alpha}^{qr}(\beta, L, \alpha, G) R_{\beta L+r\alpha}^{T_\beta T_\alpha}, \quad (\text{A.13})$$

where nonzero values of the coefficient $C_{T_\beta T_\alpha}^{qr}(\beta, L, \alpha, G)$ are given in the Table A.1.

A.2 Second-order radiative matrix element

The transition probability for an one-electron atomic system to jump from an initial state ψ_α to a final state ψ_β and absorb two photons is proportional to the square of a second-order radiative transition matrix element $M_{\beta\alpha}^2$. In terms of the first-order matrix element $M_{\beta\alpha}^1$ (A.1), the second-order matrix element is given by a perturbative sum over complete one-electron spectrum

$$M_{\beta\alpha}^2 = \sum_{\nu}^f \frac{M_{\beta\nu}^1 M_{\nu\alpha}^1}{E_\nu - E}. \quad (\text{A.14})$$

Sum over complete spectrum of atomic system includes both a sum over discrete and an integral over the continuum spectrum. The integral over continuum spectrum affects only the radial part of second-order matrix element $M_{\beta\alpha}^2$ since the angular component contains only discrete indexes κ and m . The continuum part of spectrum will be taken into account with

the Green's function method (see Chapter 2). I will rewrite the second-order transition matrix element $M_{\beta\alpha}^2$ (Goldman and Drake 1981) with a more general radial matrix element, which will be defined on an analogous manner as for first-order radial matrix element (A.12). The matrix element to be considered reads (Goldman and Drake 1981)

$$M_{\beta\alpha}^2 = \sum_{\nu, \text{ all } LMq} \frac{[e_{\lambda_2} \cdot \mathbf{Y}_{L_2 M_2}^{(q_2)}(\mathbf{k}_{\lambda_2})][e_{\lambda_1} \cdot \mathbf{Y}_{L_1 M_1}^{(q_1)}(\mathbf{k}_{\lambda_1})] \langle \beta | \tilde{a}_{L_2 M_2}^{(q_2)}(r)^* | \nu \rangle \langle \nu | \tilde{a}_{L_1 M_1}^{(q_1)}(r')^* | \alpha \rangle}{E_\nu - E}, \quad (\text{A.15})$$

where sum over intermediate states ν can be separated

$$\begin{aligned} & \sum_{\nu} \frac{\langle \beta | \tilde{a}_{L_2 M_2}^{(q_2)}(r)^* | \nu \rangle \langle \nu | \tilde{a}_{L_1 M_1}^{(q_1)}(r')^* | \alpha \rangle}{E_\nu - E} = \\ & = \sum_{\kappa_\nu m_\nu} (-1)^{j_\beta - m_\beta} \begin{pmatrix} j_\nu & L_2 & j_\beta \\ -m_\nu & M_2 & m_\beta \end{pmatrix} (-i)^{L_2 + q_2 - 1} (-1)^{j_\beta - 1/2} \left(\frac{4\pi}{2L_2 + 1} \right)^{1/2} [j_\beta, j_\nu]^{1/2} \times \\ & \times \begin{pmatrix} j_\nu & L_2 & j_\beta \\ 1/2 & 0 & -1/2 \end{pmatrix} (-1)^{j_\nu - m_\nu} \begin{pmatrix} j_\alpha & L_1 & j_\nu \\ -m_\alpha & M_1 & m_\nu \end{pmatrix} (-i)^{L_1 + q_1 - 1} (-1)^{j_\nu - 1/2} \left(\frac{4\pi}{2L_1 + 1} \right)^{1/2} \times \\ & \times [j_\nu, j_\alpha]^{1/2} \begin{pmatrix} j_\alpha & L_1 & j_\nu \\ 1/2 & 0 & -1/2 \end{pmatrix} \Pi(\kappa_\beta, L_2, q_2, \kappa_\nu) \Pi(\kappa_\nu, L_1, q_1, \kappa_\alpha) \overline{M}_{\beta\nu\alpha}^{q_2 L_2; q_1 L_1}, \quad (\text{A.16}) \end{aligned}$$

where the second-order matrix element $\overline{M}_{\beta\nu\alpha}^{q_2 L_2; q_1 L_1}$ can be written in form of a sum

$$\overline{M}_{\beta\nu\alpha}^{q_2 L_2; q_1 L_1} = \sum_{r_2 r_1} \sum_{\text{all } T} C_{T_\beta T_{2\nu}}^{q_2 r_2}(\beta, L_2, \nu, G) C_{T_{1\nu} T_\alpha}^{q_1 r_1}(\nu, L_1, \alpha, G) U_{\beta L_2 + r_2 \nu L_1 + r_1 \alpha}^{T_\beta T_{2\nu} T_{1\nu} T_\alpha}. \quad (\text{A.17})$$

The second-order radial matrix element $U_{\beta L_2 \nu L_1 \alpha}^{T_\beta T_{2\nu} T_{1\nu} T_\alpha}$ is defined to

$$U_{\beta L_2 \nu L_1 \alpha}^{T_\beta T_{2\nu} T_{1\nu} T_\alpha} = \int_0^\infty \int_0^\infty g_\beta^{T_\beta}(r) j_{L_2}(k_2 r) g_\nu^{T_{2\nu} T_{1\nu}}(r, r') j_{L_1}(k_1 r') g_\alpha^{T_\alpha}(r') dr dr' \quad (\text{A.18})$$

and a radial Green's function $g_\nu^{T_{2\nu} T_{1\nu}}(r, r')$ is defined in Section 4.3.

Appendix B

Calculation of Kummer and Tricomi functions by means of a self-validation algorithm

The radial part of central-field Green's function can be obtained with a numerical algorithm. The algorithm, which I implemented, requires an accurate computation of two confluent hypergeometric functions: regular at the origin ${}_1F_1(a, b; z) \equiv M(a, b, z)$ or Kummer function and regular at the infinity $U(a, b, z)$ or Tricomi function. Since, the algorithm uses a *general solution* (4.21) and (4.22) within a wide range of parameters, the range of arguments of Kummer and Tricomi functions is also very wide. Hence, Kummer and Tricomi functions have to be calculated very reliable even the efficiency of algorithm is affected.

In this chapter, I will detail the calculation of Kummer and Tricomi functions. First, I show standard formulae from Abramowitz and Stegun (1965) to define the mathematical background of our algorithm. Second, I discuss a simple algorithm for Kummer function by Thompson (1997). Pointing to lacks of this algorithm, I come to a better solution. Third, I describe the calculation of Tricomi function. Since in computation of Tricomi function the Kummer function is used, the highest precision and reliability of Kummer function is required. In order to ensure this precision and reliability, I found a *self-validation arithmetics* as only means to handle the problem. Finally, I will show algorithms for Kummer and Tricomi functions in the form of graphs and discuss them.

B.1 Mathematical formulae for Kummer and Tricomi functions

Both Kummer and Tricomi functions satisfy the differential equation

$$z \frac{d^2 M}{dz^2} + (b - z) \frac{dM}{dz} - aM = 0 \quad (\text{B.1})$$

with border conditions $M(a, b, z \rightarrow 0) \rightarrow 0$ and $U(a, b, z \rightarrow \infty) \rightarrow 0$.

In computation practice, there is convenient to calculate the Kummer function $M(a, b, z)$

with well known hypergeometric series

$$M(a, b, z) = 1 + \frac{a}{b} z + \frac{a(a+1)}{b(b+1)} z^2 + \frac{(a)_n}{(b)_n} z^n \dots \quad (\text{B.2})$$

where $(a)_n$ denotes Pochhammer symbols and Tricomi function $U(a, b, z)$ with an linear independent to $M(a, b, z)$ combination

$$U(a, b, z) = \frac{\pi}{\sin \pi b} \left[\frac{M(a, b, z)}{\Gamma(1+a-b)\Gamma(b)} - z^{1-b} \frac{M(a+1-b, 2-b, z)}{\Gamma(a)\Gamma(2-b)} \right], \quad (\text{B.3})$$

Additionally, when b is an integer number, the later expression is invalid because $\Gamma(2-b)$ or $\Gamma(b)$ receive negative integer argument for which Gamma function is not defined. In this case, one uses a logarithmic series in order to calculate the regular at the infinity function $U(a, b, z)$

$$U(a, n+1, z) = \frac{(-1)^{n+1}}{n!\Gamma(a-n)} \left\{ \sum_{k=0}^{\infty} \frac{(a)_k z^k}{(n+1)_k k!} [\psi(a+k) - \psi(1+k) - \psi(1+n+k)] + \right. \\ \left. + \ln(z) \sum_{k=0}^{\infty} \frac{(a)_k z^k}{(n+1)_k k!} \right\} + \frac{(n-1)!}{\Gamma(a)} \sum_{k=0}^{n-1} \frac{(a-n)_k}{(1-n)_k k!} z^{-n+k}, \quad (\text{B.4})$$

where $n = 0, 1, 2, \dots$ and the last sum is zero when $n = 0$.

Another formulae concern the asymptotic expansions. They are useful when $|z| \rightarrow \infty$

$$M(a, b, z) = \frac{\Gamma(b)}{\Gamma(a)} e^z z^{a-b} \left[\sum_{k=0}^{S-1} \frac{(b-a)_k (1-a)_k}{k! z^k} + O(|z|^{(-S)}) \right] + \\ + \frac{\Gamma(b) z^{-a}}{\Gamma(b-a)} e^{\pm i\pi a} z^{a-b} \left[\sum_{k=0}^{R-1} \frac{(a)_k (1+a-b)_k}{k! (-z)^k} + O(|z|^{(-R)}) \right], \quad (\text{B.5})$$

where '+' is taken if $\pi/2 < \arg(z) < 3\pi/2$ and '-' is taken if $-3\pi/2 < \arg(z) \leq -\pi/2$.

$$U(a, b, z) = z^{-a} \left[\sum_{k=0}^{R-1} \frac{(a)_k (1+a-b)_k}{k! (-z)^k} + O(|z|^{(-R)}) \right], \quad (\text{B.6})$$

$$\left(-\frac{3\pi}{2} < \arg(z) < \frac{3\pi}{2} \right).$$

Last formulae concern a *Kummer transformation*. They allow "to reflect" the calculation with respect to third argument z

$$M(a, b, z) = e^z M(b-a, b, -z) \quad (\text{B.7})$$

$$U(a, b, z) = z^{1-b} U(1+a-b, 2-b, -z). \quad (\text{B.8})$$

B.2 Round-off error in the realization of numerical algorithms

Although the latter set of formulae can be easily programmed, it is difficult to write an algorithm which calculates the confluent hypergeometric functions in a wide range of arguments. One can find many textbooks which deal either algorithms (Luke 1977, and Spanier and Keith 1987) or even computer programs (Zhang and Jin 1996, and Thompson 1997) to calculate the Kummer and Tricomi functions. However, all these algorithms had been found insufficient to calculate the Kummer and Tricomi functions safely. Main reason of the unreliability lies in realization of floating point arithmetics in a computer program. A *double precision variable*, realized on all the computer platforms, provides a relative uncertainty $\varepsilon = (\Delta a)/|a|$ about 10^{-16} . Hence, if one subtracts two variables which are, for example, up to 10 positions equal, then the uncertainty of result will amount already only 10^{-6} . This *round-off error* is a main obstacle in building of a reliable routine for Kummer and Tricomi functions. It affects all algorithms which are realized in a computer program. However, there is a tool available by means of which one can reliably treat the round-off errors. The tool calls *self-validation*. It will be explained below, together with algorithm for computing of Kummer function.

B.3 Self-validation algorithm for the computation of the Kummer function

A simplest method to calculate the Kummer function is to sum up the hypergeometric series (B.2) up to a T_n -th term which is small enough comparing with the calculated sum $S = \sum_n T_n$

$$|T_n|/|S| < \varepsilon, \quad (\text{B.9})$$

where ε represents a *desired accuracy*.

This method has two serious lacks. First, quite obvious lack, the round-off error can easily exceed the accuracy estimation $|T_n|/|S|$. Second, *convergency problem*, the inequality (B.9) can be fulfilled for a certain term T_p , or even for a group of terms $T_p \dots T_q$, although higher terms $T_r \dots T_s$ could have a much larger magnitude and contribute to the hypergeometric sum significantly.

To solve the round-off problem, Thompson (1997) had suggested to restrict the hypergeometric series to 1000 terms without taking into account the magnitude of following terms. With this method, he limited the round-off errors, although they still can affect the final result. The second, convergency problem, is not at all taken into account in Thompson's algorithm. As a consequence, this algorithm could not be successfully used in our program for a computation of any Green's function.

The convergency problem is solved in the handbook by Spanier and Keith (1987). They pointed to the condition for a term T_J in hypergeometric series, after which all terms have a falling magnitude

$$J > 2|a| + |b| + 1 \quad \text{and} \quad |T_J| < |T_{J-1}|. \quad (\text{B.10})$$

I will use this convergency criterion later on in our algorithm.

In order to control the round-off error, one must calculate this error together with each arithmetic operation. Although, such *self-validation* looks superfluous, it provides (a) the *most reliable* estimation of computation accuracy and (b) allows to obtain the *most exact* result which is possible within a floating point arithmetic within a given algorithm. Both these properties are needful when the result of computation is used again in another computation. For instance, if one computes Tricomi function by formula (B.3), then one often meets an unpleasant situation when summands in square brackets have almost equal magnitude but different signs. This round-off danger can be recognized in only case if one has a reliable estimation of accuracy for both terms. Moreover, most exact result for Tricomi function can be obtained if one has a highest possible precision of each Kummer function.

Theory behind *self-validation algorithms* calls "Theory of uncertainties and error propagation". This theory is well known in experimental physics. An experimentalist always deals with unprecise values of measurements and should predict the precision of result if the arithmetic operations involve unprecise values. The situation in computational physics resembles the calculation of experimental errors, although precision of computer variables is usually much higher than precision of experimental measurements.

Each floating point variable a has its own uncertainty Δa . This uncertainty is equal to the smallest distance between a and a nearest to a floating point number. Uncertainty Δa is similar to the absolute error in experimental physics. Hence, I adopt the experience of experimentalists in dealing with uncertain values. Table B.1 summarizes the simplest rules of error propagation. Here, I consider two variables a and b with uncertainties Δa and Δb in the four arithmetic operations (add, subtract, multiply, and divide) and give the uncertainty of computed result.

Operation	Uncertainty
$c = a + b$	$\Delta c = \Delta a + \Delta b$
$c = a - b$	$\Delta c = \Delta a + \Delta b$
$c = a \times b$	$\Delta c = \Delta a b + \Delta b a $
$c = a \div b$	$\Delta c = (\Delta a b + \Delta b a) / b^2$

Table B.1: Rules of uncertainty propagation in basic arithmetic operations

The other rules of error propagation, for instance in calculation of a trigonometric function, can be derived by means of the differential calculus: one must take a table of derivatives and simply replace each differential by according uncertainty $dx \rightarrow \Delta x$, all other values to their absolute values $x \rightarrow |x|$ and change each subtraction to summation " - " \rightarrow " + ". This prescription is useful when the complex valued variables are to be evaluated and in case of the elementary functions like power, trigonometric, exponential and logarithm functions. If one calculates the—more complex—special functions like Gamma function, Psi function or Tricomi functions, the uncertainties should be calculated (propagated) together with computation of the function. This is because it is often difficult to calculate the derivatives of special functions since they require a calculation of the same or another special functions.

In principle, in order to propagate the uncertainties, one can write for each special function a particular algorithm which would propagate the absolute errors in some additional computer

variables. However, such an *explicit* realization of the self-validation algorithm makes the programs too difficult to write and to debug: even a simple algorithm looks by explicit self-validation very vast.

On another hand, one can realize the uncertainty propagation *implicitly*. It means, that one introduces a new data type—a *self-validation variable*—to represent the value and its uncertainty, define the arithmetic operations and functions for this new data type, and write the algorithms already using these self-validation variables instead of usual floating point variables. Such *implicitly-validated algorithm* does not already look vast, although it will be a self-validated algorithm.

In the program for calculation of Kummer and Tricomi functions, I just accepted the *implicit validation*. Our algorithm for Kummer function looks much simpler (see Figure B.1) than suggested by Luke (1977), Zhang and Jin (1996), or Muller (2001). However, due to the self-validation, this algorithm is stable enough to afford a reliable calculation of either Coulomb- or central-field Green's functions. Moreover, it provides a reliable estimation of the result uncertainty what is crucial if one calculates the Tricomi function using the Kummer functions (B.3).

On the first step, I follow Spanier and Keith (1987) and perform the Kummer transformation (B.7) in order to calculate the Kummer function for negative third argument z . After, I compute the asymptotic expansion (B.5) independently on the magnitude of third argument z . If the asymptotic expansion provides an accuracy less than desired, I calculate the hypergeometric series. The calculation of hypergeometric series runs at least up to the term T_J for which the convergency criterion (B.10) is fulfilled. Further on, I calculate hypergeometric series up to the term T_n when either desired accuracy is achieved $|T_n|/|S| < \varepsilon$ or uncertainty becomes greater than desired accuracy $\Delta S/|S| > \varepsilon$ or uncertainty becomes greater than achieved accuracy $\Delta S/|S| > |T_n|/|S|$. If a desired accuracy is not reached, than I do again Kummer transformation and repeat the outlined algorithm. Finally, the routine returns most accurate result in a self-validation variable.

B.4 Self-validation algorithm for the computation of the Tricomi function

Our algorithm for Tricomi function looks similar to these suggested by Zhang and Jin (1996) and Thompson (1997). It is shown in the Figure B.2.

First, I calculate the asymptotic expansion (B.6). If the accuracy of asymptotic expansion is not sufficient, then I analyze second argument and decide whether linear combination of Kummer functions (B.3) or logarithmic series (B.4) is to be used. If I calculate the linear combination (B.3) of the Kummer functions, I set the desired accuracy to the highest possible ($\varepsilon_{\text{desired}} = 10^{-16}$ in case of double precision and $\varepsilon_{\text{desired}} = 10^{-34}$ in case of quad precision).

After calculation, if the accuracy of Tricomi function is worse than desired, than the same algorithm runs again, but with the Kummer transformation (B.8) at the beginning. Finally, the routine returns the best result in a self-validation variable.

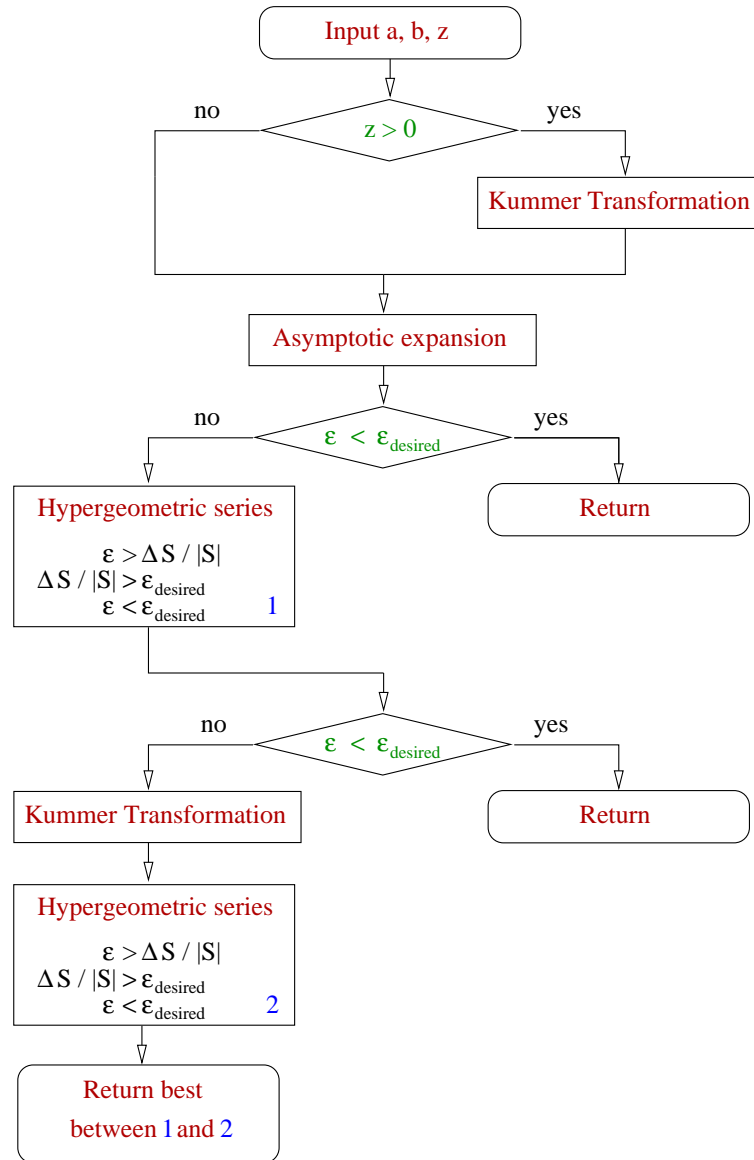


Figure B.1: Self-validation algorithm for computation of Kummer function

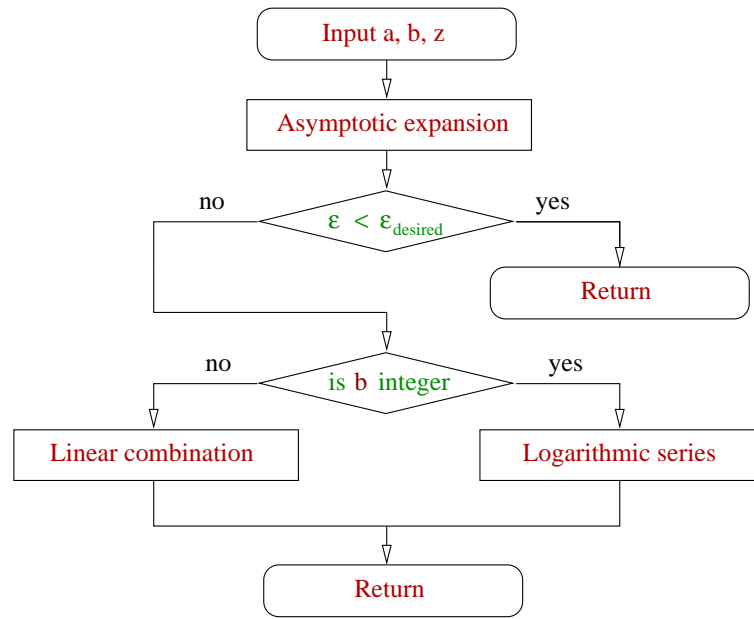


Figure B.2: Self-validation algorithm for computation of Tricomi function

Appendix C

Calculation of Hartree potentials

C.1 Hartree potential

Hartree potential includes a direct-part of Coulomb interaction between nucleus and electron and an average Coulomb interaction between electron and other electrons (Cowan 1981). I calculated this potential out of a multi-configuration expansion of an *atomic state function*

$$\Psi(\Gamma P J M) = \sum_{r=1}^{n_c} c_{r\Gamma} \psi(\gamma_r P J M), \quad (\text{C.1})$$

where $c_{r\Gamma}$ are mixing coefficients and $\psi(\gamma_r P J M)$ represents a *configuration state function*.

Hartree potential is defined for a certain subshell a and reads

$$Z(r)^H = Z_{\text{nuc}} - \sum_b^{\text{all subshells}} (w_b - \delta_{ba}) Y^0(b, b; r), \quad (\text{C.2})$$

where Z_{nuc} is nuclear charge, $Y^k(a, b; r)$ is Hartree function defined to (Dyall *et al* 1989)

$$Y^k(a, b; r) = r \int_0^\infty ds \frac{r_{<}^k}{r_{>}^{k+1}} (P_{n_a \kappa_a}(s) P_{n_b \kappa_b}(s) + Q_{n_a \kappa_a}(s) Q_{n_b \kappa_b}(s)). \quad (\text{C.3})$$

A generalized occupation number w_b in Equation (C.2) depends on mixing coefficients of chosen atomic state function and on the subshell $b = \{n_b, \kappa_b\}$ for which the potential is calculated

$$w_b = \sum_{r=1}^{n_c} \sum_a^{\text{all subshells}} c_{r\Gamma}^2 d_{ra}, \quad (\text{C.4})$$

where d_{ra} are integer occupation numbers of subshell a in configuration r . Delta-symbol δ_{ba} in Equation (C.2) decreases by one the generalized occupation number of subshell a . In this way one "takes out one electron" from the subshell a for which the Hartree potential is calculated.

At the origin, the effective nuclear charge function $Z(r)$ strives to the nuclear charge $Z(r \rightarrow 0) = Z_{\text{nuc}}$, and at the infinity, the effective nuclear charge function $Z(r)$ strives to $Z_{\text{nuc}} - N_e - 1$ where N_e is number of electrons in the atom.

C.2 Hartree-plus-statistical-exchange potential

Hartree-plus-statistical-exchange potential includes the direct part of electrostatic interaction like Hartree potential, and, additionally, it takes approximately a non-local part of Hartree-Fock energy into account. Construction of this potential was described by Cowan (1967, 1981) who introduced also a shortening HX-potential. HX-potential is constructed by adding an *exchange term* $Z_a^{xs}(r)$ to the Hartree potential $Z(r)^H$ (C.2)

$$Z(r)^{HX} = Z_{\text{nuc}} - \sum_b^{\text{all subshells}} (w_a - \delta_{ab}) Y^0(b, b; r) + Z_a^{xs}(r). \quad (\text{C.5})$$

The exchange term contains two parameters and a power of the full electronic density $\rho(r)$

$$Z_a^{xs}(r) = k_x f(r) \left[\frac{\rho'(r)}{\rho'(r) + 0.5/(n_a - l_a)} \right] \left(\frac{\rho'(r)}{\rho(r)} \right) \left(\frac{24\rho(r)}{\pi} \right)^{1/3}, \quad (\text{C.6})$$

where $k_x \approx 0.7$. A factor function $f(r)$ is of minor importance and defined to

$$f(r) = \begin{cases} 1, & r \geq r_0 \\ 1 + 0.7(1 - r/r_0), & r < r_0 \end{cases}, \quad (\text{C.7})$$

where r_0 is the location of the k -th node of the wave function $P_{n_a \kappa_a}(r)$ where k is the number of orbitals having $l = l_a$ and $n < n_a$.

A modified electron density $\rho'(r)$ is defined to

$$\rho'(r) = \rho(r) - \min(2, w_a) \rho^a(r), \quad (\text{C.8})$$

where w_a is occupation number according to Equation (C.4) and $\rho^a(r)$ is one-electron density for a subshell a

$$\rho^a(r) = (P_{n_a \kappa_a}^2(r) + Q_{n_a \kappa_a}^2(r)) / (4\pi r^2). \quad (\text{C.9})$$

Finally, the full electronic density is defined to

$$\rho(r) = \sum_a^{\text{all subshells}} w_a (P_{n_a \kappa_a}^2(r) + Q_{n_a \kappa_a}^2(r)) / (4\pi r^2). \quad (\text{C.10})$$

HX-potential, although is more complicated than Hartree potential, remains still a local, central-field potential. The one-electron energies and dipole oscillator strengths, which are provided by HX-potential, are in a fair agreement with—much more complicated—Hartree-Fock values. Moreover, I had compared three single-active-electron calculations of two-photon ionization cross section with a two-active-electron calculation in Section 4.5. This comparison reveals the HX-potential as the best amongst pure Coulomb and Hartree potentials.

Appendix D

Numerical tests for the Dirac-central-field Green's function

Since the program for computation of the radial part of Dirac-central-field Green's function is rather complex (see Section 4.3.3), it is worth to prepare a check of generated Green's function. For this purpose, a rather strong check of the generated Green's functions can be applied. The checking is based on a simple relation for the Green's function $G_E(\mathbf{r}, \mathbf{r}')$ and corresponding eigen state $\psi_n(\mathbf{r})$

$$\psi_n(\mathbf{r}') = (E_n - E) \int \psi_n^\dagger(\mathbf{r}) G_E(\mathbf{r}, \mathbf{r}') d\mathbf{r}. \quad (\text{D.1})$$

Reducing the angular integration in latter formula, we derive a relation which is directly applicable for checking of the radial part of the Dirac-central-field Green's function.

$$\begin{pmatrix} P_{n\kappa}(r') \\ -Q_{n\kappa}(r') \end{pmatrix} = (E_{n\kappa} - E) \int_0^\infty (P_{n\kappa}(r), Q_{n\kappa}(r)) \begin{pmatrix} g_{E\kappa}^{LL}(r, r') & g_{E\kappa}^{LS}(r, r') \\ g_{E\kappa}^{SL}(r, r') & g_{E\kappa}^{SS}(r, r') \end{pmatrix} dr, \quad (\text{D.2})$$

where $P_{n\kappa}(r)$ and $Q_{n\kappa}(r)$ are large and small components of Dirac radial spinor (Grant 1988).

Another possibility to check the program is provided by the symmetry property of the Green's function Equation (4.5). This property can be reduced to the radial part of the Dirac-central-field Green's function

$$g_{E\kappa}^{LL}(r, r') = g_{E\kappa}^{LL}(r', r), \quad (\text{D.3})$$

$$g_{E\kappa}^{LS}(r, r') = -g_{E\kappa}^{SL}(r', r), \quad (\text{D.4})$$

$$g_{E\kappa}^{SL}(r, r') = -g_{E\kappa}^{LS}(r', r), \quad (\text{D.5})$$

$$g_{E\kappa}^{SS}(r, r') = g_{E\kappa}^{SS}(r', r). \quad (\text{D.6})$$

The Formulae (D.2, D.3, D.4, D.5, D.6) provide the reliable check for the Dirac-central-field Green's function.

Appendix E

Publications

The list of publications which have been prepared during period of my PhD study is presented below. In this Chapter, the full-text of these papers is included.

1. *Relativistic wave and Green's functions for hydrogen-like ions*

Koval P and Fritzsche S

2003 *Comput. Phys. Commun.* **152** 191.

2. *Relativistic and retardation effects in the two-photon ionization of hydrogen-like ions*

Koval P, Fritzsche S and Surzhykov A

2003 *J. Phys. B: At. Mol. Phys.* **36** 873.

3. *Electron angular distributions in the two-photon ionization of hydrogen-like ions: a relativistic description*

Koval P, Fritzsche S and Surzhykov A

2004 *J. Phys. B: At. Mol. Phys.* **37** 375.

E.1 Relativistic wave and Green's functions for hydrogen-like ions

Koval P and Fritzsche S 2003
Comput. Phys. Commun. **152** 191-207.

Relativistic wave and Green's functions for hydrogen-like ions[☆]

Peter Koval^{*}, Stephan Fritzsche

Fachbereich Physik, Universität Kassel, Heinrich-Plett-Str. 40, D-34132 Kassel, Germany

Received 17 September 2002

Abstract

The GREENS library is presented which provides a set of C++ procedures for the computation of the (radial) Coulomb wave and Green's functions. Both, the nonrelativistic as well as relativistic representations of these functions are supported by the library. However, while the wave functions are implemented for all, the bound and free-electron states, the Green's functions are provided only for bound-state energies ($E < 0$). Apart from the Coulomb functions, moreover, the implementation of several special functions, such as the Kummer and Whittaker functions of the first and second kind, as well as a few utility procedures may help the user with the set-up and evaluation of matrix elements.

© 2002 Elsevier Science B.V. All rights reserved.

PROGRAM SUMMARY

Title of program: GREENS

Catalogue identifier: ADRJ

Program Summary URL: <http://cpc.cs.qub.ac.uk/summaries/ADRJ>

Program obtainable from: CPC Program Library, Queen's University of Belfast, N. Ireland

Licensing provisions: none

Computer for which the program is designed and has been tested: PC Pentium III, PC Athlon

Installation: University of Kassel (Germany)

Operating systems: Linux 6.1+, SuSe Linux 7.3, SuSe Linux 8.0, Windows 98

Program language used: C++

Memory required to execute with typical data: 300 kB

No. of bits in a word: all real variables are of type **double** (i.e. 8 bytes long)

No. of bytes in distributed program including test data, etc.: 343 153

Distribution format: tar gzip file

CPC Program Library subprograms required: none

Keywords: Confluent hypergeometric function, Coulomb–Green's function, hydrogenic wave function, Kummer function, nonrelativistic, relativistic, two-photon ionization cross section, Whittaker function

[☆] This program can be downloaded from the CPC Program Library under catalogue identifier: <http://cpc.cs.qub.ac.uk/summaries/ADRJ>

^{*} Corresponding author.

E-mail address: kovalp@mail.ru (P. Koval).

Nature of the physical problem

In order to describe and understand the behaviour of hydrogen-like ions, one often needs the Coulomb wave and Green's functions for the evaluation of matrix elements. But although these functions have been known analytically for a long time and within different representations [1,2], not so many implementations exist and allow for a simple access to these functions. In practice, moreover, the application of the Coulomb functions is sometimes hampered due to *numerical instabilities*.

Method of solution

The radial components of the Coulomb wave and Green's functions are implemented in position space, following the representation of Swainson and Drake [2]. For the computation of these functions, however, use is made of Kummer's functions of the first and second kind [3] which were implemented for a wide range of arguments. In addition, in order to support the integration over the Coulomb functions, an adaptive Gauss–Legendre quadrature has also been implemented within one and two dimensions.

Restrictions onto the complexity of the problem

As known for the *hydrogen atom*, the Coulomb wave and Green's functions exhibit a rapid oscillation in their radial structure if either the principal quantum number or the (free-electron) energy increase. In the implementation of these wave functions, therefore, the bound-state functions have been tested properly only up to the principal quantum number $n \approx 20$, while the free-electron waves were tested for the angular momentum quantum numbers $\kappa \leq 7$ and for all energies in the range $0 \dots 10|E_{1s}|$. In the computation of the

two-photon ionization cross sections σ_2 , moreover, only the long-wavelength approximation ($e^{i\mathbf{k}\cdot\mathbf{r}} \approx 1$) is considered both, within the nonrelativistic and relativistic framework.

Unusual features of the program

Access to the wave and Green's functions is given simply by means of the GREENS library which provides a set of C++ procedures. Apart from these Coulomb functions, however, GREENS also supports the computation of several *special functions* from mathematical physics (see Section 2.4) as well as of two-photon ionization cross sections in long-wavelength approximation, i.e. for a very first application of the atomic Green's functions. Moreover, to facilitate the integration over the radial functions, an adaptive Gauss–Legendre quadrature has been also incorporated into the GREENS library.

Typical running time

Time requirements critically depends on the quantum numbers and energies of the functions as well as on the requested accuracy in the case of a numerical integration. One value of the relativistic two-photon ionization cross section takes less or about one minute on a Pentium III 550 MHz processor.

References

- [1] H.A. Bethe, E.E. Salpeter, *Quantum Mechanics of One- and Two-Electron Atoms*, Kluwer Academic Publishers, 1977.
- [2] R.A. Swainson, G.W.F. Drake, *J. Phys. A* 24 (1991) 95.
- [3] M. Abramowitz, I.A. Stegun (Eds.), *Handbook of Mathematical Functions*, Dover, New York, 1965.

LONG WRITE-UP

1. Introduction

From the early days of quantum mechanics on, the 'hydrogen atom' has served not only as a well-known textbook problem but also as one of the fundamental models in the physics of atoms, molecules, and nuclei. When combined with the (atomic) shell model, namely, the—analytic—solutions for the hydrogen-like ions help understand most atomic processes in Nature, at least qualitatively. For this reason also, the 'hydrogen atom' has found its way into quite different fields of physics including, for example, astro- and plasma-physics, quantum optics or even the search for more efficient X-ray lasers schemes.

Despite of the success of the *hydrogen model*, however, the Coulomb problem is not always that simple to deal with, in particular, if a relativistic treatment is required. Therefore, various program tools have been developed over the years to help with either the analytic or numerical manipulation of the Coulomb functions and their matrix elements. For the nonrelativistic Coulomb problem, for example, the bound-electron states can be obtained from the codes of Noble and Thompson [1], who applied a continued fraction representation of the Whittaker functions, Bell and Scott [2], or simply by using the GNU Scientific Library [3]. These functions are incorporated also into a recent library by Madsen and coworkers [4], which has been designed to support the computation of the multipole matrix elements for circular and linear polarized light. —Less attention, in contrast, has been paid to the *relativistic* wave functions for which a CPC program is provided only by Salvat et al. [5]. This program help integrate the radial equation for any spherical-symmetric potential for both, the (one-particle) Schrödinger and Dirac equations and also provides separate procedures to compute the Coulomb wave functions.

Apart from the bound and free-electron wave functions, however, the Coulomb Green's functions play a similar important role, in particular, if the interaction of atoms with external fields is to be studied. In second- and higher-order perturbation theory, for instance, these functions help to carry out the summation over the complete spectrum in a rather efficient way. But although different analytic representations are known for the Green's functions [6–10], until today, there are almost no reliable codes freely available.

Therefore, to facilitate the further application of the 'hydrogen atom' in different contexts, here we present the GREENS library which provides a set of C++ procedures for the computation of the Coulomb wave and Green's functions. In GREENS, these *hydrogenic* functions are supported *both*, within a nonrelativistic as well as relativistic framework. Beside of the various routines for the computation (of the radial parts) of these functions, however, we also supply the user with a Gauss–Legendre quadrature and a set of special functions to simplify the evaluation of matrix elements. —But before we shall present details about the organization of the GREENS library, in the following section, we first compile the basic formulas from the theory of the 'hydrogen atom' with emphasize especially to those expressions, which have been implemented explicitly. In Section 3, later, the program structure will be discussed and how the library is to be distributed. This section also lists all user-relevant commands, although not much is said here about the underlying algorithms. In most cases, we followed the expressions from Sections 2 but care has been taken in order to provide a *reliable* code for a rather wide range of parameters which, sometimes, required quite additional effort. In Section 4, we explain how (easily) the hydrogenic wave and Green's functions can be accessed not only for a particular set of arguments but also for the computation of matrix elements. These examples may serve, therefore, also as a test bed for the installation of the code. Section 5, finally, gives a brief summary and an outlook into our future work.

2. Theoretical background

Since the theory of the 'hydrogen atom' has been presented at quite many places before (see, for instance, the texts of Messiah [11] and Drake [12]), we shall restrict ourselves to rather a short compilation of formulas, just enough in order to provide the basic notations and those expressions which are implemented in the code. In the next two subsections, therefore, we first recall the (analytic) form of the Coulomb wave and Green's functions while, in Section 2.3, these functions are applied to calculate the two-photon ionizations cross sections for linear and circular polarized light. In all these sections, the nonrelativistic and relativistic formulas are always presented in turn of each other in order to display the similarities but also the differences in the numerical treatment of these functions. Section 2.4, moreover, provides reference to a few *special functions* from mathematical physics, which frequently occur in the computations of the Coulomb wave or Green's functions and, hence, need to be part of the GREENS library.

2.1. Coulomb wave functions

2.1.1. Nonrelativistic wave function

In a time-independent external field, the motion of a particle is described by the stationary Schrödinger equation

$$(\hat{H}(\mathbf{r}) - E)\psi(\mathbf{r}) = 0 \quad (1)$$

which, obviously, is an eigenvalue equation for the total energy E of the particle. As known from the nonrelativistic Schrödinger theory, the Hamiltonian \hat{H} just includes the kinetic and potential energy of the particle and, thus, takes the form¹

$$\hat{H}(\mathbf{r}) = -\frac{\nabla^2}{2} - \frac{Z}{r} \quad (2)$$

¹ Here and in the following, we use *atomic units* ($m_e = \hbar = e^2/4\pi\epsilon_0 = 1$) if not stated otherwise.

in the case of a (pure) Coulomb field of a nucleus with charge Z . For such a spherical-symmetric potential, of course, Eq. (1) and the wave functions $\psi(\mathbf{r})$ can be separated

$$\psi_{nlm}(r, \theta, \varphi) = \frac{P_{nl}(r)}{r} Y_{lm}(\theta, \varphi) \quad (3)$$

into a *radial* and an *angular* part where, in most practical computations, the angular structure of the wave functions is often treated by means of the techniques from Racah's algebra [14]. In expression (3), n and l denote the principal and orbital angular momentum quantum numbers, respectively, while m describes the projection of the z -component of the orbital angular momentum onto the quantization axis and is called the magnetic quantum number. The radial part of the wave function, $P_{nl}(r)/r$, is a solution of the *radial* Schrödinger equation

$$\left[\frac{1}{r^2} \frac{\partial}{\partial r} \left(r^2 \frac{\partial}{\partial r} \right) - \frac{l(l+1)}{r^2} + \frac{2Z}{r} + 2E \right] \frac{P_{nl}(r)}{r} = 0 \quad (4)$$

which has (normalizable) *physical solutions* for a discrete set of negative energies

$$E_n = -\frac{Z^2}{2n^2} < 0, \quad n = 1, 2, \dots, \quad (5)$$

the so-called *bound* states, as well as for all positive energies $E > 0$, i.e. the *continuum* or *free-electron* states. Both, the bound and continuum solutions of (4) can be represented in terms of a single Whittaker function of the first kind $M_{a,b}(z)$

$$P_{nl}(r) = C(n, l, Z) M_{n, l+1/2}(2Zr/n), \quad (6)$$

$$P_{El}(r) = C(E, l, Z) M_{i\sqrt{Z/2E}, l+1/2}(-2i\sqrt{2EZ}r) \quad (7)$$

with real or complex arguments, and where $C(n, l, Z)$ and $C(E, l, Z)$, respectively, denote the corresponding normalization factors. The Whittaker functions are closely related to the Kummer functions of first and second kind as we will discuss in Section 2.2.1. In the standard theory, moreover, the radial wave functions (6) and (7) are often normalized due to

$$\int_0^\infty P_{nl}^2(r) dr = 1, \quad (8)$$

$$\int_0^\infty P_{El}^*(r) P_{E'l}(r) dr = \delta(E - E'), \quad (9)$$

in order to represent a single particle per bound state or *per energy unit*, respectively, if particles in the continuum are concerned.

2.1.2. Relativistic wave functions

An eigenvalue equation analogue to (1) also applies, if the motion of the particle is described within the relativistic theory. For an electron with spin $s = 1/2$, however, then the Hamiltonian \hat{H} needs to be replaced by the Dirac–Hamiltonian [11]

$$\hat{H}_D(\mathbf{r}) = -ic\boldsymbol{\alpha} \cdot \nabla + \beta c^2 - \frac{Z}{r} \quad (10)$$

which, apart from the kinetic and potential energy of the electron in the field of the nucleus, now also incorporates the rest energy of the electron as well as energy contributions owing to its spin. As in the nonrelativistic case, a separation of the wave function

$$\psi_{n\kappa m}(\mathbf{r}) = \frac{1}{r} \begin{pmatrix} P_{n\kappa}(r)\Omega_{\kappa m}(\theta, \varphi) \\ iQ_{n\kappa}(r)\Omega_{-\kappa m}(\theta, \varphi) \end{pmatrix} \quad (11)$$

into a radial and angular part is possible for any spherical-symmetric potential, where the two radial functions $P_{n\kappa}(r)$ and $Q_{n\kappa}(r)$ are often called the *large* and *small* components. These two functions also form a radial spinor $\begin{pmatrix} P_{n\kappa}(r) \\ Q_{n\kappa}(r) \end{pmatrix}$ and have to be obtained as solutions of the first-order, coupled equations [13]

$$\left[-\frac{Z}{r} - E \right] \frac{P_{n\kappa}(r)}{r} + \left[\frac{\kappa}{\alpha r} - \frac{1}{\alpha r} \frac{\partial}{\partial r} \right] \frac{Q_{n\kappa}(r)}{r} = 0, \quad (12)$$

$$\left[\frac{1}{\alpha r} \frac{\partial}{\partial r} + \frac{\kappa}{\alpha r} \right] \frac{P_{n\kappa}(r)}{r} - \left[\frac{2}{\alpha^2} + \frac{Z}{r} + E \right] \frac{Q_{n\kappa}(r)}{r} = 0, \quad (13)$$

where, however, the (total) energy E is taken here to represent the energy of the electron without its rest energy² c^2 , similar to Eq. (4) in the Schrödinger theory. In Eqs. (11)–(13), moreover, $\kappa = \pm(j + 1/2)$ for $l = j \pm 1/2$ is called the *relativistic* angular momentum quantum number and carries information about both, the total angular momentum j as well as the parity $(-1)^l$ of the wave function. Again, (normalizable) *physical solutions* to the Dirac operator (10) can be found for a discrete set of negative energies

$$E_{n\kappa} = \alpha^{-2} \left[1 + \left(\frac{\alpha Z}{n - \kappa + \sqrt{\kappa^2 - \alpha^2 Z^2}} \right)^2 \right]^{-1/2} - \alpha^{-2} < 0, \quad (14)$$

$n = 1, 2, \dots; \kappa = -n, \dots, n - 1, \kappa \neq 0$

and for all positive energies $E \geq 0$ as well as for the (negative) energies $E \leq -2c^2$. The two latter—continuous—parts of the spectrum are also called the *positive* and *negative* continuum whereby the negative branch, in particular, requires some re-interpretation of the theory (in terms of positron states, for example) and often introduces additional complications in the treatment of many-electron systems. When compared with the nonrelativistic energies (5), however, the degeneracy of the (relativistic) energies (14) is partially resolved and now depends on both, the principal quantum number n and the relativistic quantum number κ .

Explicit representation of the bound and free-electron solutions of Eqs. (12), (13) are known from the literature (cf. [13,15]) but typically result in rather lengthy expressions. For the bound states, for example, the two radial components are given by

$$P_{n\kappa}(r) = C_P(n, \kappa, Z) r^s e^{-qr} [(-n + |\kappa|)M(-n + |\kappa| + 1, 2s + 1; 2qr) - (\kappa - Zq^{-1})M(-n + |\kappa|, 2s + 1; 2qr)], \quad (15)$$

$$Q_{n\kappa}(r) = C_Q(n, \kappa, Z) r^s e^{-qr} [-(n + |\kappa|)M(-n + |\kappa| + 1, 2s + 1; 2qr) - (\kappa - Zq^{-1})M(-n + |\kappa|, 2s + 1; 2qr)], \quad (16)$$

where $M(a, b; z)$ is the Kummer function of the first kind, $s = \sqrt{\kappa^2 - (\alpha Z)^2}$, and $q = Z[(\alpha Z)^2 + (n - |\kappa| + s^2)]^{-1/2}$, while even more elaborate expressions arise for the free-electron states [15]. Similar to (8) and (9), the bound and free-electron radial wave functions can be normalized also due to

$$\int_0^\infty (P_{n\kappa}^2(r) + Q_{n\kappa}^2(r)) dr = 1, \quad (17)$$

$$\int_0^\infty (P_{E\kappa}(r)P_{E'\kappa}(r) + Q_{E\kappa}(r)Q_{E'\kappa}(r)) dr = \delta(E - E') \quad (18)$$

to represent one electron per bound state or per energy unit, respectively.

² In atomic units, the speed of light $c = 1/\alpha$ is the inverse of the fine-structure constant.

In the GREENS library, the radial functions of the bound and free-electron states can be accessed by means of the two library procedures `greens_radial_orbital()` and `greens_radial_spinor()` in the nonrelativistic and relativistic case, respectively; for further details, see Section 3.

2.2. Coulomb Green's functions

Apart from the wave functions, which describe the electron in particular quantum states, one often needs a summation over all (unoccupied) states, especially, if parts of the atomic interaction are treated as a perturbation. A full summation is required in second- and higher-order perturbation theory, for instance, if the behaviour of the atom is studied in a—not too weak—radiation field or in the presence of external electric or magnetic fields. Although, in principle, it appears straightforward to carry out such a summation explicitly, the large number of terms and the need of *free-free* matrix elements may hamper such an approach. Instead, the use of Green's functions [16]

$$G_E(\mathbf{r}, \mathbf{r}') = \sum_v \frac{|\psi_v(\mathbf{r})\rangle\langle\psi_v(\mathbf{r}')|}{E_v - E}, \quad (19)$$

often provides a much simpler access to the *spectrum* of the atom and, hence, to a perturbative treatment of atomic processes. In the following, therefore, we first recall a representation of the radial Coulomb Green's functions as appropriate for numerical computations. The application of these functions in the computation of two-photon ionization cross sections σ_2 for hydrogen-like is discussed later in Section 2.3.

2.2.1. Nonrelativistic Green's function

Analogous to the wave functions (3), the Coulomb Green's functions $G_E(\mathbf{r}, \mathbf{r}')$ are obtained as solutions of a linear equation

$$(\widehat{H}(\mathbf{r}) - E)G_E(\mathbf{r}, \mathbf{r}') = \delta(\mathbf{r} - \mathbf{r}') \quad (20)$$

with the same Schrödinger operator as in (1) but for an additional δ -like inhomogeneity on the right-hand side, which allows for solutions for any arbitrary E . For a spherical-symmetric potential, again, this equation can be separated into a radial and angular part by using the ansatz

$$G_E(\mathbf{r}, \mathbf{r}') = \sum_{lm} \frac{g_{El}(r, r')}{rr'} Y_{lm}(\theta, \varphi) Y_{lm}^*(\theta', \varphi') \quad (21)$$

for the Green's function in spherical coordinates. By substituting ansatz (21) into Eq. (20), one easily shows that the *radial* Green's function $g_{El}(r, r')$, which just depends on the energy E and the orbital angular momentum l , must satisfy the equation

$$\left[\frac{1}{r^2} \frac{\partial}{\partial r} \left(r^2 \frac{\partial}{\partial r} \right) - \frac{l(l+1)}{r^2} + \frac{2Z}{r} + 2E \right] \frac{g_{El}(r, r')}{rr'} = -2 \frac{\delta(r - r')}{rr'}.$$

Solutions to this single equation can be determined by taking a proper superposition of the regular and irregular solutions (near the origin) of Schrödinger's equation (4). An explicit representation for the radial Green's function reads as [9]

$$g_{El}(r, r') = \frac{\Gamma(l+1-\tau)}{x\Gamma(2l+2)} M_{\tau, l+1/2}(2xr_{<}) W_{\tau, l+1/2}(2xr_{>}), \quad (22)$$

where $x = (-2E)^{1/2}$, $\tau = Z/x$, and where $r_{>} = \max(r, r')$ and $r_{<} = \min(r, r')$ refer to the *larger* and *smaller* value of the two radial coordinates, respectively. In this representation, moreover, $M_{a,b}(z)$ and $W_{a,b}(z)$ denote the two Whittaker functions of the first and second kind which can be expressed also in terms of the Kummer functions $M(a, b; z)$ and $U(a, b; z)$ of the corresponding kinds [17]

$$M_{a,b}(z) = z^{b+1/2}e^{-z/2}M(b-a+1/2, 2b+1; z), \quad (23)$$

$$W_{a,b}(z) = z^{b+1/2}e^{-z/2}U(b-a+1/2, 2b+1; z). \quad (24)$$

In practice, the two *Kummer functions* are used more frequently (than the Whittaker functions) in the mathematical literature and in various program libraries since $M(a, b; z)$ is closely related to the hypergeometric series and since the Kummer function $U(a, b; z)$ of the second kind can be expressed in terms of $M(a, b; z)$. In addition, several improved algorithms have been worked out recently in order to calculate the regular Kummer function $M(a, b; z)$ more efficiently, see Section 2.4 for further details.

2.2.2. Relativistic Green's function

Of course, the relativistic Coulomb Green's function must refer to the Dirac Hamiltonian (10) and, hence, is given by a 4×4 -matrix which satisfies the equation

$$(\widehat{H}_D(\mathbf{r}) - E - c^2)G_E(\mathbf{r}, \mathbf{r}') = \delta(\mathbf{r} - \mathbf{r}')\mathbf{I}_4,$$

where \mathbf{I}_4 denotes the 4×4 unit-matrix and where, as for the wave functions from Eqs. (12), (13), the rest energy c^2 has not been incorporated into the (total) energy E . Solutions to this equation are known again from the literature for a *radial-angular* representation of the Coulomb Green's function [9]

$$G_E(\mathbf{r}, \mathbf{r}') = \sum_{km} \frac{1}{rr'} \begin{pmatrix} g_{E\kappa}^{LL}(r, r')\Omega_{\kappa m}(\mathbf{r})\Omega_{\kappa m}^\dagger(\mathbf{r}') & -ig_{E\kappa}^{LS}(r, r')\Omega_{\kappa m}(\mathbf{r})\Omega_{-\kappa m}^\dagger(\mathbf{r}') \\ ig_{E\kappa}^{SL}(r, r')\Omega_{-\kappa m}(\mathbf{r})\Omega_{\kappa m}^\dagger(\mathbf{r}') & g_{E\kappa}^{SS}(r, r')\Omega_{-\kappa m}(\mathbf{r})\Omega_{-\kappa m}^\dagger(\mathbf{r}') \end{pmatrix}, \quad (25)$$

where the *radial part* $\begin{pmatrix} g_{E\kappa}^{LL}(r, r') & g_{E\kappa}^{LS}(r, r') \\ g_{E\kappa}^{SL}(r, r') & g_{E\kappa}^{SS}(r, r') \end{pmatrix} / rr'$ of this function is now a 2×2 -matrix which must satisfy the matrix equation

$$\begin{pmatrix} [-\frac{Z}{r} - E] & [\frac{\kappa}{ar} - \frac{1}{ar} \frac{\partial}{\partial r} r] \\ [\frac{1}{ar} \frac{\partial}{\partial r} r + \frac{\kappa}{ar}] & [-\frac{2}{a^2} - \frac{Z}{r} - E] \end{pmatrix} \frac{1}{rr'} \begin{pmatrix} g_{E\kappa}^{LL}(r, r') & g_{E\kappa}^{LS}(r, r') \\ g_{E\kappa}^{SL}(r, r') & g_{E\kappa}^{SS}(r, r') \end{pmatrix} = \frac{\delta(r - r')}{rr'} \mathbf{I}_2.$$

In this representation of the Green's function, we make use of the two superscripts T and T' to denote the individual components in the 2×2 radial Green's matrix. They may take both the values $T = [L, S]$ to refer to either the *large* or *small* components, when multiplied with a wave function spinor (11). An explicit representation of the (four) components $g_{E\kappa}^{TT'}(r, r')$ of the radial Green's function is found by Swainson and Drake [9]

$$\begin{pmatrix} g_{E\kappa}^{LL} & g_{E\kappa}^{LS} \\ g_{E\kappa}^{SL} & g_{E\kappa}^{SS} \end{pmatrix} = \frac{1}{(1 - X^2)^2} \begin{pmatrix} h^{11} - X(h^{12} + h^{21}) + X^2 h^{22} & -X(h^{11} + h^{22}) + h^{12} + X^2 h^{21} \\ -X(h^{11} + h^{22}) + X^2 h^{12} + h^{21} & X^2 h^{11} - X(h^{12} + h^{21}) + h^{22} \end{pmatrix}, \quad (26)$$

with

$$h^{11}(r, r') = \frac{(1 - X^2)((E\alpha^2 + 1)\kappa\gamma^{-1} + 1)}{2\omega} \frac{\Gamma(\gamma + 1 - \nu)}{\Gamma(2\gamma + 2)} M_{\nu, \gamma+1/2}(2\omega r_{<}) W_{\nu, \gamma+1/2}(2\omega r_{>}), \quad (27)$$

$$h^{22}(r, r') = \frac{(1 - X^2)((E\alpha^2 + 1)\kappa\gamma^{-1} - 1)}{2\omega} \frac{\Gamma(\gamma - \nu)}{\Gamma(2\gamma)} M_{\nu, \gamma-1/2}(2\omega r_{<}) W_{\nu, \gamma-1/2}(2\omega r_{>}), \quad (28)$$

$$\begin{aligned} h^{21}(r, r') &= h^{12}(r', r) \\ &= \frac{(1 - X^2)\Gamma(\gamma + 1 - \nu)\alpha\gamma^{-1}}{2\Gamma(2\gamma + 2)} [2\gamma(2\gamma + 1)\theta(r' - r)M_{\nu, \gamma-1/2}(2\omega r)W_{\nu, \gamma+1/2}(2\omega r') \\ &\quad - (\nu + \gamma)\theta(r - r')W_{\nu, \gamma-1/2}(2\omega r)M_{\nu, \gamma+1/2}(2\omega r')], \end{aligned} \quad (29)$$

and

$$\begin{aligned} X &= (-\kappa + \gamma)(\alpha Z)^{-1}, & \gamma &= (\kappa^2 - \alpha^2 Z^2)^{1/2}, \\ \omega &= \alpha^{-1}(1 - (E\alpha^2 + 1)^2)^{1/2}, & \nu &= Z(E\alpha^2 + 1)\omega^{-1}, \end{aligned}$$

and where $\theta(x)$ denotes the Heaviside function.

In the GREENS library, we provide the two procedures `greens_radial_function()` and `greens_radial_matrix()` which support the computation of the radial functions (22) and (26) for any proper set of parameters.

2.3. Two-photon transition amplitudes and ionization cross sections

The Green's function (21) and (25) can be utilized directly to evaluate, for instance, the two-photon cross sections σ_2 for a *non-resonant* excitation, ionization, or decay process. They also occur rather naturally in the theory of the photon scattering on hydrogen-like ions. In the following, we briefly outline the perturbative calculation of the two-photon ionization cross section for hydrogen-like ions which, for an unpolarized target and in atomic units,³ is given by

$$\sigma_2 = \frac{8\pi^3 \alpha^2}{E_\gamma^2} \sum_{\kappa_f m_f} \frac{1}{2j_i + 1} \sum_{m_i} |M_{fi}|^2, \quad (30)$$

where E_γ is the photon energy and M_{fi} the two-photon transition amplitude

$$M_{fi} = \sum_v \frac{\langle \psi_f | \mathbf{u}_{\lambda_2} e^{i\mathbf{k}_2 \cdot \mathbf{r}} \cdot \mathbf{p} | \psi_v \rangle \langle \psi_v | \mathbf{u}_{\lambda_1} e^{i\mathbf{k}_1 \cdot \mathbf{r}} \cdot \mathbf{p} | \psi_i \rangle}{E_v - E_\gamma - E_i}. \quad (31)$$

In this amplitude, moreover, (ψ_i, E_i) , (ψ_v, E_v) , and (ψ_f, E_f) denote the wave functions and energies of the initial, intermediate and final atomic states, respectively. Here, the energy of the final state, E_f , does not appear explicitly in (31) but follows from

$$E_f = E_i + 2E_\gamma$$

due to the conservation of energy. Furthermore, the two vector quantities \mathbf{u}_λ and \mathbf{p} in the transition amplitude (31) refer to the polarization of the two photons as well as to the electron momentum operator.

As mentioned before, the summation over v in (31) runs over the *complete spectrum* of the atom including the continuum. This summation can be replaced, therefore, by a single Green's function (19), so that the transition amplitude (31) finally takes the form

$$M_{fi} = \int \psi_f^\dagger(\mathbf{r}) \mathbf{u}_{\lambda_2} e^{i\mathbf{k}_2 \cdot \mathbf{r}} \cdot \mathbf{p} G_{E_i + E_\gamma}(\mathbf{r}, \mathbf{r}') \mathbf{u}_{\lambda_1} e^{i\mathbf{k}_1 \cdot \mathbf{r}'} \cdot \mathbf{p}' \psi_i(\mathbf{r}') d\mathbf{r}'. \quad (32)$$

It is this form of the transition amplitude which has often been used in the literature to study non-resonant, two-photon processes [10,18].

2.3.1. Nonrelativistic ionization cross sections

For the sake of brevity, let us restrict ourselves to the two-photon ionization cross sections within the *long-wavelength* approximation, i.e. we assume $e^{i\mathbf{k} \cdot \mathbf{r}} \equiv 1$ for the coupling of the radiation field in (32). Apart from the electric-dipole field, of course, this approximation neglects the contribution from all higher multipoles, but is

³ The cross section σ_2 has the dimension length⁴ × time and, thus, can be converted into cgs-units cm⁴·s by using the multiplication factor $1.896792 \cdot 10^{-50}$.

known to describe well the ionization of light atoms with a nuclear charge of, say, $Z \lesssim 30$ and for photon energies below the ionization threshold $E_\gamma < E_T$. By substituting $\mathbf{p} \rightarrow \mathbf{r}$ and $E_\gamma \rightarrow 1/E_\gamma$ into Eqs. (30) and (31), moreover, we may obtain the ionization cross section in *length gauge*

$$\sigma_2^{(\text{length})} = 8\pi^3 \alpha^2 E_\gamma^2 \sum_{l_f m_f} \frac{1}{2l_i + 1} \sum_{m_i} |M_{fi}^{(\text{length})}|^2, \quad (33)$$

with

$$M_{fi}^{(\text{length})} = \int \psi_f^\dagger(\mathbf{r}) \mathbf{u}_{\lambda_2} \cdot \mathbf{r} \mathbf{G}_{E_i + E_\gamma}(\mathbf{r}, \mathbf{r}') \mathbf{u}_{\lambda_1} \cdot \mathbf{r}' \psi_i(\mathbf{r}') \, d\mathbf{r} \, d\mathbf{r}'. \quad (34)$$

Using the *radial-angular* representations (3) and (21) of the wave and Green's functions, respectively, and by making use of some angular momentum algebra, the 6-dimensional integral in the transition amplitude (34) can be reduced further to just a *two-dimensional integration* over the radial coordinates r and r' . In addition, if we assume the ion initially in its $1s$ ground-state and circular polarized light, i.e. two photons with the same helicity $\lambda_1 = \lambda_2 = \pm 1$, the two-photon ionization cross section (in length gauge) simply takes the form

$$\sigma_2^{(\text{length, circular})} = 8\pi^3 \alpha^2 E_\gamma^2 \left| \int P_{E_f 2}(r) r \mathbf{g}_{E_i + E_\gamma, 1}(r, r') r' P_{10}(r') \, dr \, dr' \right|^2. \quad (35)$$

2.3.2. Relativistic two-photon ionization cross sections

The *long-wavelength* approximation for the coupling of the radiation field can be considered also within the framework of the relativistic theory. In this framework, however, an useful estimate of the total cross section σ_2 are obtained only if the photon energy is well below the threshold energy $E_\gamma < E_T$ of the two-photon ionization. In the relativistic theory, the (long-wavelength) transition amplitude (32) takes the form

$$M_{fi} = c^2 \int \psi_f^\dagger(\mathbf{r}) \mathbf{u}_{\lambda_2} \cdot \boldsymbol{\alpha} \mathbf{G}_{E_i + E_\gamma}(\mathbf{r}, \mathbf{r}') \mathbf{u}_{\lambda_1} \cdot \boldsymbol{\alpha}' \psi_i(\mathbf{r}') \, d\mathbf{r} \, d\mathbf{r}', \quad (36)$$

where $\boldsymbol{\alpha}$ denotes Dirac's velocity operator. Using the radial-angular representation (25) of the Green's functions, then the total two-photon ionization cross section σ_2 for circular-polarized light can be written as

$$\sigma_2^{(\text{velocity, circular})} = \frac{8\pi^3}{\alpha^2 E_\gamma^2} \left\{ \frac{32}{25} U^{SL}(d_{5/2}, p_{3/2}, s_{1/2})^2 + \frac{12}{2025} [5U^{LL}(d_{3/2}, p_{3/2}, s_{1/2}) + 3U^{SL}(d_{3/2}, p_{3/2}, s_{1/2}) - 5U^{LL}(d_{3/2}, p_{1/2}, s_{1/2}) - 15U^{LS}(d_{3/2}, p_{1/2}, s_{1/2})]^2 \right\}, \quad (37)$$

where we introduced the radial integral

$$U^{TT'}(\kappa_f, \kappa_v, \kappa_i) = \int \bar{\mathbf{g}}_{E_f \kappa_f}^T(r) \mathbf{g}_{E_i + E_\gamma, \kappa_v}^{TT'}(r, r') \bar{\mathbf{g}}_{n_i \kappa_i}^{T'}(r') \, dr \, dr'. \quad (38)$$

In this integral, a superscript \bar{T} refers to the conjugate of T , i.e. $\bar{T} = S$ for $T = L$ and *vice versa*, and $\mathbf{g}_{n\kappa}^L(r)$ and $\mathbf{g}_{n\kappa}^S(r)$ are used to denote the large and small components of the radial spinor (11). This notation allows for a very compact representation of the multi-photon transition amplitudes which can be applied also well beyond the long-wavelength approximation.

In the GREENS library, the procedure `greens_two_photon_cs()` is presented to compute two-photon ionization cross sections in various approximations.

2.4. Special functions

Of course, the main emphasize in developing the GREENS library has been paid to the computation of the Coulomb wave and Green's functions as appropriate for a theoretical description of hydrogen-like ions. As seen from Sections 2.1 and 2.2, however, for an explicit representation of these functions we usually need to refer to a few *special functions* such as the $\Gamma(z)$ and $\Psi(z)$ functions, or the Kummer and Whittaker functions of the first and second kind which are known from the mathematical literature [17]. Therefore, in order to facilitate the implementation of the Coulomb functions, we have to provide also a simple interface to these special functions; in the following, we briefly summarize the definition of these functions and for which type of arguments they are needed for the GREENS library.

Euler's Gamma function $\Gamma(z)$ and the Psi-function $\Psi(z)$ occur very frequently and in quite different fields of physics. While the Γ -function is defined by the integral

$$\Gamma(z) = \int_0^{\infty} t^{z-1} e^{-t} dt \quad (39)$$

the Ψ -function refers to the derivative

$$\Psi(z) = \frac{d[\ln \Gamma(z)]}{dz}. \quad (40)$$

These functions are defined for all *complex arguments* z except of the real negative integers $z \neq -1, -2, \dots$ where they have their poles. In GREENS, the $\Gamma(z)$ function with real arguments z is needed for the computation of the bound-state wave and Green's functions, respectively, while complex arguments arise in the representation of the free-electron waves (7). The Ψ -function, in addition, arises in the calculation of the Kummer function $U(a, b; z)$ of the second kind if the argument b refers to an integer in the computation of nonrelativistic Green's functions.

Although the Coulomb wave and Green's functions are often expressed in terms of the Whittaker functions $M_{a,b}(z)$ and $W_{a,b}(z)$ of the first and second kind, in practical computations one makes better use of the Kummer functions of the corresponding kind, as discussed in Section 2.2.1 above. The Kummer functions $M(a, b; z)$ and $U(a, b; z)$ of the first and second kind refer to the *regular* and *irregular* solutions of Kummer's equation

$$z \frac{d^2 M}{dz^2} + (b - z) \frac{dM}{dz} - aM = 0; \quad (41)$$

in the literature, however, also several other notations are used for these functions such as $M(a, b; z) = {}_1F_1(a; b; z)$ or $U(a, b; z) = \Psi(a, b; z)$, respectively. Usually, the function $M(a, b; z)$ of the first kind is solved for the initial value $M(a, b; 0) = 1$ and, hence, is given by the confluent hypergeometric series

$$M(a, b; z) = 1 + \frac{a}{b}z + \frac{1}{2} \frac{a(a+1)}{b(b+1)}z^2 + \dots \quad (42)$$

The Kummer function of the first kind $M(a, b; z)$ is needed for both, real a, b, z and complex arguments a, z to represent the radial wave and Green's function components. In contrast, the Kummer function $U(a, b; z)$ of the second kind is required only for real argument b , for which it can be expressed as a linear combination

$$U(a, b; z) = \frac{\pi}{\sin \pi b} \left[\frac{M(a, b; z)}{\Gamma(1+a-b)\Gamma(b)} - z^{1-b} \frac{M(a+1-b, 2-b; z)}{\Gamma(a)\Gamma(2-b)} \right] \quad (43)$$

of two Kummer functions of the first kind; the function $U(a, b; z)$ arises in the computation of the radial Green's function.

The following section explains how these *special functions* from the GREENS library can be used also in applications other than the computation of Coulomb wave and Green's functions.

3. Program organization

3.1. Overview about the GREENS library

The GREENS library has been designed mainly in order to facilitate numerical applications of the Coulomb wave and Green's functions from Section 2. It provides the user with a set of C++ procedures to compute the *radial* components of these functions within both, a *nonrelativistic* as well as *relativistic* framework. Apart from the radial components, however, we also support the numerical integration of the Coulomb functions as well as the computation of a few selected matrix elements which, below, will help us demonstrate the application of the GREENS library. To provide the user with a simple access to the various functions, the concepts of object-oriented programming such as *structures*, *classes* and *members* as well as the *overloading* of procedures and operators have been utilized carefully.

Table 1 lists the *main* procedures of the GREENS library for calculating the energies and radial components of the Coulomb functions. To simplify the use of the library, the classes `spinor2_col`, `spinor2_raw`, and `matrix_2x2` have been implemented to describe the radial spinor (11), its adjunct raw spinor, and the radial Green's matrix (26), respectively. The classes `spinor2_col` and `spinor2_raw`, for instance, contain each the two members `.L` and `.S` to represent the large and small components of a relativistic wave function, while the class `matrix_2x2` has the four members `.LL`, `.LS`, `.SL`, and `.SS` with an obvious meaning. The class `matrix_2x2`, moreover, also contains the member `.e` which just returns all the four matrix elements together within a 2×2 array.

In order to treat the bound- and free-electron states in a similar way, the two wave function procedures `green_radial_orbital()` and `green_radial_spinor()` have been *overloaded*. For these two procedures, a first *integer* argument $n \geq 1$ is used to represent the principal quantum number and to return the corresponding bound-state solution, while a (first) argument $E > 0$ of type `double` refers to the kinetic energy of a free-electron state (in Hartree units). As mentioned above, however, this energy E does not include the electron rest energy, neither in the nonrelativistic nor relativistic framework. The two additional procedures `greens_set_nuclear_charge()` and `greens_get_nuclear_charge()` from Table 1 can be called to re-define or to return the current value of the nuclear charge which is utilized for the computation of all radial functions. The default value of the nuclear charge is $Z = 1$.

In most applications, the (radial) Coulomb wave and Green's function components usually occur as part of some matrix element and, hence, first require an additional integration (over r and/or r') before any *observable* quantity is obtained. Therefore, to facilitate such applications, we also provide the utility procedure `greens_integral_GL()` which evaluates a 1- or 2-dimensional integral over a finite or infinite area with *user-defined* accuracy, see Table 2. In this procedure, a Gauss–Legendre quadrature [17] of appropriate order is applied, independently for each dimension of the integrand. Moreover, to ensure a result which is accurate up to a given number of `d` valid digits, the domain of integration is divided by steps into subdomains until the required accuracy is obtained. A `WARNING` arises during the execution, if the requested precision cannot be guaranteed by the procedure. As seen from Table 2, the procedure name `greens_integral_GL()` is *overloaded* and, thus, can be invoked with rather different lists of parameters, from which the dimension of the integral, the integration domain as well as the type of the function is deduced. Apart from a real-valued integrand $f(x)$ or $f(x, y)$, respectively, `greens_integral_GL()` also supports a `matrix_2x2`-valued integrand as appropriate for the computation of matrix elements such as (38) from the relativistic theory. In the latter case, for instance, all the four integrals U^{LL} , U^{LS} , U^{SL} and U^{SS} in (37) could be treated simultaneously.

A second utility procedure `greens_two_photon_cs()` from Table 2 enables the user to calculate two-photon ionization cross sections in various approximations. Obviously, this procedure makes use of `greens_integral_GL()` and is mainly provided for test purposes below. It helps compute the total two-photon ionization cross sections σ_2 for linear or circular polarized light and within either the nonrelativistic or relativistic framework, respectively. In all of these cases, however, the computation of the cross sections is restricted to the long-wavelength approximation $e^{i\mathbf{k}\mathbf{r}} = 1$ for the coupling of the radiation field and to the ionization of an electron from the unpolarized $1s$ ground

Table 1

Main procedures of the GREENS library to calculate the energies and radial wave and Green's functions for hydrogen-like ions. The (expected) type of parameters is shown by using the syntax of C++; all quantities below must be given in atomic units

Procedure	Arguments	Description and comments
double greens_energy	(int n)	Returns the nonrelativistic energy E_n (in a.u.) of a bound-state solution with principal quantum number n ; see Eq. (5).
	(int n, int kappa)	Returns the relativistic energy $E_{n\kappa}$ (in a.u.) of a bound-state solution quantum numbers n and κ ; see Eq. (14).
double greens_radial_orbital	(int n, int l, double r)	Computes the value of the radial function $P_{nl}(r)$ at r of a bound state (6) with principal quantum number n and orbital angular momentum l .
	(double E, int l, double r)	Computes the value of the radial function $P_{El}(r)$ at r of a free-electron state (7) with energy $E > 0$ and orbital angular momentum l .
spinor2_col greens_radial_spinor	(int n, int kappa, double r)	Computes the value of the radial spinor function $\begin{pmatrix} P_{n\kappa}(r) \\ Q_{n\kappa}(r) \end{pmatrix}$ at r of a bound state (15), (16) with principal quantum number n and relativistic angular momentum quantum number κ .
	(double E, int kappa, double r)	Computes the value of the radial spinor function $\begin{pmatrix} P_{E\kappa}(r) \\ Q_{E\kappa}(r) \end{pmatrix}$ at r of a free-electron state with energy E and relativistic angular momentum quantum number κ .
double greens_radial_function	(double E, int l, double r, double r')	Computes the radial Coulomb Green's function $g_{El}(r, r')$ at r and r' from (22) for the energy $E < 0$ and orbital angular momentum l .
matrix_2x2 greens_radial_matrix	(double E, int kappa, double r, double r')	Computes the radial Coulomb Green's matrix $\begin{pmatrix} g_{E\kappa}^{LL} & g_{E\kappa}^{LS} \\ g_{E\kappa}^{SL} & g_{E\kappa}^{SS} \end{pmatrix}$ from (26) at r and r' for the energy $E < 0$ and the relativistic angular momentum quantum number κ .

Table 2

Utility procedures of the GREENS library for the numerical integration of 1- and 2-dimensional functions and the computation of two-photon ionization cross sections σ_2 in various approximations. The same notation as in Table 1 is used

Procedure	Arguments	Description and comments
double greens_integral_GL	(double(*funct)(double x), double a, double b, int d)	Calculates the definite (1-dimensional) integral $\int_a^b f(x) dx$ with an accuracy of (at least) d valid digits.
	(double(*funct)(double x), int d)	Calculates the definite (1-dimensional) integral $\int_0^\infty f(x) dx$ with an accuracy of (at least) d valid digits if $f(x)$ does not oscillate rapidly and vanishes sufficiently fast for large values of x .
	(double(*funct)(double x, double y), double ax, double bx, double ay, double by, int d)	Calculates the definite (2-dimensional) integral $\int_{a_x}^{b_x} \int_{a_y}^{b_y} f(x, y) dx dy$ with an accuracy of (at least) d valid digits. This procedure applies an adaptive Gauss–Legendre integration formula, independently in each dimension.
	(double(*funct)(double x, double y), int d)	Calculates the definite (2-dimensional) integral $\int_0^\infty \int_0^\infty f(x, y) dx dy$ with an accuracy of (at least) d valid digits if $f(x, y)$ does not oscillate rapidly and vanishes sufficiently fast for large values of x and y .
double greens_two_photon_cs	("nonrelativistic", "circular", double E_ph, int d)	Computes the nonrelativistic two-photon ionization cross section (35) for circular polarized light, in long-wavelength approximation, and for a photon energy $E_{ph} > E_{1s}/2$. A cross section value in atomic units and with an accuracy of (at least) d valid digits is returned.
	("nonrelativistic", "linear", double E_ph, int d)	Computes the nonrelativistic two-photon ionization cross section for linear polarized light and in long-wavelength approximation.
	("relativistic", "circular", double E_ph, int d)	Computes the relativistic two-photon ionization cross section (37) for circular polarized light, in long-wavelength approximation, and for a photon energy $E_{ph} > E_{1s}/2$.
	("relativistic", "linear", double E_ph, int d)	Computes the relativistic two-photon ionization cross section for linear polarized light and in long-wavelength approximation.

Table 3

Special function procedures of the GREENS library. The same notation as in Table 1 is used. The type of all procedures is `double` if all arguments are `double`, and is of type `complex` otherwise

Procedure	Arguments	Description and comments
GAMMA	(double z) or (complex z)	Returns the $\Gamma(z)$ function (39) for either a real or complex argument z .
Psi	(double z) or (complex z)	Returns the $\Psi(z)$ function (40) for either a real or complex argument z .
KummerM	(double a, double b, double z) or (complex a, double b, complex z)	Calculates the Kummer function $M(a, b; z)$ of the first kind (42) for real and/or complex arguments a, b , and z .
KummerU	(double a, double b, double z)	Calculates the Kummer function $U(a, b; z)$ of the second kind (43) for real arguments a, b , and z .
WhittakerM	(double a, double b, double z) or (complex a, double b, complex z)	Calculates the Whittaker function $M_{a,b}(z)$ of the first kind (23) for either real or complex arguments a, b , and z ; b must be real.
WhittakerW	(double a, double b, double z)	Calculates the Whittaker function $W_{a,b}(z)$ of the second kind (24) for real arguments a, b , and z .

state. In addition, the photon energy E_γ , i.e. the third argument of the procedure `greens_two_photon_cs()` must be in the range $-E_{1s}/2 < E_\gamma < -E_{1s}$ where E_{1s} is the (negative) $1s$ -binding energy from Eqs. (5) or (14). Again, the last argument `d` refers to the requested accuracy of the cross section of (at least) `d` valid digits and is transferred directly to the underlying integration procedure `greens_integral_GL()`.

Of course, the wave and Green's functions from Section 2 can hardly be implemented without a proper set of *special function* procedures. Therefore, Table 3 displays those procedures which are provided by the GREENS library and which we briefly discussed in Section 2.4. The allowed types of the parameters are also displayed in this table.

3.2. Distribution and compilation of the GREENS library

The GREENS library will be distributed as the gzipped tar-file `greens.tar.gz` from which the `greens` root directory is obtained by `gunzip greens.tar.gz` and `tar -xvf greens.tar`. This root contains a `Read.me` file, the `src` subdirectory for the source code as well as six subdirectories for various examples. In `src`, we provide the header file `greens.h` and a `makefile` to facilitate the compilation of the (static) library `libgreens.a` in the `greens` root directory. It also incorporates about 50 source files for all of the individual procedures.

In the following section, two examples from the subdirectories `example-coulomb-funct` and `example-twophoton-cs` are discussed in more detail and are taken as the test for the installation of the library. Each of these example subdirectories, again, contain a `makefile` from which an executable (`a.out`) is generated simply by typing `make` within the corresponding subdirectory. Since these `makefiles` also compile and link the library **libgreens.a**, the user may start directly from a copy of one of these subdirectories for his own *application* of the GREENS library.

4. Examples

To illustrate the use of the GREENS library, we first show how the (radial) Coulomb wave and Green's functions can be calculated for any point r or (r, r') , respectively. Hereby, a simple comparison between the nonrelativistic


```

#include "greens.h"

int main(void){
int n, l, kappa;           // quantum numbers
double r, rp, E, wf_nr, gf_nr; // coordinates, energies, etc.
spinor2_col wf_r;        // relativistic spinor
matrix_2x2 gf_r;         // relativistic Green's matrix

print("#Test of the Coulomb radial functions");

for(double Z=1.0; Z<93.0; Z=Z+91.0) {
  print();
  greens_set_nuclear_charge(Z); // set nuclear charge
  E = -greens_energy(1) * 0.8;

  rp = 2.5/Z; n = 4; l = 2; kappa = -3;
  write("# coord wf_nr wf_r.L ");
  print(" gf_nr gf_r.e[0][0] gf_r.LL");
  for (r=0.0; r<25.0/Z; r=r+0.1/Z){
    wf_nr = greens_radial_orbital(n, l, r);
    wf_r = greens_radial_spinor (n, l, r);
    gf_nr = greens_radial_function(-E, l, r, rp);
    gf_r = greens_radial_matrix (-E, l, r, rp);

    printf("%E %E %E %E %E %E\n", r, wf_nr, wf_r.L,
          gf_nr, gf_r.e[0][0], gf_r.LL);}}
return 0;}

```

Fig. 1. Calculation of the Coulomb wave and Green's functions for nuclear charge $Z = 1$ and $Z = 92$. The printout of this procedure is shown in the Test run output and in the file `printout.txt` in the subdirectory `example-coulomb-funct`.

and relativistic theory—in the limits of a low and high nuclear charge Z —is achieved by setting $Z = 1$ (hydrogen) and $Z = 92$ (hydrogen-like uranium), respectively. Fig. 1 displays the source code which evaluates the two radial functions $P_{4d}(r)$ and $P_{4d_{5/2}}(r)$, respectively, for r -values in the range $r = 0, \dots, 25./Z$ with a stepsize of $\Delta r = 0.1/Z$. Beside of these wave function components, this code also calculates the Coulomb Green's functions at the same values of r and for a fixed $r' = 2.5/Z$. For a call of this procedure, the printout is (partially) shown in the Test run output below. The source of this example and the complete printout can be found in the subdirectory `example-coulomb-funct`. In order to obtain the full radial part of the Coulomb wave and Green's functions, of course, the results of `greens_radial_orbital()` and `greens_radial_spinor()` must be multiplied with $1/r$, while the values from `greens_radial_function()` and `greens_radial_matrix()` have to be multiplied with $1/r'$, respectively.

A second example concerns the computation of the two-photon ionization cross sections for the two ions from above. For these ions, the $1s$ binding energies are $-1/2$ and -4232 Hartrees within the nonrelativistic theory. In the TEST RUN OUTPUT below, the two-photon ionization cross sections for circular and linear polarized light and within both, the nonrelativistic and relativistic approximation. For each of these ions, the cross sections are calculated with an accuracy of about six digits for the ten energies $E_o, E_o + 0.01 * Z^2, \dots, E_o + 0.09 * Z^2$ where $E_o = 0.3 * Z^2$ corresponds to 60% of the nonrelativistic $1s$ binding energy. Again, the full source of this example is provided with the GREENS library in the subdirectory `example-twophoton-cs` and, thus, can easily be modified for any other photon energy.

5. Summary and outlook

To facilitate applications of the ‘hydrogen ion model’ in quite different fields of physics, the GREENS library is presented and provides a set of C++ procedures for the computation of the Coulomb wave and Green’s functions within both, a nonrelativistic as well as relativistic framework. Since C++ is today freely available for most architectures, an object-oriented approach to the Coulomb problem could be realized without the need for special compilers or other mathematical libraries. Apart from the radial Coulomb functions, however, GREENS also provides a set of special functions as well as a few utility procedures to evaluate, for instance, the two-photon ionization cross sections in long-wavelength approximation.

In the future, various extensions of the GREENS library might be of great interest for the physics community. Owing to the current design of several *free-electron laser* (FEL) facilities worldwide, for example, systematic investigations on multiphoton processes become more and more likely also in the EUV and X-ray region, where the inner-shell electron get involved. For such investigations, which will consider also many-electron atoms and ions, the generation of *effective* one-particle Green’s functions are certainly desirable. First steps into this direction, including the combination with the well-known RATIP package [19], are currently under work in our group.

References

- [1] C.J. Noble, I.J. Thompson, *Comput. Phys. Commun.* 33 (1984) 413.
- [2] K.L. Bell, N.S. Scott, *Comput. Phys. Commun.* 20 (1980) 447.
- [3] <http://sources.redhat.com/gsl/>.
- [4] L.B. Madsen, J.P. Hansen, H.M. Nilsen, *Comput. Phys. Commun.* 120 (1999) 231.
- [5] F. Salvat, et al., *Comput. Phys. Commun.* 90 (1995) 151.
- [6] L. Hostler, *J. Math. Phys.* 5 (1964) 591.
- [7] L. Hostler, *J. Math. Phys.* 11 (1970) 2966.
- [8] J. Mlodzki, *Comput. Phys. Commun.* 34 (1984) 211.
- [9] R.A. Swainson, G.W.F. Drake, *J. Phys. A* 24 (1991) 95.
- [10] A. Maquet, V. Veniard, T.A. Marian, *J. Phys. B* 31 (1998) 3743.
- [11] A. Messiah, *Quantum Mechanics*, North-Holland, Amsterdam, 1999.
- [12] G.W.F. Drake, *Atomic, Molecular, and Optical Physics Handbook*, Woodbury, New York, 1996.
- [13] R.A. Swainson, G.W.F. Drake, *J. Phys. A* 24 (1991) 79.
- [14] D.A. Varshalovich, A.N. Moskalev, V.K. Khersonskii, *Quantum Theory of Angular Momentum*, World Scientific, Singapore, 1988.
- [15] J. Eichler, W.E. Meyerhof, *Relativistic Atomic Collisions*, Academic Press, New York, 1995.
- [16] P. Morse, H. Feshbach, in: *Methods of Theoretical Physics*, Vol. 1, McGraw-Hill, New York, 1953, p. 821.
- [17] M. Abramowitz, I.A. Stegun (Eds.), *Handbook of Mathematical Functions*, Dover, New York, 1965.
- [18] G.W. Series (Ed.), *The Spectrum of Atomic Hydrogen: Advances*, World Scientific, New Jersey, 1988.
- [19] S. Fritzsche, *J. Electr. Spec. Rel. Phenom.* 114–116 (2001) 1155.

TEST RUN OUTPUT

A. Computation of the radial Coulomb wave and Green's functions

#Test of the Coulomb radial functions

#Nuclear charge is changed to 1.000000

#coord	wf_nr	wf_r.L	gf_nr	gf_r.e[0][0]	gf_r.LL
0.000000E+00	0.000000E+00	0.000000E+00	0.000000E+00	0.000000E+00	0.000000E+00
1.000000E-01	6.758392E-06	6.761076E-06	9.861696E-05	9.865164E-05	9.865164E-05
2.000000E-01	5.228909E-05	5.230066E-05	7.642130E-04	7.643481E-04	7.643481E-04
...					
2.480000E+01	-2.307241E-01	-2.307229E-01	8.979656E-09	8.980284E-09	8.980284E-09
2.490000E+01	-2.295400E-01	-2.295388E-01	8.243999E-09	8.244579E-09	8.244579E-09

#Nuclear charge is changed to 92.000000

#coord	wf_nr	wf_r.L	gf_nr	gf_r.e[0][0]	gf_r.LL
0.000000E+00	0.000000E+00	0.000000E+00	0.000000E+00	0.000000E+00	0.000000E+00
1.086957E-03	6.482422E-05	4.344695E-04	1.071923E-06	5.170738E-06	5.170738E-06
2.173913E-03	5.015393E-04	1.952599E-03	8.306663E-06	2.311893E-05	2.311893E-05
...					
2.706522E-01	-2.201670E+00	-2.088423E+00	8.960868E-11	1.641947E-10	1.641947E-10
2.717391E-01	-2.190133E+00	-2.074839E+00	8.226637E-11	1.512671E-10	1.512671E-10

B. Computation of two-photon ionization cross sections

#Test of the two-photon ionisation cross sections

#Digits is changed to 6

#Nuclear charge is changed to 1.000000

#E	cs_nr_c	cs_r_c	cs_nr_l	cs_r_l
3.000000E-01	8.728681E-01	8.727765E-01	5.849625E-01	5.849002E-01
3.100000E-01	8.819793E-01	8.818399E-01	5.889291E-01	5.888364E-01
3.200000E-01	9.143732E-01	9.143980E-01	6.095973E-01	6.096138E-01
...				
3.800000E-01	5.778480E+00	5.794808E+00	4.829547E+00	4.843563E+00
3.900000E-01	1.792990E-01	1.796899E-01	2.330477E-01	2.333333E-01

#Nuclear charge is changed to 92.000000

#E	cs_nr_c	cs_r_c	cs_nr_l	cs_r_l
2.539200E+03	1.439533E-12	6.927729E-13	9.647196E-13	4.629667E-13
2.623840E+03	1.454559E-12	6.763950E-13	9.712612E-13	4.510878E-13
2.708480E+03	1.507983E-12	6.588038E-13	1.005347E-12	4.392479E-13
...				
3.216320E+03	9.529863E-12	6.744809E-13	7.964884E-12	4.646710E-13
3.300960E+03	2.956996E-13	7.498654E-13	3.843421E-13	5.232579E-13

E.2 Relativistic and retardation effects in the two-photon ionization of hydrogen-like ions

Koval P, Fritzsche S and Surzhykov A
2003 *J. Phys. B: At. Mol. Phys.* **36** 873-878.

Relativistic and retardation effects in the two-photon ionization of hydrogen-like ions

Peter Koval¹, Stephan Fritzsche and Andrey Surzhykov

Fachbereich Physik, Universität Kassel, Heinrich-Plett Straße 40, D-34132 Kassel, Germany

E-mail: kovalp@physik.uni-kassel.de

Received 22 November 2002, in final form 20 January 2003

Published 14 February 2003

Online at stacks.iop.org/JPhysB/36/873

Abstract

The non-resonant two-photon ionization of hydrogen-like ions is studied in second-order perturbation theory, based on the Dirac equation. To carry out the summation over the complete Coulomb spectrum, a Green function approach has been applied to the computation of the ionization cross sections. Exact second-order relativistic cross sections are compared with data as obtained from a relativistic long-wavelength approximation as well as from the scaling of non-relativistic results. For high- Z ions, the relativistic wavefunction contraction may lower the two-photon ionization cross sections by a factor of two or more, while retardation effects appear less pronounced but still give rise to non-negligible contributions.

1. Introduction

The multi-photon ionization of atoms has been widely studied during the last few decades. While, however, most previous atomic experiments focused on the multi-photon ionization of the valence-shell electrons of the alkaline metal and group I elements (Jaouen *et al* 1984, Antoine *et al* 1996), theoretical investigations instead often dealt with the excitation and ionization of low- Z , hydrogen- and helium-like ions, owing to their simplicity (Karule 1985, Maquet *et al* 1998). With the recent progress in the development and set-up of coherent light sources in the EUV and x-ray domain, such as the various free-electron lasers, it now becomes much more likely that two- and multi-photon processes will also be observed for the inner-shell electrons of medium and heavy elements in the near future (Kornberg *et al* 2002). Since, generally, a relativistic theory is needed to describe such elements, the primary interest in studying multi-photon processes may concern first the importance of relativistic effects along the hydrogen isoelectronic sequence. In the past, similar investigations have been carried out only for the decay of the $2s_{1/2}$ metastable level (Santos *et al* 2001) as well as for the two-photon excitation from the $1s$ ground states of hydrogen-like ions (Szymanowski *et al* 1997).

¹ Author to whom any correspondence should be addressed.

To the best of our knowledge, however, no attempt has been made so far to explore two- and multi-photon ionization for medium- and high- Z ions by means of a relativistic theory.

In this paper, we consider the two-photon ionization of hydrogen-like ions in second-order perturbation theory, based on the Dirac equation. To obtain the total ionization cross sections, a Green function approach is applied in section 2 to perform the summation over the *complete hydrogen spectrum* appropriately. Using such an approach, cross sections for the two-photon ionization of the 1s ground state of hydrogen-like ions are calculated for nuclear charges in the range $Z = 1, \dots, 100$ in order to explore both the relativistic contraction of the wavefunctions as well as those effects which arise from the higher multipoles in the decomposition of the radiation field, i.e. the so-called *retardation effects*. Section 3, later, provides a comparison of the cross sections from the relativistic theory (as obtained in two different approximations) as well as from the scaling of non-relativistic results. Finally, a few conclusions are given in section 4.

2. Two-photon ionization cross section. Perturbative treatment

In second-order perturbation theory, the two-photon ionization cross section σ_2 is given by (Laplanche *et al* 1976)

$$\sigma_2 = \frac{8\pi^3 \alpha^2}{E_\gamma^2} \left| \sum_{\nu} \frac{\langle \psi_f | \mathbf{p} \cdot \mathbf{u}_{\lambda_2} e^{ik_2 \cdot r} | \psi_\nu \rangle \langle \psi_\nu | \mathbf{p} \cdot \mathbf{u}_{\lambda_1} e^{ik_1 \cdot r} | \psi_i \rangle}{E_\nu - E_i - E_\gamma} \right|^2, \quad (1)$$

where (ψ_i, E_i) , (ψ_ν, E_ν) and (ψ_f, E_f) denote the wavefunctions and the energies of the initial, intermediate and final atomic states, respectively². In this expression, as usual, the electron–photon interaction is described in terms of the transition operator $\mathbf{p} \cdot \mathbf{u}_\lambda e^{ik \cdot r}$ which includes the momentum \mathbf{p} of the electron and the photon wave $\mathbf{u}_\lambda e^{ik \cdot r}$. As appropriate for laser experiments, here and in the following we assume that the two photons have equal wavevectors $\mathbf{k}_1 = \mathbf{k}_2 = \mathbf{k}$ and equal helicities $\lambda_1 = \lambda_2 = \lambda = \pm 1$, i.e. that they have the same circular polarization. Then, the energy $E_f = E_i + 2E_\gamma$ of the emitted electron simply follows from the energy conservation and is given by the energy of the initial state and twice the photon energy E_γ .

2.1. Green function method

Apart from the usual integration over the spatial coordinates, the evaluation of the transition amplitude in equation (1) also requires a *summation* over the complete spectrum of the (hydrogen) ion. Obviously, this summation includes the sum over all discrete states as well as an integration over the continuum. In particular, the second part, i.e. the integration over the continuum, is rather difficult to carry out in practice since it implies the computation of *free–free* electronic transitions. An alternative to carrying out the summation over the spectrum explicitly in the transition amplitude is given by a change in the sequence of summation and integration from $\int \int d\mathbf{r} dE_\nu$ to $\int \int dE_\nu d\mathbf{r}$.

Then, the summation over the complete hydrogen spectrum can be replaced by the Coulomb–Green function (Swainson and Drake 1991)

$$G_E(\mathbf{r}, \mathbf{r}') = \sum_{\nu} \frac{|\psi_\nu(\mathbf{r})\rangle \langle \psi_\nu(\mathbf{r}')|}{E_\nu - E} \quad (2)$$

which is zero at the origin and tends to zero if $r \rightarrow \infty$ or $r' \rightarrow \infty$. This particular property

² Here and in the following, we use Hartree atomic units. Since the two-photon ionization cross section σ_2 has the dimension $\text{length}^4 \times \text{time}$, it can easily be converted to other units such as $\text{cm}^4 \text{s}$ by using the *conversion factor* 1.89679×10^{-50} .

of the Coulomb–Green function ensures that the second-order transition amplitudes in (1) can be evaluated even if the continuum wavefunctions ψ_f remain oscillating at large r .

Using the Green function (2), the ionization cross section (1) can be rewritten in the form (Maquet *et al* 1998)

$$\sigma_2 = \frac{8\pi^3\alpha^2}{E_\gamma^2} |\langle \psi_f | \mathbf{p} \cdot \mathbf{u}_\lambda e^{ik \cdot \mathbf{r}} G_{E_i+E_\gamma}(\mathbf{r}, \mathbf{r}') \mathbf{p}' \cdot \mathbf{u}_\lambda e^{ik \cdot \mathbf{r}'} | \psi_i \rangle|^2, \quad (3)$$

including a new *double* integration over \mathbf{r} and \mathbf{r}' . For hydrogen-like ions, the Coulomb–Green functions $G_E(\mathbf{r}, \mathbf{r}')$ are known analytically, within both the non-relativistic and the relativistic theory. Based on the Dirac Hamiltonian with a hydrogen potential, $H_D = c\boldsymbol{\alpha} \cdot \mathbf{p} + \beta mc^2 - Z/r$, a radial–angular representation of the relativistic Coulomb–Green function was given earlier by Swainson and Drake (1991). In the evaluation of matrix elements, such a representation allows for analytic integration over all angles using the techniques of Racah algebra, while the radial integration often has to be carried out numerically.

2.2. Multipole expansion of the photon wave

To evaluate the *angular part* of the transition amplitude in expression (3), of course, we need first to represent the photon wave in terms of its electric and magnetic multipole fields (Rose 1957):

$$\mathbf{u}_\lambda e^{ikz} = \sqrt{2\pi} \sum_{L=1}^{\infty} i^L \sqrt{2L+1} (\mathcal{A}_{L\lambda}^{(m)} + i\lambda \mathcal{A}_{L\lambda}^{(e)}), \quad (4)$$

where, for the sake of simplicity, we have taken the quantization axis, i.e. the z -axis, along the photon momenta direction \mathbf{k} . For a proper radial–angular representation of all Coulomb wave and Green functions, then, the transition amplitude can be reduced to a (finite) sum of products of the type *angular coefficient* \times *radial integral*, depending on the number of multipoles and on further approximations which are made for the (coupling of the) radiation field. In our computations, the angular coefficients were obtained algebraically, using the RACAH program (Fritzsche 1997, Fritzsche *et al* 2001). For the radial integrals, in contrast, we applied the procedures from the GREENS library (Koval and Fritzsche 2003). Owing to the structure of the radial Green function (matrix), this implies a double integration over a two-dimensional area with $0 \leq r < \infty$ and $0 \leq r' \leq \infty$, for which an adaptive numerical integration algorithm with a user-defined precision was developed. This algorithm is based on the Gauss–Legendre quadrature and has also been implemented in the GREENS library.

3. Results and discussion

3.1. Relativistic Z -scaling rule

Different approximations can be applied to investigate the two-photon ionization of hydrogen-like ions, depending on the photon frequency and the nuclear charge. In non-relativistic quantum theory, for instance, the total non-resonant cross section in the long-wavelength approximation is known to scale down like

$$\sigma_2(Z, E_\gamma Z^2) = \frac{1}{Z^6} \sigma_2(Z = 1, E_\gamma), \quad (5)$$

i.e. with the sixth power of the nuclear charge, if—at the same time—the photon energy is scaled with Z^2 (Zernik 1964). This scaling rule for the non-resonant part of the cross section applies for all photon energies $\text{Ryd}/2 \leq E_\gamma < \text{Ryd}$ below of the one-photon threshold of

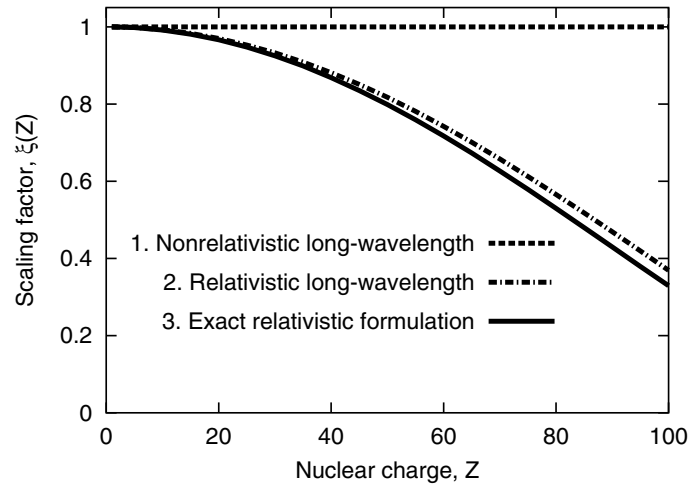


Figure 1. The dependence of the scaling factor $\xi(Z)$ on the nuclear charge Z for $\varepsilon = 1.05$, i.e. for a two-photon excess energy of 5%. (1) The non-relativistic long-wavelength approximation; (2) the relativistic long-wavelength approximation; (3) the exact relativistic second-order results.

hydrogen ($Z = 1$), where $\text{Ryd} \simeq 13.6$ eV refers to the hydrogen ground-state energy. To display the deviations of the cross sections in the different relativistic approximations from the non-relativistic scaling, we may rewrite equation (5) in the form

$$\sigma_2(Z, E_\gamma(Z)) = \frac{\xi(Z)}{Z^6} \sigma_2(Z = 1, E_\gamma(Z = 1)), \quad (6)$$

where the photon energy $E_\gamma(Z) \equiv \varepsilon |E_{1s}(Z)|/2$ now depends on the relativistic binding energy and, thus, shows a slightly more complicated Z -dependence than the non-relativistic $\sim Z^2$ behaviour. As above, we may restrict ourselves to photon energies with $1 \leq \varepsilon < 2$, below of the one-photon threshold of all hydrogen ions. With this definition of ε , however, the interpretation of the scaling rule (6) becomes quite simple as, say, a value $\varepsilon = 1.05$ obviously specifies the photon energy, so the total energy of the two photons together exceeds the 1s threshold by just 5%; a definition which can also be used in the non-relativistic case. Thus, the *net* deviation between the various approximations is shown in the scaling factor $\xi(Z)$ which, in the non-relativistic limit, is $\xi(Z) \equiv 1$.

3.2. Relativistic and retardation effects

Figure 1 displays the scaling factor $\xi(Z)$ as a function of the nuclear charge $1 \leq Z \leq 100$ for $\varepsilon = 1.05$, i.e. for a two-photon excess energy of 5% which is well within the non-resonant region. Three different approximations are shown in this figure: apart from the trivial non-relativistic factor $\xi(Z) = 1$, the scaling factors are given for the relativistic long-wavelength approximation $e^{ik \cdot r} = 1$ (dashed-dotted curve) as well as for the exact second-order perturbation treatment of all retardation effects (solid curve). In practice, only the multipole fields up to $L_{max} = 5$ are needed in (4) in order to obtain convergence of the corresponding cross sections at about the 1% level.

When compared with the non-relativistic decrease of the two-photon ionization cross sections, owing to the $1/Z^6$ scaling of the cross sections in equation (5), a further significant reduction arises for multiply and highly charged ions mainly because of the relativistic contraction of the wavefunctions towards the nucleus. This contraction can lower the cross sections easily by a factor of two or more in the high- Z domain. The incorporation of

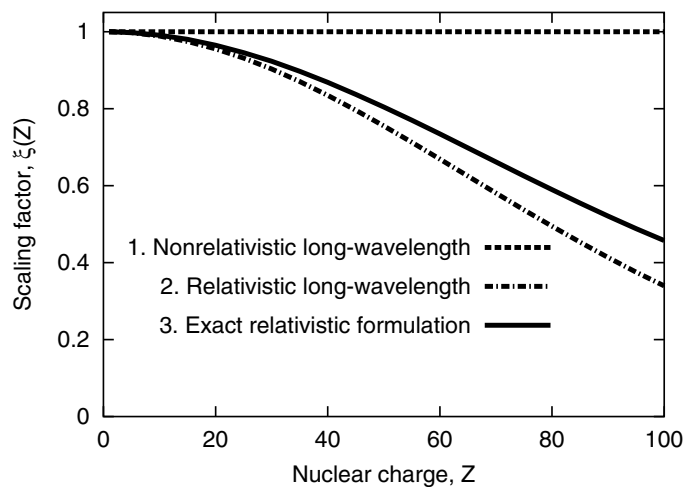


Figure 2. The dependence of the scaling factor $\xi(Z)$ on the nuclear charge Z for $\varepsilon = 1.40$. All other notation is the same as in figure 1.

higher multipoles beyond the E1–E1 dipole approximation, in contrast, contributes even for large values of $Z \sim 100$ only to $\leq 5\%$ for photon energies near the two-photon threshold. Somewhat larger retardation effects, however, are found for higher photon energies. For a two-photon excess energy of, say, 40% above the threshold (cf figure 2), the *retarded* two-photon cross sections (solid curve) are now larger than the cross sections in the long-wavelength approximation with deviation up to about 30% at the high- Z end of the sequence. The behaviour of the retarded cross sections with respect to the long-wavelength approximation clearly shows the importance of higher multipoles which, otherwise, are usually seen only in angle-differential measurements (Surzhykov *et al* 2002).

4. Conclusions

In conclusion, the non-resonant two-photon ionization of hydrogen-like ions has been studied in detail within the relativistic theory. Emphasis was placed, in particular, on the relativistic contraction of the wavefunctions as well as on the retardation in the cross sections which arise from higher multipoles of the radiation field. However, our computations also showed that a Green function approach may provide reliable access to second-order properties other than the total two-photon ionization cross sections. Investigations of the angle-differential emission of electrons as well as the two-photon decay of few-electron ions are currently under way (see, for example, Manakov *et al* 1999).

Acknowledgment

This work has been supported by the Deutsche Forschungsgemeinschaft (DFG) within the framework of the Schwerpunkt ‘Wechselwirkung intensiver Laserfelder mit Materie’.

References

- Antoine P, Essarroukh N-E, Jureta J, Urbain X and Brouillard F 1996 *J. Phys. B: At. Mol. Opt. Phys.* **29** 5367
 Fritzsche S 1997 *Comput. Phys. Commun.* **103** 51
 Fritzsche S, Inghoft T, Bastug T and Tomaselli M 2001 *Comput. Phys. Commun.* **139** 314

- Jaouen M, Laplanche G and Rachman A 1984 *J. Phys. B: At. Mol. Phys.* **17** 4643
- Karule E 1985 *J. Phys. B: At. Mol. Phys.* **18** 2207
- Kornberg M A, Godunov A L, Ortiz S I, Ederer D L, McGuire J H and Young L 2002 *J. Synchrotron Radiat.* **9** 298
- Koval P and Fritzsche S 2003 *Comput. Phys. Commun.* at press
- Laplanche G, Durrieu A, Flank Y, Jaouen M and Rachman A 1976 *J. Phys. B: At. Mol. Phys.* **9** 1263
- Manakov N L, Maquet A, Marmo S I, Vénierard V and Ferrante G 1999 *J. Phys. B: At. Mol. Opt. Phys.* **32** 3747
- Maquet A, Vénierard V and Marian T A 1998 *J. Phys. B: At. Mol. Opt. Phys.* **31** 3743
- Rose M E 1957 *Elementary Theory of Angular Momentum* (New York: Wiley)
- Santos J P, Patte P, Parente F and Indelicato P 2001 *Eur. J. Phys. D* **13** 27
- Surzhykov A, Fritzsche S, Gumberidze A and Stöhlker Th 2002 *Phys. Rev. Lett.* **88** 153001
- Swainson R A and Drake G W F 1991 *J. Phys. A: Math. Gen.* **24** 95
- Szymanowski C, Vénierard V, Taïeb R and Maquet A 1997 *Europhys. Lett.* **6** 391
- Zernik W 1964 *Phys. Rev. A* **135** 51

E.3 Electron angular distributions in the two-photon ionization of heavy hydrogen-like ions: a relativistic description

Koval P, Fritzsche S and Surzhykov A
2004 *J. Phys. B: At. Mol. Phys.* **37** 375-388.

Electron angular distributions in the two-photon ionization of hydrogen-like ions: a relativistic description

Peter Koval, Stephan Fritzsche and Andrey Surzhykov¹

Fachbereich Physik, Universität Kassel, Heinrich-Plett Straße 40, D-34132 Kassel, Germany

E-mail: surz@physik.uni-kassel.de

Received 28 August 2003

Published 17 December 2003

Online at stacks.iop.org/JPhysB/37/375 (DOI: 10.1088/0953-4075/37/2/006)

Abstract

The angular distribution of the emitted electrons, following the two-photon ionization of hydrogen-like ions, is studied within the framework of second order perturbation theory *and* the Dirac equation. Using a density matrix approach, we have investigated the effects which arise from the polarization of the incoming light as well as from the higher multipoles in the expansion of the electron–photon interaction. For medium- and high- Z ions, in particular, the non-dipole contributions give rise to a significant change in the angular distribution of the emitted electrons, if compared with the electric dipole approximation. This includes a strong forward emission while, in the dipole approximation, the electron emission always occurs symmetrically with respect to the plane which is perpendicular to the photon beam. Detailed computations for the dependence of the photoelectron angular distributions on the polarization of the incident light are carried out for the ionization of H, and Xe⁵³⁺ and U⁹¹⁺ (hydrogen-like) ions.

1. Introduction

During the last decades, the multi-photon ionization of atoms and ions has been widely studied, both experimentally and theoretically. While, however, the majority of experiments were first of all concerned with the multi-photon ionization of complex atoms, most theoretical investigations instead dealt with the ionization (and excitation) of the much simpler hydrogen-like and helium-like systems. For atomic hydrogen, in contrast, multi-photon experiments have been rather scarce so far (Wolff *et al* 1988, Rottke *et al* 1990, Antoine *et al* 1996), mainly because of the lack of sufficiently intensive (and coherent) light sources in the UV and EUV region. With the recent progress in the set-up of intensive light sources in the EUV

¹ Author to whom any correspondence should be addressed.

and x-ray domain, such as the fourth-generation synchrotron facilities or variously proposed free-electron lasers, two- and multi-photon studies on the ionization of inner-shell electrons are now becoming more likely to be carried out in the future (Kornberg *et al* 2002), including case studies on medium- Z and high- Z *hydrogen-like* ions. With increasing charge (and intensity of the light), of course, relativistic effects will become important, and these have been investigated in the past for the two-photon excitation and decay (Goldman and Drake 1981, Szymanowski *et al* 1997, Santos *et al* 2001) as well as ionization (Koval *et al* 2003) of hydrogen-like ions. So far, however, all of these studies were focused on the total (excitation or decay) rates and ionization cross sections while, to the best of our knowledge, no attempts have been made to analyse the effects of relativity on *angular* resolved studies.

In this contribution, we explore the angular distribution of the electrons following the two-photon ionization of hydrogen-like ions. Second-order perturbation theory, based on Dirac's equation, is applied to calculate the two-photon amplitudes including the full (relativistic) electron–photon interaction. The angular distribution of the photoelectrons is then derived by means of the density matrix theory which has been found appropriate for most collision and ionization processes and, in particular, for the—*nonrelativistic*—two-photon angular-dependent studies (Laplanche *et al* 1986). Since, however, the basic concepts of the density matrix theory have been presented elsewhere (Blum 1981, Balashov *et al* 2000), we will restrict ourselves to a rather short account of this theory in section 2.1. Apart from a few basic relations, here we only show how the angular distribution of the electrons can be traced back to the two-photon transition amplitudes. The evaluation of these amplitudes in second-order perturbation theory and by means of Coulomb–Green functions are discussed later in sections 2.2 and 2.3, and including the full decomposition of the photon field in terms of its multipole components in section 2.4. Using such a decomposition, we have calculated the electron angular distributions for the two-photon ionization of the 1s ground state of hydrogen (H) as well as hydrogen-like xenon (Xe^{53+}) and uranium (U^{91+}). By comparing the angular distributions for different nuclear charges Z , we were able to analyse both the effects of the polarization of the (incoming) light and the contributions from higher (i.e. non-dipole) multipoles in the decomposition of the electron–photon interaction. These results are displayed in section 3 and clearly show that, with increasing charge Z , the higher multipole components lead to a strong emission in the forward direction (i.e. parallel to the propagation of the light), while the electric dipole approximation alone gives rise to a symmetric electron emission around the polar angle $\theta = 90^\circ$, similar to that obtained by nonrelativistic computations (Zernik 1964, Lambropoulos 1972, Arnous *et al* 1973). Finally, a brief summary on the two-photon ionization of medium and high- Z ions is given in section 4.

2. Theory

2.1. Density matrix approach

Within the density matrix theory, the state of a physical system is described in terms of so-called *statistical* (or *density*) operators (Fano and Racah 1959). These operators can be considered to represent, for instance, an ensemble of systems which are—altogether—in either a *pure* quantum state or in a *mixture* of different states with any degree of coherence. Then, the basic idea of the density matrix formalism is to *accompany* such an ensemble through the collision process, starting from a well-defined ‘initial’ state and by passing through one or, possibly, several intermediate states until the ‘final’ state of the collision process is attained.

In the two-photon ionization of hydrogen-like ions, the ‘initial’ state of the (combined) system ‘ion *plus* photons’ is given by the bound electron $|n_b j_b \mu_b\rangle$ and the two incoming

photons, if we assume a zero nuclear spin $I = 0$. For the sake of simplicity, we also restrict our treatment to the case that both photons will have *equal* momentum, $\mathbf{k}_1 = \mathbf{k}_2 = \mathbf{k}$, while the spin states of the photons may still differ from each other and are characterized in terms of the *helicity* parameters $\lambda_1, \lambda_2 = \pm 1$ (i.e. by means of their spin projections onto the direction of propagation \mathbf{k}). Of course, the case of equal photon momenta \mathbf{k} corresponds to the most frequent experimental set-up of the two-photon ionization of atoms and ions using, for instance, lasers or synchrotron radiation sources. With these assumptions in mind, the initial spin state of the overall system is determined by the direct product of the statistical operators of the ion and the two incident photons

$$\hat{\rho}_i = \hat{\rho}_b \otimes \hat{\rho}_\gamma \otimes \hat{\rho}_\gamma \quad (1)$$

or, explicitly, in a representation of the density matrix in terms of the individual momenta by

$$\langle n_b j_b \mu_b, \mathbf{k}\lambda_1, \mathbf{k}\lambda_2 | \hat{\rho}_i | n_b j_b \mu'_b, \mathbf{k}\lambda'_1, \mathbf{k}\lambda'_2 \rangle = \langle n_b j_b \mu_b | \hat{\rho}_b | n_b j_b \mu'_b \rangle \langle \mathbf{k}\lambda_1 | \hat{\rho}_\gamma | \mathbf{k}\lambda'_1 \rangle \langle \mathbf{k}\lambda_2 | \hat{\rho}_\gamma | \mathbf{k}\lambda'_2 \rangle. \quad (2)$$

In the ‘final’ state of the ionization, after the electron has *left* the nucleus, we just have a free electron with asymptotic momentum \mathbf{p} and spin projection m_s (as well as the bare residual ion with nuclear charge Z). Therefore, the final spin state is described by the statistical operator of the emitted (free) electron $\hat{\rho}_e$ which, in the framework of the density matrix theory, can be obtained from the initial-state density operator $\hat{\rho}_i$ owing to the relation (Blum 1981, Balashov *et al* 2000)

$$\hat{\rho}_f = \hat{\rho}_e = \hat{R} \hat{\rho}_i \hat{R}^\dagger. \quad (3)$$

In this simple relation, \hat{R} is called the transition operator and must describe the interaction of the electron with the (two photons of the) radiation field. Of course, the particular form of the transition operator \hat{R} depends on the framework in which we describe the coupling of the radiation field to the atom. As is appropriate for high- Z ions, below we will always refer to a *relativistic* treatment of the electron–photon interaction, based on Dirac’s equation and the *minimal coupling* of the radiation field (Berestetskii *et al* 1971).

Instead of applying equation (3), in practice, it is often more convenient to rewrite the statistical operators in a matrix representation. Using, for example, the initial spin density matrix (2), we easily obtain the density matrix of the (finally) emitted electron by

$$\begin{aligned} \langle \mathbf{p}m_s | \hat{\rho}_e | \mathbf{p}m'_s \rangle &= \sum_{\mu_b \mu'_b} \sum_{\lambda_1 \lambda'_1 \lambda_2 \lambda'_2} \langle n_b j_b \mu_b | \hat{\rho}_b | n_b j_b \mu'_b \rangle \langle \mathbf{k}\lambda_1 | \hat{\rho}_\gamma | \mathbf{k}\lambda'_1 \rangle \langle \mathbf{k}\lambda_2 | \hat{\rho}_\gamma | \mathbf{k}\lambda'_2 \rangle \\ &\times M_{\mathbf{b}\mathbf{p}}(m_s, \mu_b, \lambda_1, \lambda_2) M_{\mathbf{b}\mathbf{p}}^*(m'_s, \mu'_b, \lambda'_1, \lambda'_2), \end{aligned} \quad (4)$$

where use is made of the abbreviation

$$M_{\mathbf{b}\mathbf{p}}(m_s, \mu_b, \lambda_1, \lambda_2) = \langle \mathbf{p}m_s | \hat{R} | \mathbf{k}\lambda_1, \mathbf{k}\lambda_2, n_b j_b \mu_b \rangle \quad (5)$$

in order to represent the transition amplitudes for the two-photon ionization. The final-state density matrix (4) still contains the *complete* information about the ionization process (i.e. the properties of the bare ion *and* the electron) and, thus, can be used to derive all the observable properties of the photoelectrons. Obviously, however, the outcome of some considered experiment will depend on the particular set-up and the capability of the detectors for *resolving* the individual properties of the particles. In density matrix theory, this set-up of the experiment is typically described in terms of a (so-called) *detector operator* \hat{P} which characterizes the detector system as a whole. In fact, this detector operator can be considered to project out all those quantum states of the final-state system which lead to a ‘count’ at the detectors; in the language of the density matrix, therefore, the probability for an ‘event’

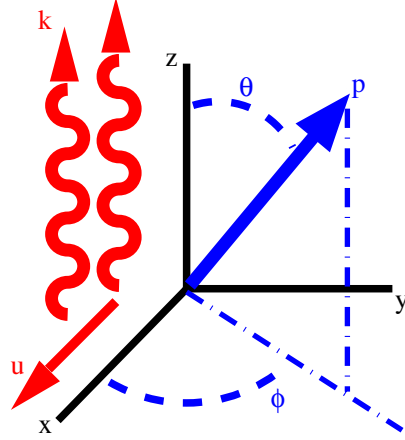


Figure 1. Geometry of the two-photon ionization. The photoelectron is emitted along the unit vector $\hat{\mathbf{p}} = (\theta, \phi)$ where θ is the (polar) angle between the incident photon momenta \mathbf{k} (chosen as the z -axis) and the electron momentum \mathbf{p} . Moreover, the (azimuthal) angle ϕ defines the angle of \mathbf{p} with respect to the x - z plane which, in the case of linearly polarized light, contains the polarization vector \mathbf{u} .

at the detector is simply given by the trace of the detector operator with the density matrix: $W = \text{Tr}(\hat{P}\hat{\rho})$.

To determine, for instance, the angular distribution of the emitted (photo-) electrons, we may assume a detector operator in a given direction $\hat{\mathbf{p}} = (\theta, \phi)$ (cf figure 1) which is *insensitive* to the polarization of the electrons

$$\hat{P} = \sum_{m_s} |\mathbf{p}m_s\rangle\langle\mathbf{p}m_s|, \quad (6)$$

i.e. a projection operator along \mathbf{p} and including a summation over the spin state m_s of the electrons. From this operator, and by taking the trace over the product $(\hat{P}\hat{\rho}_f)$ with the final-state density matrix (4), we obtain immediately the electron angular distribution in the form

$$W(\hat{\rho}) = \text{Tr}(\hat{P}\hat{\rho}_f) = \frac{1}{2j_b + 1} \sum_{\mu_b m_s} \sum_{\lambda_1 \lambda_1' \lambda_2 \lambda_2'} \langle \mathbf{k}\lambda_1 | \hat{\rho}_\gamma | \mathbf{k}\lambda_1' \rangle \langle \mathbf{k}\lambda_2 | \hat{\rho}_\gamma | \mathbf{k}\lambda_2' \rangle \\ \times M_{\mathbf{b}\mathbf{p}}(m_s, \mu_b, \lambda_1, \lambda_2) M_{\mathbf{b}\mathbf{p}}^*(m_s, \mu_b, \lambda_1', \lambda_2'), \quad (7)$$

where, for the sake of simplicity, we have assumed that the hydrogen-like ion is initially unpolarized. Apart from this additional assumption, however, equation (7) still represents the general form of the electron angular distribution for the process of the two-photon ionization of hydrogen-like ions. As is seen from this equation, the emission of the photoelectron will depend on the spin state of the incident photons, defined by the photon density matrices $\langle \mathbf{k}\lambda | \hat{\rho}_\gamma | \mathbf{k}\lambda' \rangle$. For any further evaluation of this distribution function, therefore, we shall first specify these density matrices or, in other words, the polarization of the incoming light. For example, if both photons are *unpolarized*, the (two) photon density matrices simply reduce to a constant $1/2$, $\langle \mathbf{k}\lambda | \hat{\rho}_\gamma | \mathbf{k}\lambda' \rangle = \delta_{\lambda\lambda'}/2$ (cf appendix, equation (A.2)) and lead us to the angular distribution

$$W^{\text{unp}}(\hat{\rho}) = \frac{1}{4(2j_b + 1)} \sum_{\mu_b m_s} \sum_{\lambda_1 \lambda_2} |M_{\mathbf{b}\mathbf{p}}(m_s, \mu_b, \lambda_1, \lambda_2)|^2. \quad (8)$$

For many (modern) light sources such as lasers or synchrotron radiation, it is not very practical to consider only *unpolarized* light from the very beginning. In general, instead, the angular distribution of the emitted electrons will depend both on the *type* as well as the *degree* of the polarization of the incident light. For *circularly* polarized light with degree P_C , for instance, the photon density matrix from equation (7) becomes $\langle \mathbf{k}\lambda | \hat{\rho}_\gamma | \mathbf{k}\lambda' \rangle = (1 + \lambda P_C) \delta_{\lambda\lambda'} / 2$ and, hence, gives rise to the angular distribution

$$W_{P_C}^{\text{circ}}(\hat{p}) = \frac{1}{4(2j_b + 1)} \sum_{\mu_b m_s \lambda_1 \lambda_2} (1 + \lambda_1 P_C)(1 + \lambda_2 P_C) |M_{\text{bp}}(m_s, \mu_b, \lambda_1, \lambda_2)|^2, \quad (9)$$

while, for *linearly* polarized light along the x -axis and with a polarization degree P_L , the photon density matrix is $\langle \mathbf{k}\lambda | \hat{\rho}_\gamma | \mathbf{k}\lambda' \rangle = \delta_{\lambda\lambda'} / 2 + (1 - \delta_{\lambda\lambda'}) P_L / 2$. If we evaluate equation (7) again with this latter density matrix, we obtain the angular distribution

$$\begin{aligned} W_{P_L}^{\text{lin}}(\hat{p}) = & \frac{1}{4(2j_b + 1)} \sum_{\mu_b m_s} \left((1 - P_L)^2 \sum_{\lambda_1 \lambda_2} |M_{\text{bp}}(m_s, \mu_b, \lambda_1, \lambda_2)|^2 \right. \\ & + P_L^2 \left| \sum_{\lambda_1 \lambda_2} M_{\text{bp}}(m_s, \mu_b, \lambda_1, \lambda_2) \right|^2 + 2P_L(1 - P_L) \\ & \left. \times \sum_{\lambda_1} \left| \sum_{\lambda_2} M_{\text{bp}}(m_s, \mu_b, \lambda_1, \lambda_2) \right|^2 \right) \end{aligned} \quad (10)$$

for the electrons as emitted in the two-photon ionization of hydrogen-like ions with linearly polarized light.

2.2. Two-photon transition amplitude in second-order perturbation theory

For any further analysis of the electron angular distributions, following the two-photon ionization of a hydrogen-like ion, we need to calculate the transition amplitude $M_{\text{bp}}(m_s, \mu_b, \lambda_1, \lambda_2)$ as seen from equations (8)–(10). This amplitude describes a *bound-free* transition of the electron under the (simultaneous) absorption of two photons. For a moderate intensity of the photon field, of course, this amplitude is most simply calculated by means of second-order perturbation theory (Laplanche *et al* 1976)

$$M_{\text{bp}}(m_s, \mu_b, \lambda_1, \lambda_2) = \frac{\sqrt{8\pi^3}}{\alpha E_\gamma} \sum_{\nu} \frac{\langle \psi_{\mathbf{p}m_s} | \alpha \mathbf{u}_{\lambda_1} e^{i\mathbf{k}\mathbf{r}} | \psi_{\nu} \rangle \langle \psi_{\nu} | \alpha \mathbf{u}_{\lambda_2} e^{i\mathbf{k}\mathbf{r}} | \psi_{n_b j_b \mu_b} \rangle}{E_{\nu} - E_b - E_\gamma}, \quad (11)$$

where the transition operator $\alpha \mathbf{u}_\lambda e^{i\mathbf{k}\mathbf{r}}$ describes the (relativistic) electron–photon interaction, the unit vector \mathbf{u}_λ the polarization of the photons, and where the summation runs over the complete one-particle spectrum. In equation (11), we added the factor $\sqrt{8\pi^3} / \alpha E_\gamma$ in order to ensure that the squared transition amplitude $|M_{\text{bp}}(m_s, \mu_b, \lambda_1, \lambda_2)|^2$ has a proper dimension of cross section. From the energy conservation, moreover, it follows immediately that the energies of the initial bound state, E_b , and the final continuum state, E_f , are related to each other by $E_f = E_b + 2E_\gamma$, owing to the energy of the incoming photons, which can be written in Hartree atomic units as $E_\gamma = k/\alpha$. Although known for a long time, the *relativistic* form of the transition amplitude (11) has been used only recently in studying multi-photon ionization processes and, in particular, in order to calculate the total ionization cross sections along the hydrogen isoelectronic sequence (Koval *et al* 2003). In such a relativistic description of the transition amplitude (11), the initial state $\psi_{n_b j_b \mu_b}(\mathbf{r}) = \langle \mathbf{r} | n_b j_b \mu_b \rangle$ and the final state $\psi_{\mathbf{p}m_s}(\mathbf{r}) = \langle \mathbf{r} | \mathbf{p}m_s \rangle$ are the (analytically) well-known solutions of the Dirac Hamiltonian for a bound and continuum electron, respectively (Berestetskii *et al* 1971).

As is seen from equation (11), the evaluation of the transition amplitude requires a summation over the *discrete* (bound) states as well as an integration over the *continuum* of the Dirac Hamiltonian, (ψ_ν, E_ν) . In fact, such a ‘summation’ over the complete spectrum is difficult to carry out explicitly since, in particular, the integration over the continuum requires the calculation of *free–free* transitions. This summation, therefore, is sometimes restricted to some small—*discrete*—basis, assuming that the contribution from the continuum is negligible. In practice, however, such a limitation seems justified only to estimate the behaviour of the cross sections near the resonances where the ion is rather likely excited by the first photon into some—*real*—intermediate state of the ion from which it is later ionized by means of a second photon. In the *non-resonant* region of the photon energies, in contrast, the integration over the continuum may give rise to a rather remarkable contribution to the total cross section and, hence, has to be carried out. Apart from a *direct summation* over the continuum states, however, it is often more favourable to apply Green functions, at least if these functions can be generated efficiently. For hydrogen-like ions, for example, such Green functions are known analytically, both in the nonrelativistic as well as relativistic theory (Swainson and Drake 1991).

2.3. Green function approach

As usual, Green functions are defined as solutions to some inhomogeneous (differential) equation

$$(\hat{H} - E)G_E(\mathbf{r}, \mathbf{r}') = \delta(\mathbf{r} - \mathbf{r}'), \quad (12)$$

where, in our present investigation, \hat{H} refers to the Dirac Hamiltonian and E denotes the energy of the atom or ion. For realistic systems, of course, such Green functions are not easy to obtain, even if only *approximate* solutions are needed. However, a formal solution is given by (Morse and Feshbach 1953)

$$G_E(\mathbf{r}, \mathbf{r}') = \sum_{\nu} \frac{|\psi_{\nu}(\mathbf{r})\rangle\langle\psi_{\nu}(\mathbf{r}')|}{E_{\nu} - E}, \quad (13)$$

including a summation (integration) over the complete spectrum (of \hat{H}) as discussed in the previous section. In the two-photon transition amplitude (11), therefore, we may simply replace this summation by the corresponding Green function

$$M_{\text{bp}}(m_s, \mu_b, \lambda_1, \lambda_2) = \frac{\sqrt{8\pi^3}}{\alpha E_{\gamma}} \langle \psi_{\mathbf{p}m_s}(\mathbf{r}) | \alpha \mathbf{u}_{\lambda_1} e^{i\mathbf{k}\mathbf{r}} G_{E_b+E_{\gamma}}(\mathbf{r}, \mathbf{r}') \alpha \mathbf{u}_{\lambda_2} e^{i\mathbf{k}\mathbf{r}'} | \psi_{n_b\kappa_b\mu_b}(\mathbf{r}') \rangle. \quad (14)$$

For hydrogen-like ions, the Coulomb–Green functions from equation (12) are known analytically today in terms of (various) special functions from mathematical physics and, in particular, in terms of the confluent hypergeometric function ${}_1F_1(a, b; z)$. Here, we will not display these functions explicitly but refer the reader instead to the literature (Swainson and Drake 1991, Koval and Fritzsche 2003). For the further evaluation of the transition amplitudes (14) let us note only that, in addition to the one-particle Dirac Hamiltonian, the Coulomb–Green function can be decomposed into a radial and an angular part

$$G_E(\mathbf{r}, \mathbf{r}') = \frac{1}{rr'} \sum_{\kappa m} \begin{pmatrix} g_{E\kappa}^{LL}(r, r') \Omega_{\kappa m}(\hat{r}) \Omega_{\kappa m}^{\dagger}(\hat{r}') & -i g_{E\kappa}^{LS}(r, r') \Omega_{\kappa m}(\hat{r}) \Omega_{-\kappa m}^{\dagger}(\hat{r}') \\ i g_{E\kappa}^{SL}(r, r') \Omega_{-\kappa m}(\hat{r}) \Omega_{\kappa m}^{\dagger}(\hat{r}') & g_{E\kappa}^{SS}(r, r') \Omega_{-\kappa m}(\hat{r}) \Omega_{-\kappa m}^{\dagger}(\hat{r}') \end{pmatrix}, \quad (15)$$

where the $\Omega_{\kappa m}(\hat{r})$ denote standard Dirac spinors and where the radial Green function is given in terms of four components $g_{E\kappa}^{TT'}(r, r')$ with $T = L, S$ referring to the *large* and *small* components of the associated (relativistic) wavefunctions. The computation of the radial Green function for hydrogen-like ions has been described and implemented previously into the GREENS library (Koval and Fritzsche 2003); this code has been used also for the computation of all transition amplitudes and (angle-differential) cross sections as shown and discussed below.

2.4. Exact relativistic formulation of the two-photon amplitude

Equation (14) displays the two-photon transition amplitude in terms of the (relativistic) wave and Green functions of hydrogen-like ions. For the further evaluation of this amplitude, we need to decompose both the photon as well as the free-electron wavefunctions into partial waves in order to make later use of the techniques of Racah's algebra. As discussed previously for the capture of electrons by bare, high- Z ions (Surzhykov *et al* 2002b), we first have to decide about a proper quantization axis (z -axis) for this decomposition, depending—of course—on the particular process under consideration. For the photoionization of atoms, the only really *preferred* direction of the overall system is given by the photon momenta $\mathbf{k}_1 = \mathbf{k}_2 = \mathbf{k}$ which we adopt as the quantization axis below. Then, the multipole expansion of the radiation field reads as

$$\mathbf{u}_\lambda e^{i\mathbf{k}\mathbf{r}} = \mathbf{u}_\lambda e^{ikz} = \sqrt{2\pi} \sum_{L=1}^{\infty} i^L [L]^{1/2} (\mathbf{A}_{L\lambda}^{(m)} + i\lambda \mathbf{A}_{L\lambda}^{(e)}), \quad (16)$$

where $[L] = (2L + 1)$ and the standard notation $\mathbf{A}_{LM}^{(e,m)}$ is used for the electric and magnetic multipole fields, respectively. Each of these multipoles can be expressed in terms of the spherical Bessel functions $j_L(kr)$ and the vector spherical harmonics $\mathbf{T}_{L,\Lambda}^M$ of rank L as (Rose 1957)

$$\begin{aligned} \mathbf{A}_{LM}^{(m)} &= j_L(kr) \mathbf{T}_{L,L}^M, \\ \mathbf{A}_{LM}^{(e)} &= j_{L-1}(kr) \sqrt{\frac{L+1}{2L+1}} \mathbf{T}_{L,L-1}^M - j_{L+1}(kr) \sqrt{\frac{L}{2L+1}} \mathbf{T}_{L,L+1}^M. \end{aligned} \quad (17)$$

Using the expressions (16) and (17) for the photon field, we can rewrite the two-photon transition amplitude (14) in terms of its *electric-magnetic* components

$$\begin{aligned} M_{\mathbf{b}\mathbf{p}}(m_s, \mu_b, \lambda_1, \lambda_2) &= \frac{2\pi \sqrt{8\pi^3}}{\alpha E_\gamma} \sum_{L,L'=1}^{\infty} \sum_{\Lambda,\Lambda'} i^{L+L'} [L, L']^{1/2} \xi_{\Lambda L}^{\lambda_1} \xi_{\Lambda' L'}^{\lambda_2} \\ &\times \langle \psi_{\mathbf{p}m_s} | \alpha j_\Lambda(kr) \mathbf{T}_{L,\Lambda}^{\lambda_1} G_{E_b+E_\gamma}(\mathbf{r}, \mathbf{r}') \alpha j_{\Lambda'}(kr') \mathbf{T}_{L',\Lambda'}^{\lambda_2} | \psi_{n_b k_b \mu_b} \rangle, \end{aligned} \quad (18)$$

where the coefficients $\xi_{L\Lambda}^\lambda$ are defined as

$$\xi_{L\Lambda}^\lambda = \begin{cases} 1 & \text{if } \Lambda = L \\ i\lambda \sqrt{\frac{L+1}{2L+1}} & \text{if } \Lambda = L-1 \\ -i\lambda \sqrt{\frac{L}{2L+1}} & \text{if } \Lambda = L+1. \end{cases} \quad (19)$$

As is seen from the expansion (18), we can distinguish between different multipole components such as $E1E1$, $E1M1$, $E1E2$, and others owing to the symmetries of the two vector spherical harmonics, i.e. due to the particular combination of the summation indices L , L' , Λ , Λ' in this expansion. In the second line of (18), however, the electromagnetic multipole matrix elements still contain the wavefunction $\psi_{\mathbf{p}m_s}(\mathbf{r})$ of the free electron with well-defined asymptotic momentum \mathbf{p} . In another expansion, therefore, we have to decompose it into partial waves to allow for a further simplification of the two-photon transition amplitude (18). Again, also the expansion of the free-electron wave will depend on the choice of the quantization axis and requires—by using a quantization along the photon momentum—that we have to carry out a rotation of the space part of the electron wavefunction from the z -direction into the \mathbf{p} -direction (Eichler and Meyerhof 1995)

$$\psi_{\mathbf{p}m_s}(\mathbf{r}) = 4\pi \sum_{\kappa_f \mu_f} i^{l_f} e^{-i\Delta_{\kappa_f}} \langle l_f \mu_f - m_s | j_f \mu_f \rangle Y_{l_f \mu_f - m_s}^*(\hat{p}) \begin{pmatrix} g_{E \kappa_f}^L(r) \Omega_{\kappa_f \mu_f}(\hat{r}) \\ i g_{E \kappa_f}^S(r) \Omega_{-\kappa_f \mu_f}(\hat{r}) \end{pmatrix}, \quad (20)$$

where the summation runs over all partial waves $\kappa_f = \pm 1, \pm 2 \dots$, i.e. over all possible values of the Dirac angular momentum quantum number $\kappa_f = \pm(j_f + 1/2)$ for $l_f^L = j_f \pm 1/2$. In this notation, the (nonrelativistic angular) momentum l_f^L represents the parity of the partial waves and Δ_{κ_f} is the Coulomb phase shift. Moreover, as seen from expression (20), the partial waves

$$\psi_{E\kappa\mu_f}(\mathbf{r}) = \begin{pmatrix} g_{E\kappa_f}^L(r)\Omega_{\kappa_f\mu_f}(\hat{r}) \\ ig_{E\kappa_f}^S(r)\Omega_{-\kappa_f\mu_f}(\hat{r}) \end{pmatrix} \quad (21)$$

separate into a radial and an angular parts, where the two radial functions

$$g_{E\kappa}^L(r) \equiv P_{E\kappa}(r), \quad g_{E\kappa}^S(r) \equiv Q_{E\kappa}(r)$$

are often called the *large* and *small* components and the corresponding angular parts $\Omega_{\kappa_f\mu_f}(\hat{r}) \equiv |l_f^L j_f \mu_f\rangle = \sum_{m_l m_s} \langle l_f^L m_l 1/2 m_s | j_f \mu_f \rangle Y_{l_f^L m_l}(\hat{r}) \chi_{1/2 m_s}$ and $\Omega_{-\kappa_f\mu_f}(\hat{r}) \equiv |l_f^S j_f \mu_f\rangle = \sum_{m_l m_s} \langle l_f^S m_l 1/2 m_s | j_f \mu_f \rangle Y_{l_f^S m_l}(\hat{r}) \chi_{1/2 m_s}$ are the standard Dirac spin-angular functions.

Using the partial-wave decomposition (21) for the free-electron wavefunction and a similar expansion (15) for the Green functions, we now can carry out the angular integration in the transition amplitude (18) analytically:

$$\begin{aligned} M_b(m_s, \mu_b, \lambda_1, \lambda_2) &= \frac{8\pi^2 \sqrt{8\pi^3}}{\alpha E_\gamma} \sum_{L\Lambda L'\Lambda'} \sum_{\kappa_f \mu_f} \sum_{\kappa m T T'} i^{L+L'} i^{-l_f^L} P^T P^{T'} e^{i\Delta_{\kappa_f}} \\ &\times [L, L']^{1/2} \xi_{L\Lambda}^{\lambda_1} \xi_{L'\Lambda'}^{\lambda_2} \langle l_f^L \mu_f - m_s 1/2 m_s | j_f \mu_f \rangle \\ &\times \langle \kappa_f l_f^T \mu_f | \sigma \mathbf{T}_{L\Lambda}^{\lambda_1} | \kappa l^T m \rangle \langle \kappa l^{T'} m | \sigma \mathbf{T}_{L'\Lambda'}^{\lambda_2} | \kappa_b l_b^T \mu_b \rangle U_{\Lambda\Lambda'}^{TT'}(\kappa_f, \kappa, \kappa_b) Y_{l_f^L \mu_f - m_s}(\hat{p}) \end{aligned} \quad (22)$$

where, apart from the Clebsch–Gordan coefficient $\langle l_f^L \mu_f - m_s 1/2 m_s | j_f \mu_f \rangle$ and some constant factors, the angular part of the amplitude is given in terms of the matrix elements of the rank L spherical tensor $\sigma \mathbf{T}_{L\Lambda}^M = [Y_\Lambda \otimes \sigma]_{L\Lambda}^M$. These matrix elements can be simplified to (Balashov *et al* 2000)

$$\begin{aligned} \langle \kappa_b l_b^T \mu_b | \sigma \mathbf{T}_{L\Lambda}^M | \kappa_a l_a^{T'} \mu_a \rangle &= \sqrt{\frac{3}{2\pi}} [j_a, L, \Lambda, l_b^{T'}]^{1/2} \langle j_a \mu_a L M | j_b \mu_b \rangle \\ &\times \langle l_b^T 0, \Lambda 0 | l_a^{T'} 0 \rangle \begin{Bmatrix} l_b^T & 1/2 & j_b \\ \Lambda & 1 & L \\ l_a^{T'} & 1/2 & j_a \end{Bmatrix}, \end{aligned} \quad (23)$$

by using a proper decomposition in terms of the orbital and spin sub-spaces. The radial part of the transition amplitude (18) is contained in (22) in the (two-dimensional) integrals

$$U_{\Lambda\Lambda'}^{TT'}(\kappa_f, \kappa, \kappa_b) = \int g_{E_f \kappa_f}^{\bar{T}}(r) j_\Lambda(kr) g_{E_b + E_\gamma \kappa}^{TT'}(r, r') j_{\Lambda'}(kr') g_{E_b \kappa_b}^{\bar{T}'}(r') dr dr', \quad (24)$$

which combines the various (large and small) components of the bound state, the Green function as well as from the free-electron wave. In this notation, again, $T = L, S$ and a superscript \bar{T} refers to the conjugate of T , i.e. $\bar{T} = L$ for $T = S$ and *vice versa*. In contrast to the angular integrals (23), the radial integrals (24) have to be computed numerically. In the present work, all the required integrals for the two-photon transition amplitudes (22) are calculated by using the GREENS (Koval and Fritzsche 2003) and RACAII (Fritzsche *et al* 2001) programs.

2.5. Electric dipole approximation

The transition amplitude (22) still describes the full interaction between the electron and photon fields. With the explicit summation over all the multipoles of the photon field (16), it

includes the so-called *retardation effects* or *non-dipole* contributions. In practice, however, the contributions from the higher multipoles decrease very rapidly with L and may therefore be neglected; in fact, the computation of these contributions also become rather tedious because of difficulties with a stable procedure for the two-dimensional radial integrals (24). In many cases, therefore, it seems justified to restrict the summation in (22) to just the (dominant) *electric dipole* term with $L = 1$ and $\Lambda = L \pm 1$. This ‘dipole approximation’ is valid if the photon wave length is much larger than the size of the atom, i.e. $ka_0 \ll 1$, where a_0 is the Bohr radius. For the two-photon ionization, this condition is well satisfied for most light ions with, say, $Z < 30$ and for photon energies below that of the one-photon ionization threshold.

From the general form (22) of the ionization amplitude, the electric dipole approximation is obtained by taking $L = L' = 1$ and $\Lambda, \Lambda' = 0, 2$ which—owing to the dipole selection rules—then also restricts the summation over κ_f , i.e. the allowed partial waves for the free electron. For K-shell ionization with (completely) *circularly* polarized light, for instance, the final-state electron can only escape in the $d_{3/2}$ or $d_{5/2}$ states. And, as seen from equation (22), the dipole transition amplitude is then indeed defined by the (second-rank) spherical harmonic, $M_{bp}(m_s, \mu_b, \lambda, \lambda) \propto Y_{2, \mu_b - m_s + 2\lambda}(\hat{p})$ which (together with equation (9)) leads us to the well-known angular distribution

$$W^{\text{circ}}(\hat{p}) = c_4 \sin^4 \theta \quad (25)$$

of the photoelectrons (Lambropoulos 1972, Arnous *et al* 1973). As expected from the axial symmetry of the overall system ‘ion plus photons’, the angular distribution (25) only depends on θ but not on the azimuthal angle ϕ . For linearly polarized light, in contrast, a *reaction plane* is naturally defined by the photon momentum \mathbf{k} and the polarization vector \mathbf{u} and, hence, the axial symmetry is broken. For a linear polarization of the incident light, therefore, the angular distribution will depend on both the polar and azimuthal angle, and is given by (Zernik 1964, Lambropoulos 1972)

$$W^{\text{lin}}(\hat{p}) = b_0 + b_2 \sin^2 \theta \cos^2 \phi + b_4 \sin^4 \theta \cos^4 \phi, \quad (26)$$

where the angle $\phi = 0$ corresponds to an electron emission within the reaction plane (cf figure 1).

3. Results and discussion

For the calculation of total two-photon ionization cross sections, the electric dipole approximation was recently found sufficient for most of the hydrogen-like ions, and not just in the low- Z domain (Koval *et al* 2003). Even for high- Z ions, for example, the total cross sections from the dipole approximation do not differ by more than about 20% from those of a full relativistic computation, including the contributions from all the higher multipoles. Larger deviations, however, can be expected for the angular distribution of the emitted electrons which is known to be sensitive to the retardation in the electron–photon interaction (Surzhykov *et al* 2002a). As is known, for instance, from the radiative recombination of high- Z ions, which is the time-inverse process for the *one-photon ionization*, a significant change in the angle-differential cross sections may arise from the higher multipoles and may lead to quite sizeable deviations when compared with the dipole approximation (Eichler and Meyerhof 1995).

In this contribution, therefore, we have analysed both the electric dipole and the exact relativistic treatment from equation (22) in order to explore the relativistic and retardation effects on the angular distributions of the electrons. Detailed computations have been carried out, in particular, for the K-shell ionization of (neutral) hydrogen as well as hydrogen-like xenon and uranium ions at an energy of both incoming photons of $E_\gamma = 1.4|E_{1s}|/2$ where the E_{1s} is

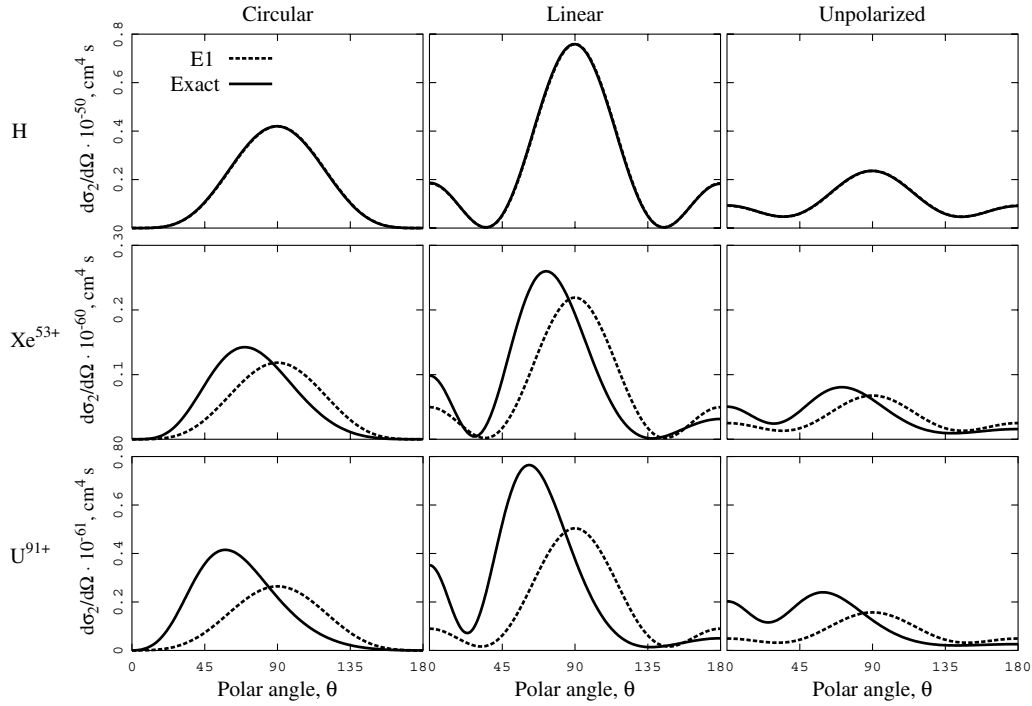


Figure 2. Angular distributions of the emitted electrons in the two-photon K-shell ionization of hydrogen-like ions by means of circularly, linearly and unpolarized light. Results are presented for both, the electric dipole (---) and the relativistic (—) approximations and for a two-photon energy which is 40% above the (one-photon) ionization threshold.

the (one-photon) ionization threshold. Moreover, to explore the dependence of the relativistic effects on the polarization of the incoming light, three cases of the polarization are considered: (i) completely circular polarized, (ii) completely linear polarized, and (iii) unpolarized light. For these three ions and types of polarization, figure 2 displays the angular distributions of the electrons as obtained within the dipole approximation (---) as well as the exact relativistic treatment (—) which is given by equations (22)–(24) and includes, therefore, all the multipoles in the electron–photon interaction. While, for hydrogen, both approximations yield virtually identical results, they start to differ as the nuclear charge Z is increased. Instead of a symmetrical emission with respect to the polar angle $\theta = 90^\circ$, then the emission occurs predominantly into the forward direction, an effect which is best seen for hydrogen-like U^{91+} ions. We therefore find that the *non-dipole* terms first of all give rise to an *asymmetrical* shift in the angular distribution of the electrons which could be observed in experiment. The maxima in the (angle-differential) cross sections, on the other hand, are less affected and deviate, even for hydrogen-like uranium, by less than a factor of 2.

In figure 2, all angular distributions are shown as a function of the polar angle θ , i.e. with respect to the incoming photon beam. As discussed above, this dependence of the differential cross sections, $d\sigma/d\Omega = d\sigma/d\Omega(\theta)$, can be the only one for circular and unpolarized light for which the electron emission must be axially symmetric. For linear polarized light, in contrast, the emission of the electrons will depend on both the polar angle θ and the azimuthal angle ϕ . For this polarization, figure 2 only displays the angular distributions *within* the reaction plane, i.e. at $\phi = 0^\circ$. To explore, in addition, the ϕ -dependence of the two-photon ionization by linear polarized light explicitly, figure 3 shows the corresponding angular distributions $d\sigma/d\Omega(\theta, \phi)$

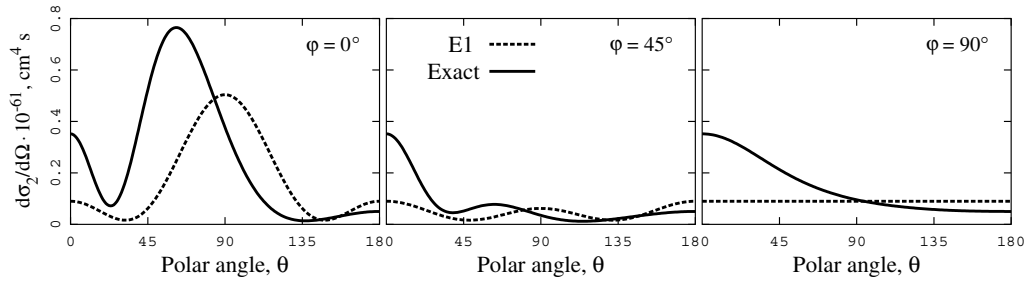


Figure 3. Angular distributions of the electrons emitted in the two-photon K-shell ionization of the hydrogen-like uranium U^{91+} by means of linear polarized light. Distributions are shown for the angles $\phi = 0^\circ$, 45° and 90° with respect to the reaction plane; cf figure 1

for the three particular angles $\phi = 0^\circ$, 45° and 90° with respect to the reaction plane; here, the left inlet ($\phi = 0^\circ$) is the same as shown in figure 2 in the middle column for U^{91+} ions. Again, the results from the electric dipole approximation are compared with those from a fully relativistic computation. As is seen from figure 1, the most pronounced effect of the higher multipoles arises for an electron emission in a plane which is perpendicular to the photon polarization vector ($\phi = 90^\circ$). In such a—perpendicular—geometry of the experiment, the cross sections from the exact treatment show strong forward emission of the photoelectrons while the electric dipole approximation (26), in contrast, results in a completely isotropic emission, if seen as a function of the polar angle θ .

Until now, we considered the two-photon ionization of hydrogen-like ions by either *completely* polarized (linear: $P_L = 1$; circular $P_C = 1$) or unpolarized light ($P_L = P_C = 0$). In most experimental investigations on two- (and multi-) photon processes, however, the incident radiation is typically polarized with some given *degree of polarization* $0 \leq P_C, P_L \leq 1$. Apart from the *type* of the polarization of the incoming light, therefore, we shall also study how the angular distributions depend on the *degree* of polarization. Figure 4, for instance, displays the angular distribution from the K-shell ionization of hydrogen-like U^{91+} ions by means of circular polarized light with a degree of polarization $P_C = 0.0$ (unpolarized case), 0.5, 0.9 and 1.0. As is seen from this figure, the probability for an electron emission increases at angles around $\theta = 60^\circ$ but decreases (towards zero) in the forward and backward direction as the degree of polarization is increased. In particular the behaviour near $\theta = 0^\circ$ and 180° can be easily explained if we consider the conservation of momentum in the overall system. Since, for *completely* circularly polarized light, the (total) spin projection of photons on the quantization axis (which is chosen along the photon momenta \mathbf{k}) becomes $\lambda_1 + \lambda_2 = \pm 2$, it obviously can not be compensated—in the final state—if the electron is emitted parallel (or antiparallel) to the incoming light and hence its spin projection is $\mu_f = m_s = \pm 1/2$. For *unpolarized* light, in contrast, the photons may have different helicities and, therefore, the projection of their angular momentum $\lambda_1 + \lambda_2 = 0$ may be conserved under a forward and backward *non spin-flip* electron emission.

4. Summary

In this paper, the two-photon ionization of hydrogen-like ions has been studied in the framework of second-order perturbation theory *and* the relativistic description of the electron and photon fields. That is, exact Dirac bound and continuum wavefunctions were applied for the description of the electron to reveal the importance of *relativity* on the angular distributions of

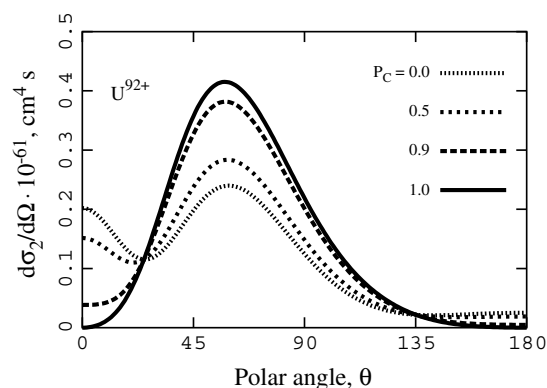


Figure 4. Angular distributions of the electrons emitted in the two-photon K-shell ionization of the hydrogen-like uranium U^{91+} by circular polarized light with different degrees of polarizations $P_C = 0, 0.5, 0.7$ and 1 .

the emitted electrons. Moreover, relativistic Coulomb–Green functions are used to perform the summation over the complete Dirac spectrum as needed in second-order perturbation theory.

To understand the angular distributions of the emitted photoelectron and, in particular, the influence of the polarization of the light on this emission, density matrix theory has been utilized to ‘combine’ the two-photon transition amplitudes in a proper way. Calculations are carried out for the K-shell ionization of the three (hydrogen-like) ions H, Xe^{53+} and U^{91+} . From the angular distribution of the electrons for different types (linear, circular, unpolarized) and degrees of polarization (i.e. in going from the completely polarized to unpolarized light), it is clearly seen that the angular emission depends much more sensitively on the contributions from higher multipoles than the total cross sections. Two rather pronounced effects, for example, concern the (asymmetrical) forward emission of the electrons as well as a significant change in the electron emission for linear polarized light, if the electrons are observed perpendicular to the reaction plane (cf figure 4). Both effects are enhanced if the nuclear charge of the ions is increased.

An even stronger influence from the non-dipole terms (of the radiation field) is expected for the spin-polarization of the photoelectrons. In common with the present investigation, density matrix theory provides a very suitable tool for such *polarization* studies. A detailed analysis of the polarization of the photoelectrons, emitted in the two-photon ionization of hydrogen-like ions, is currently in progress.

Acknowledgments

This work has been supported by the Deutsche Forschungsgemeinschaft (DFG) within the framework of the Schwerpunkt ‘Wechselwirkung intensiver Laserfelder mit Materie’. One of us (AS) is also grateful for the support from the Gesellschaft für Schwerionenforschung (GSI) project KS-FRT.

Appendix A. Photon spin density matrix

A *pure* (i.e. completely polarized) state of the photon can be characterized in terms of a polarization unit vector \mathbf{u} which always points perpendicular to the (asymptotic) photon momentum \mathbf{k} . Of course, this polarization vector, \mathbf{u} , can be rewritten by means of any *two*

(linear independent) basis vectors such as the *circular polarization* vectors $\mathbf{u}_{\pm 1}$ which are (also) perpendicular to the wavevector \mathbf{k} and which, for \mathbf{u}_{+1} respective \mathbf{u}_{-1} , are associated with right- and left-circular polarized photons (Blum 1981). In such a basis, the unit vector for the *linear* polarization of the light can be written as

$$\mathbf{u}(\chi) = \frac{1}{\sqrt{2}}(e^{-i\chi}\mathbf{u}_{+1} + e^{i\chi}\mathbf{u}_{-1}), \quad (\text{A.1})$$

where χ is the angle between $\mathbf{u}(\chi)$ and the x - z plane.

While a description of the polarization of the light in terms of either the circular polarization vectors $\mathbf{u}_{\pm 1}$ or the linear polarization vector (A.1) is appropriate for completely polarized light, it is not sufficient to deal with an ensemble of photons which have different polarization. Such a—mixed—state of the light is then better described in terms of the spin density matrix. Since the photon (with spin $S = 1$) has only two allowed spin (or helicity) states $|\mathbf{k}\lambda\rangle$, $\lambda = \pm 1$, the spin density matrix of the photon is a 2×2 matrix and, hence, can be parameterized by three (real) parameters:

$$\langle \mathbf{k}\lambda | \hat{\rho}_\gamma | \mathbf{k}\lambda' \rangle = \frac{1}{2} \begin{pmatrix} 1 + P_C & P_L e^{-2i\chi} \\ P_L e^{2i\chi} & 1 - P_C \end{pmatrix}, \quad (\text{A.2})$$

where $0 \leq P_L \leq 1$ and $-1 \leq P_C \leq 1$ denote the degrees of linear and circular polarization, respectively. The angle χ , moreover, represents the direction of the maximal linear polarization of light.

Of course, the choice of the parameters P_L , P_C and χ is not *unique* and many other—equivalent—sets of three real parameters could be applied to characterize the photon spin density matrix (A.2). In the analysis of experimental data, for instance, one often uses the three *Stokes* parameters to describe the polarization of radiation. The Stokes parameters can easily be expressed in terms of the (two) degrees of polarization, P_L and P_C , and the angle χ as:

$$P_1 = P_L \cos 2\chi, \quad P_2 = P_L \sin 2\chi, \quad P_3 = P_C. \quad (\text{A.3})$$

The use of the Stokes parameters leads to the familiar form of the spin density matrix (Blum 1981, Balashov *et al* 2000)

$$\langle \mathbf{k}\lambda | \hat{\rho}_\gamma | \mathbf{k}\lambda' \rangle = \frac{1}{2} \begin{pmatrix} 1 + P_3 & P_1 - iP_2 \\ P_1 + iP_2 & 1 - P_3 \end{pmatrix}. \quad (\text{A.4})$$

References

- Antoine P, Essarroukh N-E, Jureta J, Urbain X and Brouillard F 1996 *J. Phys. B: At. Mol. Opt. Phys.* **29** 5367
 Arnous E, Klarsfeld S and Wane S 1973 *Phys. Rev. A* **7** 1559
 Balashov V V, Grum-Grzhimailo A N and Kabachnik N M 2000 *Polarization and Correlation Phenomena in Atomic Collisions* (New York: Kluwer-Academic)
 Berestetskii V B, Lifshitz E M and Pitaevskii L P 1971 *Relativistic Quantum Theory* (Oxford: Pergamon)
 Blum K 1981 *Density Matrix Theory and Applications* (New York: Plenum)
 Eichler J and Meyerhof W 1995 *Relativistic Atomic Collisions* (San Diego, CA: Academic)
 Fano U and Racah G 1959 *Irreducible Tensorial Sets* (New York: Academic)
 Fritzsche S, Inghoff T, Bastug T and Tomaselli M 2001 *Comput. Phys. Commun.* **139** 314
 Goldman S P and Drake G W 1981 *Phys. Rev. A* **24** 183
 Kornberg M A, Godunov A L, Ortiz S I, Ederer D L, McGuire J H and Young L 2002 *J. Synchrotron Radiat.* **9** 298
 Koval P and Fritzsche S 2003 *Comput. Phys. Commun.* **152** 191
 Koval P, Fritzsche S and Surzhykov A 2003 *J. Phys. B: At. Mol. Opt. Phys.* **36** 873
 Lambropoulos P 1972 *Phys. Rev. Lett.* **28** 585
 Laplanche G, Durrieu A, Flank Y, Jaouen M and Rachman A 1976 *J. Phys. B: At. Mol. Phys.* **9** 1263
 Laplanche G, Jaouen M and Rachman A 1986 *J. Phys. B: At. Mol. Phys.* **19** 79

- Morse P and Feshbach H 1953 *Methods of Theoretical Physics* vol 1 (New York: McGraw-Hill)
- Rose M E 1957 *Elementary Theory of Angular Momentum* (New York: Wiley)
- Rottke H, Wolff B, Brickwedde M, Feldmann D and Welge K H 1990 *Phys. Rev. Lett.* **64** 404
- Santos J P, Patte P, Parente F and Indelicato P 2001 *Eur. J. Phys. D* **13** 27
- Surzhykov A, Fritzsche S, Gumberidze A and Stöhlker Th 2002a *Phys. Rev. Lett.* **88** 153001
- Surzhykov A, Fritzsche S and Stöhlker Th 2002b *J. Phys. B: At. Mol. Opt. Phys.* **35** 3713
- Swainson R A and Drake G W F 1991 *J. Phys. A: Math. Gen.* **24** 95
- Szymanowski C, Véniard V, Taïeb R and Maquet A 1997 *Europhys. Lett.* **6** 391
- Wolff B, Rottke H, Feldmann D and Welge K H 1988 *Z. Phys. D* **10** 35
- Zernik W 1964 *Phys. Rev.* **135** A51

Bibliography

Andruszkow J *et al* 2000 *Phys. Rev. Lett.* **85** 3825-3829.

Abramowitz M and Stegun I A 1965 *Handbook of Mathematical Functions* (New York: Dover).

Amusia M Ya 1990 *Atomic photoeffect* (New York: Plenum Press)

Arnous E, Klarsfeld S and Wane S 1973 *Phys. Rev. A* **7** 1559.

Avery James and Avery John 2003 *Journal of Mathematical Chemistry* **33** 145.

Aymar M and Crance M 1980 *J. Phys. B* **13** 2527.

Bebb H and Gold A 1966 *Phys. Rev.* **143** 1.

Brown G E and Ravenhall D G 1951 *Proc. Roy. Soc.* **A208** 552.

Cowan R D 1981 *The Theory of Atomic Structure and Spectra* (Los Angeles: University of California Press).

Cowan R D 1967 *Phys. Rev.* **163** 54.

Delone N B and Krainov V P 1999 *Multiphoton Processes in Atoms* (Berlin: Springer-Verlag).

Dirac P A M 1926 *Proceedings of the Royal Society of London* **A112** 661.

Drake G W F 1996 *Atomic, Molecular, & Optical Physics Handbook* (New York: AIP Press).

Dyall K G, Grant I P, Johnson C T, Parpia F A and Plummer E P 1990 *Comput. Phys. Commun.* **55** 425.

Eichler J and Meyerhof W E 1995 *Relativistic Atomic Collisions* (New York: Academic Press).

Gebarowski R, Burke P G, Taylor K T, Dörr M, Bensaid M and Joachain C J 1997 *J. Phys. B* **30** 1837.

Göppert-Mayer M 1931 *Ann. Phys.* **9** 273.

Goldman S P and Drake G W F 1981 *Phys. Rev. A* **24** 183.

- Gräf D and Hink W 1985 *J. Phys. B* **18** L803.
- Grant I P 1974 *J. Phys. B* **7** 1458.
- Grant I P 1988 in *Methods in Computational Chemistry*, (London: Plenum Press).
- Karazija R 1996 *Introduction to the Theory of X-Ray and Electronic Spectra of Free Atoms* (New York: Plenum Press).
- Karule E 1977 in *Multiphoton Processes: Proceedings of an International Conference at the University of Rochester* (New York: Wiley).
- Karule E and Pratt R H 1991 *J. Phys. B* **24** 1585.
- Klarsfeld S 1969 *Nuovo Cimento Lett.* **1** 682; **2** 548.
- Kornberg M A, Godunov A L, Ortiz S I, Ederer D L, McGuire J H and Young L 2002 *Journal of Synchrotron Radiation* **9** 298.
- Koval P and Fritzsche S 2003 *Comput. Phys. Commun.* **152** 191. (see in Appendix E)
- Koval P, Fritzsche S and Surzhykov A 2003 *J. Phys. B* **36** 873. (see in Appendix E)
- Koval P, Fritzsche S and Surzhykov A 2004 *J. Phys. B* **37** 375. (see in Appendix E)
- Lambropoulos P, Maragakis P and Zhang J 1998 *Phys. Rep.* **305** 203.
- Landau L D, Lifshitz E M 1986 *Course of theoretical physics. Quantum mechanics* (New York: Wiley).
- Laplanche G, Durrieu A, Flank Y, Jaouen M and Rachman A 1976 *J. Phys. B* **9** 1263.
- Luc-Koenig E, Lyras A, Lecomte J-M and Aymar M 1997 *J. Phys. B* **30** 5213.
- Luke Y L 1977 *Algorithms for the Computation of Mathematical Functions* (New York: Academic Press).
- Maquet A, Véniard V and Marian T A 1998 *J. Phys. B* **31** 3743.
- McGuire E J 1981 *Phys. Rev. A* **23** 186.
- McKenna C and Hugo W van der Hart 2003 *J. Phys. B* **36** 1627.
- Messiah A 1990a *Quantum Mechanics Vol. 1* (New York: Walter de Gruyter)
- Messiah A 1990b *Quantum Mechanics Vol. 2* (New York: Walter de Gruyter)
- Muller K E 2001 *Numer. Math.* **90** 179.
- Nikolopoulos L A A 2003 *Comput. Phys. Commun.* **150** 140.
- NIST atomic database 2003 Published online: <http://www.nist.gov/>

- Rapoport L, Zon B and Manakov N 1969 *Zh. Eksp. Teor. Fiz.* **56** 400; *Trans. Sov. Phys.–JETP* **34** 515.
- Ritchie B 1977 *Phys. Rev. A* **34** 4857.
- Rocca J J, Hammarsten E C, Jankowska E, Filevich J, Marconi M C, Moon S, and Shlyaptsev V N 2003 *Phys. Plasmas* **10** 2031.
- Rose M E 1957 *Elementary Theory of Angular Momentum* (New York: Wiley).
- Rus B, Mocek T, Präg A R, Kozlová M, Jamelot G, Carillon A, Ros D, Joyeux D and Phalippou D 2002 *Phys. Rev. A* **66** 063806.
- Saenz A and Lambropoulos P 1999 *J. Phys. B* **32** 5629.
- Salvat F, Fernández-Varea J M and Williamson W Jr 1995 *Comput. Phys. Commun.* **90** 151.
- Schrödinger E 1926 *Annalen der Physik* **81** 109.
- Spanier J and Keith B 1987 *An Atlas of Functions* (New York: Springer-Verlag).
- Swainson R A and Drake G W F 1991a *J. Phys. A* **24** 79.
- Swainson R A and Drake G W F 1991b *J. Phys. A* **24** 95.
- Schwartz C 1959 *Ann. Phys. (N. Y.)* **6** 156.
- Schwartz C and Tieman T J 1959 *Ann. Phys. (N. Y.)* **6** 178.
- Szmytkowski R 1997 *J. Phys. B* **30** 825.
- TESLA Home-page 2003 <http://tesla.desy.de/>.
- Thompson W J 1997 *Atlas for computing mathematical functions* (New York: Wiley).
- Varshalovich D A, Moskalev A N, Khersonskii V K 1989 *Quantum Theory of Angular Momentum* (New Jersey: World Scientific).
- Victor G A 1967 *Proc. Phys. Soc.* **91** 825.
- Wynne J J, Armstrong J A and Esherick P 1977 in *Multiphoton Processes: Proceedings of an International Conference at the University of Rochester* (New York: Wiley).
- Xingdong M and Crasemann B 1988 *Phys. Rev. A* **38** 4585.
- Zernik W 1964 *Phys. Rev.* **135** A51.
- Zhang S, Jin J 1996 *Computation of special functions* (New York: Wiley).
- Zon B, Manakov N L and Rapoport L P 1971 *Zh. Eksp. Teor. Fiz.* **61** 968; *Trans. Sov. Phys.–JETP* 1972 **34** 515.

Index

- Algorithm
 - for Dirac-central-field Green's function, 32–36
 - for Kummer function, 59
 - for Tricomi function, 59
 - self-validation, 58
- Anti-resonance, 12, 19–21
- Approximation
 - long-wavelength, 12
 - single-active-electron (SAE), 3, 30, 36, 38
- Coulomb field, 14, 16, 17, 32
- Cross section
 - one-photon ionization, 21
 - two-photon ionization, 21
 - differential, 1, 17–19
 - total, 1, 11, 12, 17, 19–21, 30
- Decay
 - one-photon, 16
 - two-photon, 14, 16, 48
- Effects
 - many-electron, 2, 3
 - multipole, 2, 14–17, 21, 25
 - relativistic, 2, 14–17, 21
- Electric dipole channel, 1, 16, 21, 42, 43
- Electron angular distribution, 18
- Equation
 - defining
 - for Kummer functions, 55
 - Green's function, 14, 31
- Excitation
 - two-photon, 14, 16
- Function
 - confluent hypergeometric, 55
 - effective nuclear charge, 32, 34
 - Green's, 2, 14, 17
 - central-field, 14, 30–32, 65
 - Coulomb, 2, 14, 17, 18
 - Hartree, 63
 - Kummer, 55
 - Tricomi, 55
- Hydrogenic nucleus, 15, 16
- Ion
 - helium-like, 38–39
 - hydrogen-like, 2, 3, 15–28
- Ionization
 - multiphoton, 1–3, 6
 - one-photon, 5, 15
 - two-photon, 1, 5–7, 11, 13–18, 21
 - argon, 39
 - helium, 13, 38
 - helium-like neon, 38
 - hydrogen, 1, 2, 11, 13–15
 - hydrogen-like ions, 2, 15–28
 - lithium, 36
- Kummer transformation, 56
- Matrix element
 - first-order, 10, 51–53
 - second-order, 6, 10, 11, 13, 53–54
- Method
 - differential equation, 2, 11, 13, 14
 - direct summation, 11, 12
 - Green's function, 2, 3, 11, 12, 14
- Nuclear charge, 16, 18, 19, 21
- Perturbation theory, 1–3, 6, 7
 - second-order, 1, 9

Polarization
 ratio, 19, 21, 40–43
 vector, 18, 51

Potential
 Hartree, 36, 63
 Hartree-plus-statistical-exchange, 36, 39, 64
 HX, 36, 39, 64

Range
 dominant, 11, 12
 non-resonance, 12
 resonance, 12

Resonance
 height, 39
 two-photon, 1, 12, 15, 19–22

Round-off error, 57

Selection rules
 electric dipole, 15, 21
 in one-photon ionization, 15
 in two-photon ionization, 15, 20

Series
 asymptotic, 56
 hypergeometric, 56
 logarithmic, 56

Shell
 inner, 2, 3, 14, 15, 39
 K, 16, 39
 L, 39
 outer, 2, 36

Spectrum
 continuum, 3, 9, 11–13, 18
 discrete, 9, 11, 12, 18

State
 bound, 12, 18
 final, 10, 15–19
 free, 18
 initial, 15, 17, 18, 21
 intermediate, 13
 metastable, 1, 13, 16

Sturmian basis set, 2, 48

Threshold energy, 11, 21

Transition amplitude
 n -th-order, 10, 13
 first-order, 10
 second-order, 10–14, 18–21

Uncertainty propagation, 58

Yield
 electronic, 11, 17
 ionic, 17

Acknowledgment

I would like to express my gratitude to **Dr. Stephan Fritzsche** who gave the initial idea for this work and have provided the constant support during the realization of the Dirac-central-field Green's function. Thanks to his recommendations, I have learned a lot in the atomic physics and in the modern programming technology.

I am grateful to **Prof. Burkhard Fricke** who leads the physics department on a very kind way, creating the friendly climate inside of the group. Many thanks I express to **Dr. Wolf-Dieter Sepp** with whom I have discussed many issues belonging to this work as well as many other interesting topics in the physics and in the everyday life. My special gratitude is directed to **Dr. Andrey Surzhykov** for his help and condolence which contributed both to my work and to my well being.

I am grateful to **Dr. Alejandro Saenz** for his fruitful remarks about the two-photon resonances and for his two-photon ionization cross sections of the helium atom.

Sincere gratitude I direct to my *alma mater* and *school* teachers **Dr. Vyacheslav Tlyachev** and **Victor Savosko**. They kept my interest in physics, gave me the necessary background and a friendly support.

During my stay in Germany, I met many people who contributed to the friendly environment. Amongst other, I would like to name here my roommates **Dr. Andrey Surzhykov** and **Cristina Sarpe-Tudoran**; colleagues: **Dr. Josef Anton**, **Dr. Turgut Bastug**, **Dr. Chenzhong Dong**, **Dr. Timo Jacob**, **Dr. Gediminas Gaigalas**, **Dr. Tomohiko Ishii**, **Eka-terina Rykhlińskaia**, **Gabriel Cristache**, **Lars Haag**, **Thorsten Inghoff**, **Alexander Rabinovitsch** and **Alexander Uvarov**; and people who hardly relate to the theoretical physics: **Elfriede Heise**, **Dr. Karl Fritz Heise** and **Nata Werner**.

I appreciate my **parents** for their constant love and faith in me.

This work has been supported by the Deutsche Forschungsgemeinschaft (DFG) within the framework of the Schwerpunkt "Wechselwirkung intensiver Laserfelder mit Materie".

Curriculum Vitae

Name: **Peter Koval**
Born: 6 April 1976 at village Tulski, Russia

School education

Sep. 1983 – May 1986 primary school, WIR, Republic Adygheya, Russia
Sep. 1986 – May 1991 secondary school, WIR, Republic Adygheya, Russia
Sep. 1991 – June 1993 high school, WIR, Republic Adygheya, Russia

University education

Sep. 1993 – June 1998 Physics Department, Adyghe State University, Maykop, Russia
June 1998 Diploma (*with honor*), speciality "Physics", major "Theoretical Physics"
Nov. 1998 – Dec. 2000 Postgraduate at Adyghe State University, Maykop, Russia

Employment

from April 2001 Scientific collaborator at University of Kassel, Germany

Erklärung

Hiermit versichere ich, daß ich die vorliegende Dissertation selbständig und ohne unerlaubte Hilfe angefertigt und andere als die in der Dissertation angegebenen Hilfsmittel benutzt habe. Alle Stellen, die wörtlich oder sinngemäß aus veröffentlichten oder unveröffentlichten Schriften entnommen sind, habe ich als solche kenntlich gemacht. Kein Teil dieser Arbeit ist in einem anderen Promotions- oder Habilitationsverfahren verwendet worden.

April 5, 2004, Kassel

Peter Koval